UNIVERSITÀ DEGLI STUDI DI NAPOLI "FEDERICO II"

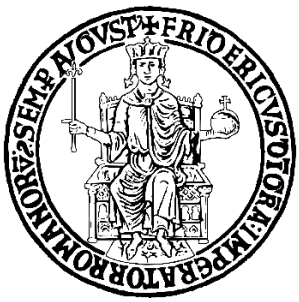

SCUOLA POLITECNICA E DELLE SCIENZE DI BASE

DIPARTIMENTO DI STRUTTURE PER L'INGEGNERIA E L'ARCHITETTURA

CORSO DI LAUREA MAGISTRALE IN INGEGNERIA STRUTTURALE E GEOTECNICA

TESI DI LAUREA SPERIMENTALE IN

TEORIA E PROGETTO DELLE COSTRUZIONI IN ACCIAIO

NUMERICAL MODELLING AND PARAMETRIC ANALYSIS OF EXISTING STEEL FRAMES RETROFITTED WITH EXTERNAL BRBs

MODELLAZIONE NUMERICA E ANALISI PARAMETRICA DI TELAI ESISTENTI IN ACCIAIO ADEGUATI SISMICAMENTE MEDIANTE L'UTILIZZO DI BRB ESTERNI

Relatore:
Chiar.mo Prof. Ing. Raffaele Landolfo

Correlatore:
Chiar.mo Dr. Ing. Fabio Freddi

Candidato:
Massimo Cicia

Matricola:
M56000873

Anno Accademico 2021/2022

UNIVERSITÀ DEGLI STUDI DI NAPOLI "FEDERICO II"

SCUOLA POLITECNICA E DELLE SCIENZE DI BASE

DIPARTIMENTO DI STRUTTURE PER L'INGEGNERIA E L'ARCHITETTURA

CORSO DI LAUREA MAGISTRALE IN INGEGNERIA STRUTTURALE E GEOTECNICA

In a joint research project with:

UNIVERSITY COLLEGE LONDON

DEPARTMENT OF CIVIL, ENVIRONMENTAL & GEOMATIC ENGINEERING

NUMERICAL MODELLING AND PARAMETRIC ANALYSIS OF EXISTING STEEL FRAMES RETROFITTED WITH EXTERNAL BRBs

MODELLAZIONE NUMERICA E ANALISI PARAMETRICA DI TELAI ESISTENTI IN ACCIAIO ADEGUATI SISMICAMENTE MEDIANTE L'UTILIZZO DI BRB ESTERNI

Relatore:
Chiar.mo Prof. Ing. Raffaele Landolfo

Correlatore:
Chiar.mo Dr. Ing. Fabio Freddi

Candidato:
Massimo Cicia

Matricola:
M56000873

Anno Accademico 2021/2022

“Non chi comincia, ma quel che persevera”

Leonardo da Vinci

Abstract

The damage experienced during historical and recent earthquakes worldwide has continued to highlight the seismic vulnerability of existing buildings designed before the introduction of modern seismic design codes.

Several innovative retrofit strategies have been developed and investigated in the past few decades. For some of them, the significant research efforts allowed the knowledge transfer from the academic research in policy-making and building codes, hence promoting the application of these solutions in practice. Some of these earthquake risk mitigation strategies include the use of passive energy dissipation devices and base isolation systems.

Nevertheless, the invasiveness of the intervention still represents a significant limitation for the implementation of retrofitting in practice. Only a few innovative solutions allow operating without interrupting the activity of the building or without removing non-structural elements. It is noteworthy that the cost of the latter two aspects often represents a significant portion of the cost of the intervention. For this reason, there is a significant need for the development and in-depth investigations of modern retrofit strategies able to address these issues.

Among others, the use of Buckling Restrained Braces (BRBs) has emerged to be an efficient retrofit strategy. BRBs are a type of yielding dissipative device where a sleeve provides buckling resistance to an unbonded core that resists the axial stress. As buckling is prevented, the BRB's core can develop axial yielding in both tension and compression, ensuring an almost symmetric hysteretic behaviour. This property allows the development of large and stable hysteretic loops, providing significant energy dissipation capacity. When included within existing frames, the BRBs provide a supplemental path for the earthquake-induced lateral loads enhancing the structure's seismic performance by adding strength, stiffness and energy dissipation capacity to the frame. BRBs are typically placed within the existing frames and require the demolition and reconstruction of non-structural components.

The present research investigated the use of BRBs for the seismic retrofitting of existing steel structures, considering an external placement of the braces. This solution aims to minimise the intervention's invasiveness and, consequently, business interruptions and indirect losses. The research is based on advanced 3D numerical simulations of a case study steel frame retrofitted with BRBs externally placed with respect to the frame. The numerical model has been validated against the results of large-scale Pseudo-Dynamic tests and successively used to perform extensive parametric analyses. The results provide valuable insights and design recommendations on the effective implementation of this retrofit solution.

Table of contents

List of Figures

List of Tables

1 Introduction

1.1 Background and motivations

Most of the existing buildings (> 80%) in Europe have been built before the introduction of the seismic design codes. Therefore, they exhibit low energy dissipation capacity and are prone to experiencing local failure mechanisms as a consequence of high-intensity seismic events. This has been demonstrated by the post-earthquake scenarios in many historical and recent events. The situation is similar in most seismic-prone regions worldwide.

Among others, the recent central Italy earthquakes in 2016 have caused widespread damage to low-to-medium rise steel buildings that do not incorporate ductile seismic detailing. The insufficient lateral stiffness of existing steel frames led to significant lateral drifts and buckling in the steel components, especially in the columns. Local damage (buckling) has also been observed at the beam-column connections due to the strut-action induced by the masonry infills. Therefore, a mass-scale intervention on the existing building stock seems to be required in order to reach current safety standards.

Nowadays, several effective retrofit strategies are currently available for earthquake risk mitigation, including passive energy dissipating devices and base isolation systems. Nevertheless, invasiveness of the intervention represents a common limitation of these methods; only a few of them allow operating without interrupting the activity of the building or without removing non-structural elements. It is worth mentioning that the latter two aspects usually account for a significant portion of the whole intervention cost. For this reason, the development and in-depth investigation of retrofit strategies that can be implemented without interrupting construction use still represent a significant challenge that needs to be addressed.

To this end, within the HITFRAMES project [1], a two-story one-bay substructure of a prototype building retrofitted with eccentric Buckling Restrained Braces (BRBs), was tested at the Structures Laboratory (STRULAB) of the University of Patras in Greece. The prototype building under consideration has been selected to be representative of typical existing steel frames and consists of a multi-story steel Moment Resisting Frame (MRF) that was designed primarily for gravity loads with insufficient seismic detailing.

Within this framework, the research activity reported in the following thesis investigates the effectiveness of a retrofit strategy that allows applying dissipative devices externally, avoiding prolonged business interruption and the related indirect losses.

1.2 Research Objectives

The aim of this research activity is to provide advancements in the field of Steel Structures Rehabilitation by investigating the feasibility of an innovative low-invasive retrofit strategy for existing steel buildings based on the use of BRBs placed externally to the frame plane, in continuity with the outcomes of a previous European Research Project HITFRAMES. To fulfil this aim, the following research objectives have been identified:

- To develop a simplified numerical modelling strategy for BRB devices and validate it against experimental results;
- To develop an advanced 3D non-linear numerical model of a two-storey steel MRF retrofitted with external BRBs and validate it against the results of the large-scale Pseudo-Dynamic experimental tests performed within the European Research Project HITFRAMES;
- To evaluate the feasibility and effectiveness of the retrofit strategy;
- To identify the key design parameters which affect the effectiveness of the intervention and perform an extensive parametric analysis to quantify their influence on the seismic response;
- To define design recommendations aimed at improving the effectiveness of the retrofit intervention.

1.3 Thesis Outline

The present Thesis is organised as follows:

- **Chapter 2**: covers a literature review in the fields of interest. Attention is first drawn to the assessment of existing steel structures, starting from the definition of seismic risk and concluding with a detailed description of the assessment procedure according to both EC8-1[2] and EC8-3[3]. Successively, a brief description of the main retrofit intervention strategies is provided. Relevance is given to the application of bracing systems as retrofit strategies, including an extensive description of BRBs and the typical connection used in conventional interventions. Finally, alternative solutions involving an external damping solution connected to the structure are presented;
- **Chapter 3**: introduces the preliminary work performed within the European Research Project (HITFRAMES) on which this thesis lays its foundations. The first section presents the prototype building considered as a representative of typical non-seismically designed, low-ductility, low-rise existing steel MRFs. Then, the scaled sub-structure representing the test specimens is introduced in all the considered configurations: the bare and retrofitted frame. Furthermore, the BRB's specifications, together with the material properties obtained from the coupon tests, are presented. This

chapter is concluded with a description of the Pseudo-dynamic tests carried out throughout the experimental campaign and an illustration of the test setup and instrumentation. Finally, different observations on the outcomes of the experimental test are presented;

- **Chapter 4**: describes the numerical modelling and validation process undertaken throughout this research work. At first, the model of the bare frame is presented and validated against the experimental results. This task was essential to gain confidence in the numerical results. Then, the BRB frame model is described, giving particular attention to modelling the BRB device cyclic behaviour. The numerical models' calibration was performed at the materials, components, and system level. Different modelling strategies were investigated to provide satisfactory solutions with regard to modelling accuracy and the computational effort required. Finally, the limitations included in the previously described models are presented, and different conclusions are outlined;
- **Chapter 5**: identifies the key parameters affecting the effectiveness of the intervention and presents a parametric analysis in which the influence of these parameters on the structural response is quantified. Furthermore, a complete structure model was considered to investigate the performance of the retrofit system by explicitly accounting for the influence of the other structural and non-structural elements. The results provide valuable insights and design recommendations on the effective implementation of this retrofit solution. Finally, the main conclusions are drawn, and future works in the field are suggested.

2 Literature review

2.1 Assessment of existing steel structures

2.1.1 Seismic risk

Earthquakes are among natural hazards causing the highest number of casualties and economic losses worldwide. However, the problem is not related to the earthquake itself but to its effects on the built environment. In this context, the seismic design of structures and infrastructures represents a crucial issue of modern societies.

Seismic Risk quantification is a key aspect of seismic design. It can be defined as the probability of losses occurring due to earthquakes within a given period of time; these losses can include human lives, social and economic disruption as well as material damage. In order to assess seismic risk, it is useful to split it into three simpler assessment terms, which are interlinked but can be almost separately studied: seismic *hazard*, *vulnerability*, and *exposure*.

Seismic Hazard may be defined as the probability of a potentially damaging earthquake effect (*e.g.*, ground shaking, ground failure, etc.) occurring at a site within a given period of time. It is commonly expressed as a relationship between the level of the seismic effect and the corresponding probability of its occurrence. Seismic hazard is therefore considered as an external factor, *i.e.*, not directly controllable except by relocating the civil works in question.

Seismic Vulnerability is the likelihood (or probability) of the occurrence of damage in a building (or series of buildings) when exposed to a particular earthquake effect. Therefore, it is typically represented by a relationship between an intensity measure of the earthquake effect and the level of damage expected. The latter definition (in terms of structural damage) is what is typically used by engineers. However, it is worth mentioning that vulnerability is usually seen as a function of fragility (expected damage in different types of buildings given different levels of earthquake ground motion) and damage cost (expected cost of repair, downtime, or human casualties, given different levels of damage). It is clear that vulnerability assessment and control, *e.g.*, through seismic design, is an earthquake engineering competence.

Exposure quantifies the number of people and buildings, the amount of commercial and industrial activity, and the amount and type of important infrastructure and constructions concentrated in the area assessed. It can be seen as a vulnerability consequences (losses) measure. It is worth mentioning that exposure depends on the function of the structure and the items it may contain. For example, two identical structures with different uses, a warehouse and a school, given all other conditions

being equal, are unlikely to be characterised by the same exposure for seismic risk assessment purposes. Therefore, exposure is a strictly anthropogenic factor and thus considered controllable [4].

Seismic Risk reduction strategies are based on the reduction of the individual factors mentioned above. As previously mentioned, the *Seismic Hazard* of a site is an external factor; therefore, it is only possible to act on it by trying to refine the seismic classification of the territory. Despite being an anthropogenic factor, the only way to reduce the *Exposure* would be to declassify particularly vulnerable buildings. However, this will not provide an effective solution to the problem. Therefore, operating on the reduction of the *Seismic Vulnerability* represents the only effective solution. This can be achieved in several ways, and many research studies investigated the problem offering different solutions. Among others, common aspects of these strategies include *1)* removing the criticalities (elements of vulnerability) of the construction; *2)* increase of the global capacity of the structure. Retrofit strategies, in agreement with the objectives for new constructions, aim at meeting different performance objectives with respect to different seismic intensities established according to the Performance-Based Earthquake Engineering (PEER)Framework [5–8].

2.1.2 Assessment of existing buildings

This section aims at providing the essential background information on standardised procedures for the seismic assessment of existing steel MRFs based on the Eurocode 8–Part 3 (EC8–3) [3]. In this regard, comparisons will also be made with some recommendations from Eurocode 8–Part 1 (EC8-1) [2].

It is worth noting that while EC8-1 aims to guide the seismic design for new structures, the EC8-3 represents the main European reference for the assessment and retrofit of existing structures. Therefore, although these two codes have a common background, their aims are slightly different, thus resulting in some substantial differences that affect both structural analysis and verification.

It is noteworthy that the performance-based approach is the most widely used design and assessment technique in current regulations worldwide. This method aims at requiring different levels of performance in the structure for different levels of seismic intensity. To this aim, several limit states are defined.

The EC8–3 defines three limit states, namely Damage Limitation (DL), Significant Damage (SD) and Near Collapse (NC) limit states. On the other hand, the EC8–1 considers two limit states only, namely Damage Limitation (DLS) and Ultimate (ULS) limit states. As summarised in Table 2-1, each limit state has a specific seismic hazard against which the structure under consideration must be designed or assessed.

***Table 2-1** Return period and probability of exceedance for limited states in EC8-3 and EC8-1*

	EC8-3			EC8-1	
Limit States	DL	SD	NC	DLS	USL
Return Period $P_{failure}$	225 *yrs.* 20% in 50*yrs*	475 *yrs.* 10% in 50*yrs*	2475 *yrs.* 2% in 50*yrs*	95 *yrs.* 10% in 10*yrs*	475 *yrs.* 10% in 50*yrs*

Table 2-1 shows that substantial differences exist between the limit states considered in the two codes. Regarding the Damage Limit state (DL), the two codes differ for the return period considered. This aspect can be explained by their different purpose. On the one hand, the EC8-1 considers more frequent earthquakes at the DLS in order to limit the reparation cost of the non-structural components in newly designed structures. On the other hand, the EC8-3 states to limit structural damage for a rarer seismic event. Concerning USL and SD limit states, the two codes are similar; since these two limit states have almost the same objectives, they also are associated with the same return period. In contrast, considerable differences exist between the two codes regarding the NC limit state, which is not defined in EC8-1. This can be explained because EC8–1 is a design code which prescribes the design and detailing rules that ensure adequate sources of ductility and overstrength to cover the demand at NC. Therefore, the code is calibrated to implicitly satisfy the performance at NC because the designer has to comply with specific measures that are properly (or supposed to be) calibrated by the code drafter. On the contrary, the EC8–3 deals with existing structures that are not code-compliant. Therefore, it is explicitly necessary to assess their performance at NC as well.

The assessment procedure begins with the definition of the knowledge level (KL). The EC8-3 identifies three KLs to account for the epistemic uncertainties related to the existing building (*e.g.*, lack of information on geometry, material properties, detailing, etc.). Depending on the level of knowledge achieved, different types of analysis are allowed. In particular, linear analysis methods are allowed for all three KLs, while non-linear approaches are only allowed for "normal knowledge" (KL2) and "full knowledge" (KL3). In addition, each knowledge level is associated with a confidence factor (CF) that must be used to reduce the mean value of the material strength. The CFs are 1.35, 1.20 and 1.00 for KL1 (*i.e.*, "limited knowledge"), KL2 and KL3, respectively. Therefore, this approach encourages the practitioner to collect additional, detailed information about the structure to reduce the conservatism of the assessment. At this stage, the numerical model of the structure can be defined with the modified material properties.

Once identified the knowledge level and created the structural model, it is necessary to define the seismic demand. As mentioned above, KL1 only allows the use of linear analyses, such as lateral force procedure (LF) or Modal Response Spectrum analysis (MRS). On the other hand, for KL2 and KL3, non-linear analysis methods such as Non-linear Static (pushover) Analysis and Non-linear Time-history Analysis may also be used.

However, given that time-history analyses generally involve a higher computational work, the pushover analysis procedure has become the most widely used analysis method within the context of the seismic assessment of existing structures. According to EC8-3, two lateral load patterns need to be applied in pushover analysis, named "uniform" and "modal". The "uniform" distribution is characterised by the assumption of uniform displacements over the height, while the "modal" distribution must be consistent with the force distribution that would be adopted in a linear, static or dynamic analysis. In the first case, the distribution of forces turns out to be similar, through the mass matrix, to a linear distribution of displacements; it is worth noting that this distribution can be adopted only if the applicability conditions of the linear static analysis are satisfied. In the second case, the force distribution adopted is similar to the shape of the first mode of vibration. It is worth noting that the EC8-3, in contrast to the EC8-1, requires that whenever the fundamental period of the structure exceeds 2 seconds or $4T_c$, an analysis that explicitly takes into account the contribution of higher modes (multimodal analysis) or a non-linear time-history analysis must be used. However, at the end of this procedure, it is possible to obtain the capacity curve of the structure. At this stage, the seismic demand is determined through the N2 method [9], which transfers the structures into an equivalent SDOF system based on the first mode shape and compares it with the target response spectrum in the ADRS plane.

On the other hand, the time-history analysis turns out to be more complex since it requires an accurate definition of the non-linear hysteretic behaviour of components calibrated against experimental results. In this regard, the EC8-3 requires at least three ground motion records to be considered whose mean response spectrum turns out to be consistent with the target spectrum, *i.e.*, the mean spectrum should not be less than 90% of the target spectrum within the range $[0.2T_1, 2T_1]$, where T_1 is the fundamental period of the structure. In addition, it is worth mentioning that EC8-3 also requires to apply simultaneously two horizontal ground motions when a spatial model is used in the analysis.

In the final stage of the assessment procedure, it is necessary to verify that the required performance levels are guaranteed. This is achieved by comparing appropriate Engineering Demand Parameters (EDPs) obtained from the analysis (demand) against acceptance criteria (capacity) for the desired performance level. The acceptance criteria for seismic performance may vary depending on whether static or dynamic nonlinear analysis is used and how uncertainties associated with the demands and acceptance criteria are handled. For example, the component models, demand parameters, and acceptance criteria used in nonlinear static procedures need to implicitly account for cyclic degradation effects that are not modelled in the static analysis. On the other hand, some dynamic analysis models may directly incorporate degradation due to cyclic loading, in which case different models and acceptance criteria may be used [10].

Acceptance criteria for structural components are generally distinguished between "deformation-controlled" (ductile components that can tolerate inelastic deformations) and "force-controlled" (non-ductile components whose capacities are governed by strength). Consequently, when a KL1 is reached (and hence the structure evaluation is carried out using linear analysis methods), force-based safety checks are conducted because a linear analysis does not allow reliable estimation of capacity and demand displacements. On the other hand, where a KL2 is reached, the use of non-linear analysis allows the displacement demand to be derived. Therefore, with reference to this displacement demand, the safety verifications for the given limit state considered are carried out in terms of displacement (for ductile elements/mechanisms) and forces (for brittle elements/mechanisms).

In steel MRFs, the EDPs related to the main damage patterns and conventionally considered by assessment codes include the chord rotations in beams and columns and shear strain in panel zones. An extensive discussion on the capacity limits for these EDPs can be found in [11] .

2.2 Retrofit strategies

2.2.1 Introduction

The retrofit intervention allows for increasing the safety level of the existing structure (Figure 2-1) and could be classified into two categories:

- *Upgrading interventions*, which increase the safety level of the building, while keeping it below the unit, *i.e.*, without reaching the minimum safety level for new buildings;
- *Retrofitting interventions* allow reaching the safety level of a new building (equal to or higher than 1) required by the current standards.

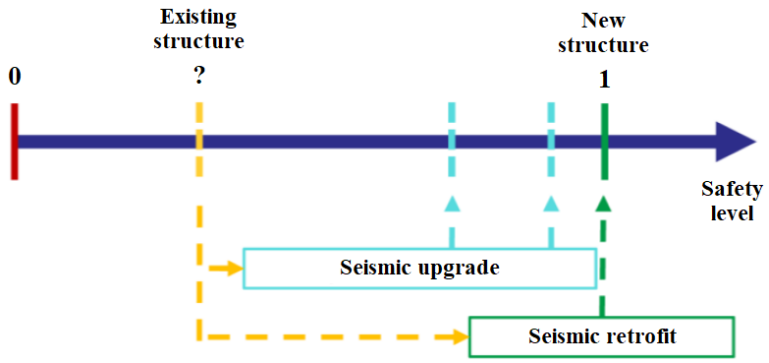

Figure 2-1 *Miglioramento ed adeguamento sismico*

At this point, it is up to the engineer and the owner to decide which type of intervention is suitable. After setting a target, *i.e.*, the safety level desired, several intervention strategies are available to achieve it. A brief outline of the actual retrofit strategies will be provided in the following.

2.2.2 Classification

Classifying seismic interventions is not an easy task because most of them modify the seismic behaviour of the structure in several aspects at the same time. Therefore, there is no single way to carry out this classification. However, it is indispensable to give a clear overview of possible interventions. Thus, in the following, the different types of intervention will be differentiated according to their main effects on the structure.

When the assessment process of an existing structure is completed, a situation similar to the one shown in Figure 2-2 is likely to be obtained. The intersection of the radial line corresponding to the elastic period of the idealized bilinear system (T^*) with the elastic demand spectrum (S_{ae}) defines the acceleration demand (strength) required for elastic behaviour and the corresponding elastic displacement demand (S_{de}). The yield acceleration (S_{ay}) represents both the acceleration demand and the capacity of the inelastic system. The inelastic displacement demand (S_d), as well as the ductility demand (μ), can be obtained by applying the R_μ-μ-T relations [12]. At this stage, the performance point (i.e. the inelastic demand in terms of acceleration and displacement that the structure has to guarantee) corresponds to the intersection point of the capacity curve with the demand spectrum corresponding to the ductility demand (μ) [9]. For existing structures, it is extremely likely that the capacity curve does not reach the performance point (*i.e.*, the displacement capacity D_c is smaller than the displacement demand S_d).

Considering that the response of a structure subject to seismic actions depends on its strength, stiffness and ductility, in order to seismically rehabilitate existing deficient structures, it would be possible to modify these three parameters and/or reduce the input actions. In a more general way, in order to increase the safety level, two different ways can be followed: increasing capacity or reducing demand.

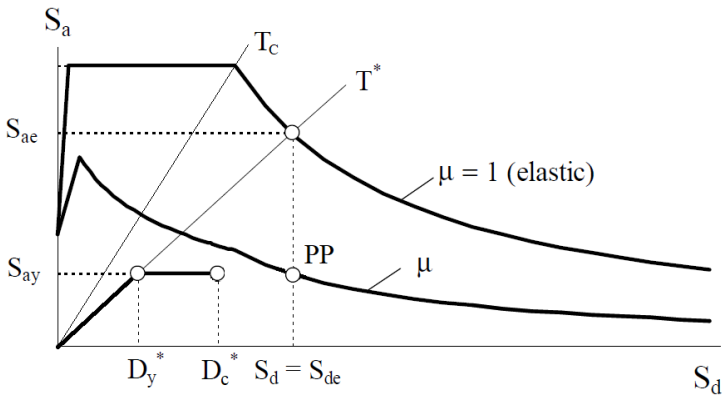

Figure 2-2 *Comparison between capacity curve e demand spectrum in ADRS plane ($T^*>T_C$) (Adapted from Fajfar, 2000[9])*

The increase of the *Seismic Capacity* can be achieved through two different strategies:

- by increasing the strength of the structure (capacity to carry higher spectral accelerations);
- by increasing the ductility of the structure. It is worth mentioning that this strategy also allows the increase of the energy dissipation capacity and hence a reduction of the seismic design forces.

The reduction of the *Seismic Demand* can be achieved through two different strategies:

- by reducing energy input;
- by increasing energy dissipation.

Accordingly, a classification of interventions can be carried out, distinguishing between interventions aimed at *increasing capacity* and interventions aimed at *reducing demand*.

For steel structures, some typical capacity-increasing interventions include the introduction of welded or bolted plates in order to increase the frame elements' cross-sectional area and/or node stiffness, the introduction of bracing systems, and the implementation of exoskeletons. On the other hand, demand-reducing measures include mass reduction, base isolation, and the introduction of dissipative devices.

However, it is worth mentioning that usually, interventions achieve the result through a combination of these effects. As an example, the ductility of a structure can be increased by increasing the ductility of its elements; however, such operations generally also increase its strength and/or stiffness.

Within this thesis, the feasibility of a retrofit strategy involving BRBs placed outside the frame plane is investigated. The use of a steel bracing system, *i.e.*, capacity-increasing systems, within the existing structure, allows to enhance its strength, stiffness, and sometimes modify its seismic response. On the other hand, the introduction of dissipative elements, *i.e.*, demand-reducing systems, into the bracing system allows for improving its dissipative capacity. Moreover, arranging these systems outside the frame plane minimises the invasiveness of the intervention and avoids business interruption. Therefore, the investigated solution is characterised by multiple advantages.

2.2.3 Bracing systems

Bracing systems are, among the possible retrofit solutions, a simple and effective retrofit system, especially when it is necessary to limit storey drifts. This is because they allow the structure to resist horizontal forces through complete truss action. The aim of bracing structures is to design systems that are both strong enough to withstand seismic forces and sufficiently light to preserve existing structural elements from requiring further reinforcement [13].

The usual way to seismically protect both new and existing framed structures is by using concentrically braced steel members arranged in a network of frames (Concentrically Braced Frame - CBF), according to single bracing, cross bracing, chevron bracing, and any other concentric bracing scheme. Although these systems provide high lateral stiffness and strength under moderate earthquakes, the low dissipation capacity of the whole system due to brace buckling under strong earthquakes must be considered. (Figure 2-3a).

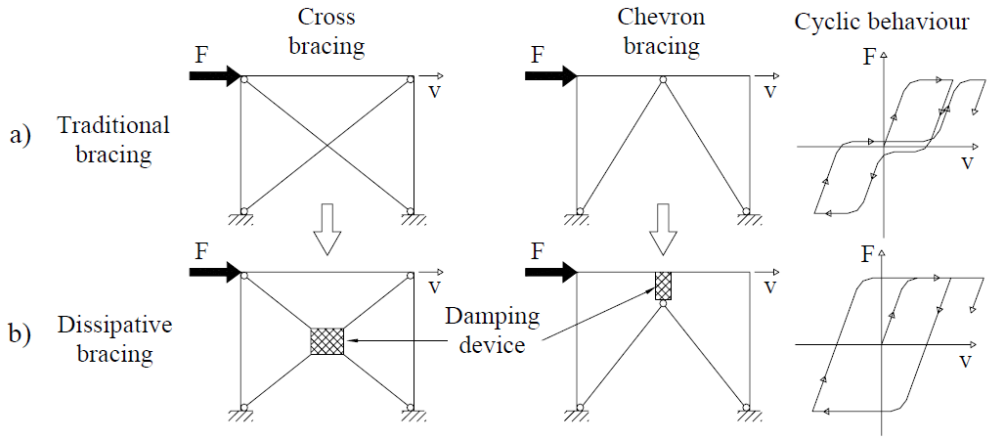

Figure 2-3 *Traditional and dissipative bracing system (from D'Aniello et al. [13])*

In seismic retrofitting, besides strengthening the existing frame, the overall seismic performance of the structure must be improved, including dissipative capacity. Therefore, the aforementioned drawback must be avoided by preventing buckling and premature failure of braces. This can be achieved by placing in the conventional bracing system some special devices that dissipate the input seismic energy before severe damage to the primary structure occurs. In Figure 2-3b, some solutions to modify an ordinary bracing system into a dissipative bracing system are shown in a schematic manner. One of several advantages of such systems is that these devices are designed to be replaceable after possible earthquake damage.

Another way to improve the cyclic performance of traditional cross-bracing systems is based on the use of special types of bracing members, which are notoriously called Buckling-Restrained Braces (BRBs) [14] or also Unbonded Brace (UB) [15]. Figure 2-4 shows examples of BRB frame configurations [16].

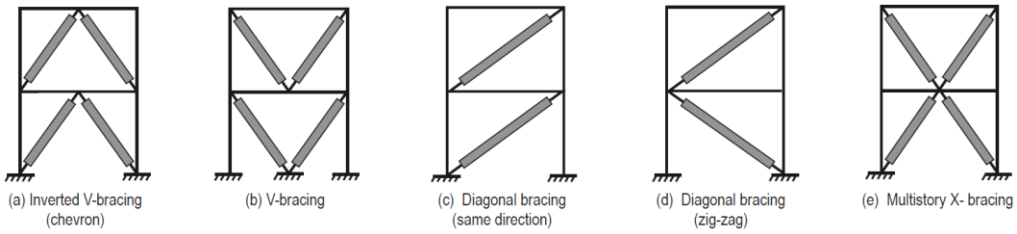

Figure 2-4 *Examples of BRB configurations. (from Kersting et al.[16])*

2.2.4 Buckling Restrained Braced Frames

2.2.4.1 General characteristics of dissipative structural solutions

Dissipative structural solutions were first introduced into earthquake engineering as an alternative to the traditional linear elastic design in the second half of the 20th century.

These systems aim at dissipating most of the kinetic energy transmitted by an earthquake by exploiting the material's non-linear behaviour (especially if it is made of metal such as steel) or by using damping devices. Energy dissipation leads to a mitigation of seismic effects and eventually to more economical structural solutions.

Concerning structures that dissipate energy by taking advantage of the material, inelastic behaviour is concentrated in the so-called dissipative zones to provide the designer control over the expected global mechanism and avoid premature failure. Beams end in MRFs, and diagonal braces in CBFs are an example of these dissipative zones. To provide adequate resistance after yielding, the dissipative member is required to have sufficient inelastic capacity in terms of both force and displacement.

As a consequence of yielding, the stiffness of the dissipative element decreases considerably. This may result in a reduction of the overall building stiffness with a consequent variation of its dynamic properties (period elongation). In particular, an elongation of the structure's vibration period corresponds to a reduction in spectral acceleration and an increase in spectral displacement. Therefore, a dissipative system must have a large deformation capacity at both local (element) and global (structural) levels. According to current earthquake engineering standards, the advantageous ductile behaviour of dissipative frames can be taken into account through the behaviour factor, which allows reducing the demand spectrum by taking into account the dissipative capacity of the structure.

2.2.4.2 Buckling restrained brace

Buckling Restrained Brace (BRB) represents a relatively innovative component for braced frames that typically concentrate dissipative zones in their diagonal braces, *i.e.*, Buckling Restrained Braced Frames (BRB frame). The main advantage of BRBs over a conventional steel brace is their balanced hysteretic cycle.

Due to their typically high slenderness, conventional steel braces buckle before reaching their yield point under compression. They are therefore characterised by cyclical degradation and a limited energy dissipation capacity. On the other hand, BRB buckling is prevented by its special configuration, and, as a result, it does not exhibit any degradation of stiffness and strength [17–19]. Such different behaviour under cyclic axial load is shown in Figure 2-5 [20].

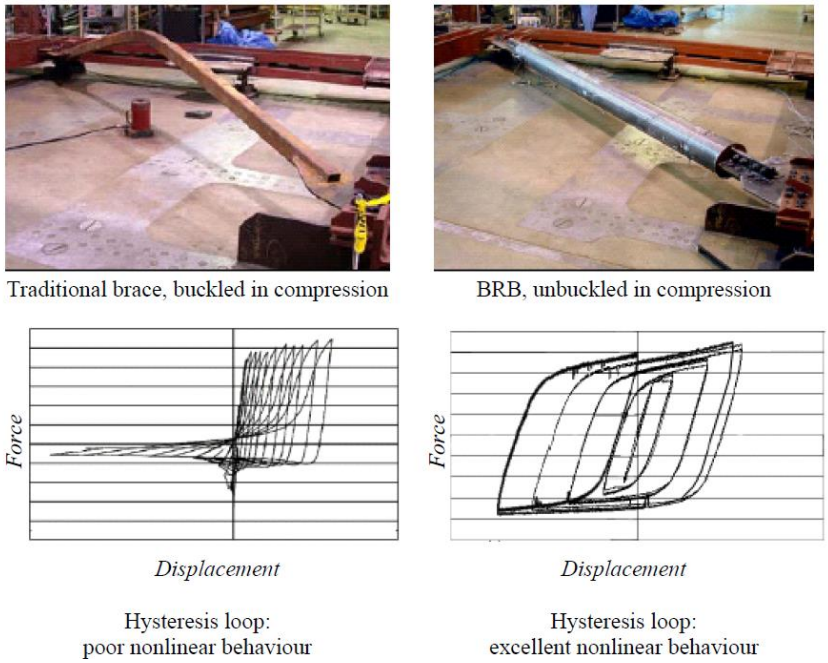

Figure 2-5 *Traditional brace vs buckling restrained brace (from Ballio et al.[20])*

The same advantage is also achieved when BRB bracing is included in the complete structural scheme (Figure 2-6) [20].

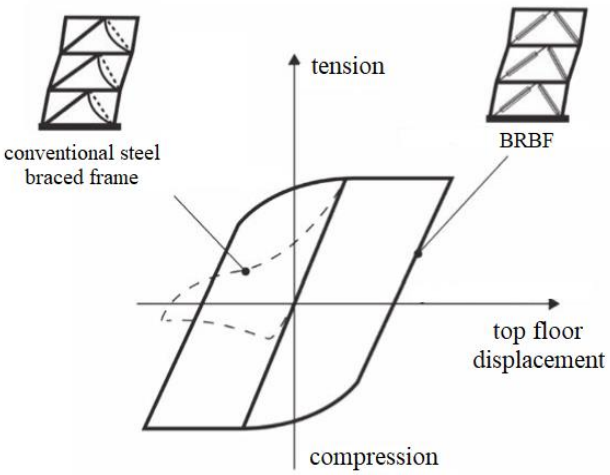

Figure 2-6 *Advantages of BRB bracing on structural cyclic behaviour (from Ballio et al[20]).*

It is worth mentioning that, usually, the BRB cyclic behaviour turns out to be asymmetrically characterized by an ultimate compressive force of 10-15% higher than the ultimate tensile force. This is related to friction between core and sleeve as well as nonlinear geometric effects in compression given by limited buckling made possible by the clearance left between the core and the sleeve [21].

A typical BRB configuration is illustrated in Figure 2-7. The main component of this dissipative device is its ductile steel core, which is designed to yield both in

tension and compression. In order to avoid buckling in compression, the steel core is placed inside a steel tube filled with mortar. In addition, to prevent the contribution of the casing to the axial load resistance, the core and the casing are decoupled by a gap (filled with unbonding material or left empty). It is worth mentioning that the gap must be designed to accommodate the expansion of the steel core due to the Poisson effect in compression.

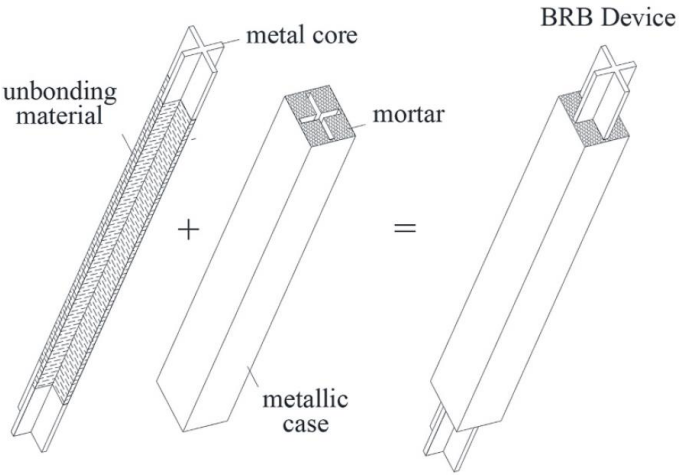

Figure 2-7 *Concept type of buckling-restrained brace (from Freddi et al.[22])*

Figure 2-8 shows the main components of a BRB. The following portions can be identified [23]:

- *Restrained yielding segment*: this steel segment can be rectangular or cruciform in cross-section. Given that this segment is designed to yield under cyclic loading, mild steel that exhibits high ductility is generally preferred. In addition to this, to ensure a reliable capacity design of the frame equipped with BRBs, steel materials with a predictable yield strength with small variations must be favoured;
- *Restrained non-yielding segment*: this segment, surrounded by the casing and the mortar, is generally an extension of the restrained yielding element but with an enlarged reinforced area to ensure a fully elastic behaviour;
- *Unrestrained non-yielding segment*: this segment is the projection of the steel core from the casing and mortar, which ensures the connection (generally pinned) with the frame;
- *De-bonding agent and expansion material*: an inert material (rubber, polyethylene, mastic tape or silicon grease) is required to reduce the transfer of shear forces between the restrained yielding segment and the mortar. The air gap must be large enough to allow for the expansion of the steel core in compression but not that much large to increase the buckling amplitude of the steel core;
- *Buckling-restrained mechanism*: the system is made of mortar, and the external casing prevents the buckling of the inner steel core [24].

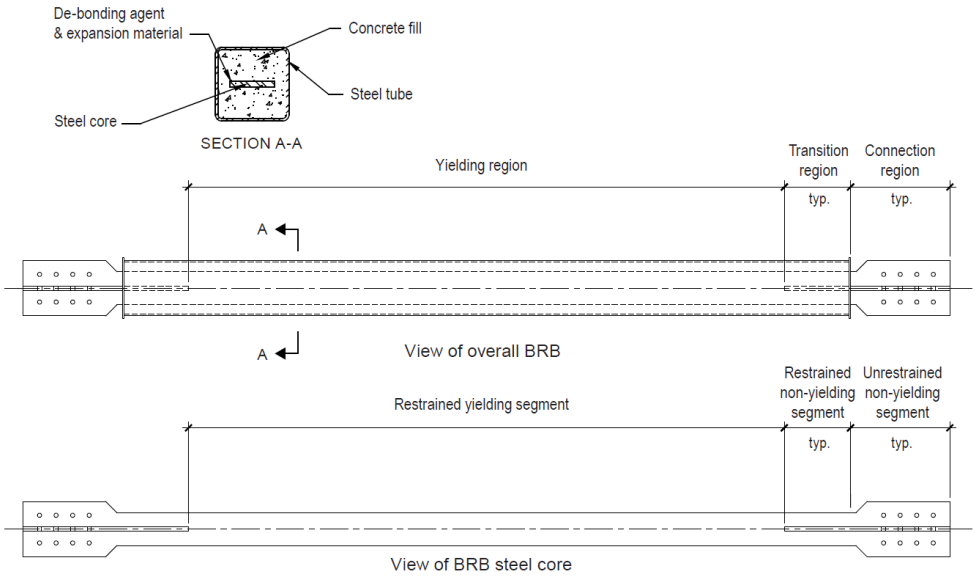

Figure 2-8 *Common BRB assembly (from Kersting et al.[16])*

The use of BRBs has gained popularity worldwide, especially in Japan, USA, Chile and New Zealand [25] in the last two decades for both new constructions and rehabilitation of existing buildings, given that:

- Frames incorporating BRBs can rely on a higher elastic lateral stiffness at low levels of seismic input compared to steel MRFs, making it extremely easier to meet code drift requirements [26];
- The low hardening of the post-elastic branch in BRBs' constitutive law maximises their energy dissipation. This effect, combined with the prevention of buckling in compression, ensures a large and stable dissipation for frames with BRBs even at high levels of seismic input [27];
- BRBs act as a replaceable structural fuse, minimising damage to other elements (assumed that capacity design provisions keep the latter in the elastic regime). Therefore, the reparability of damaged BRBs significantly increases the resilience of the global system.

However, regardless of the several advantages previously mentioned, a limitation in the application of BRBs has been generally observed in Europe. This mainly accounts for the lack of specific Eurocodes provisions addressing the design of frames incorporating BRBs. Codification of Eurocode conforming design of BRB frames has been recently proposed in some research works [28], but European practising engineers can currently rely on American AISC 341-16 [29] and ASCE 7-10 [30] standards and on some technical guidelines, as the NEHRP Report 11 [16], only.

2.2.4.3 Connections

Usually, steel braces are introduced within steel structures through gusset plates. The design and details of the gusset plate connections are one of the most delicate aspects of BRB frame systems. Although the excellent ductility capacity of isolated BRBs has been clearly established, the ability of BRBs to develop their full ductility when installed in frames is greatly affected by the adopted connection type. Several large-scale test of BRB frames characterised by bolted connections, stiff beam-column-brace connections and long brace-gusset plate connection regions [31] [32] [33] [34] [35] [36], demonstrated the development of failure modes that prevented the ductility capacity of BRB from being fully utilised. The above types of BRB frames exhibited reasonable performance for story drifts up to 0.02 rad, while gusset plate distortion and brace instability have been observed for story drifts between 0.02 and 0.025 rad. An example of these connection types is represented in Figure 2-9a.

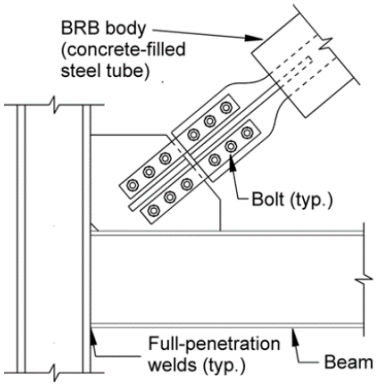

Figure 2-9 *BRB frames connection details: continuous beam, bolted brace (from Aiken et al.[31])*

As a result of these studies, special attention was given to the beam-column-brace connections. Among others, Fahnestock et al. [37] tested a connection detailed to allow rotation while limiting flexural demands on the connection regions (Figure 2-10a). The 'true' pinned brace-gusset connection allows limiting the moments on the BRB caused by the beam-column connection region, while the bolted beam splice limits the moment developed in the beam and column at the beam-column connection region. In order to isolate the contribution of the pinned connection, another type of connection was tested in which full-penetration groove welds were used to join the beam to the beam stubs, simulating a continuous beam (Figure 2-10b). Both connection types have shown excellent performance, exhibiting only a lower yield for story drift of about 0.048rad, thus demonstrating that short and stocky connection regions and pinned BRB connections with end collars prevented the undesirable failure modes observed in previous BRB frame test.

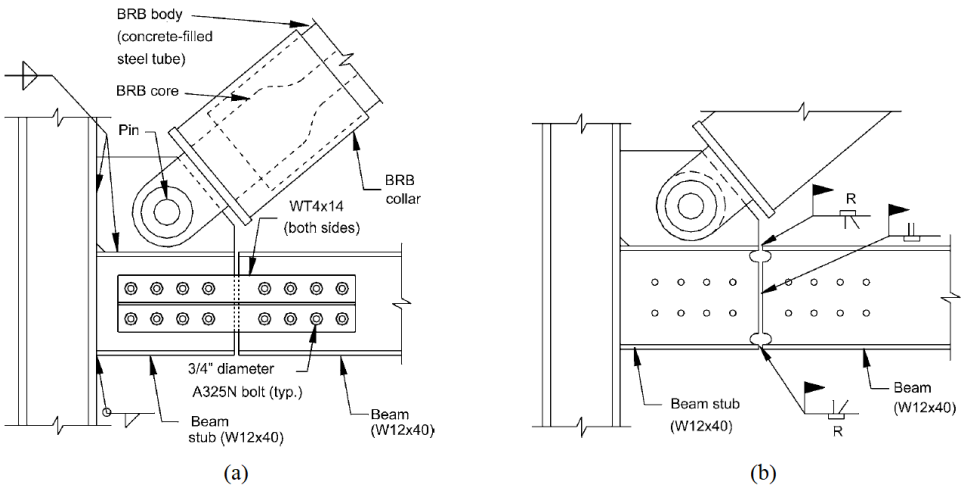

Figure 2-10 *BRB frame connection details: (a) bolted spliced beam, pinned brace; (b) welded spliced beam, pinned brace. (from Fahnestock et al.[37])*

Guidance on the design of gusset plates in BRB frames can be found in AISC standards [29]. However, it is worth mentioning that BRB frame gusset plates are not intended to develop a hinge zone the way CBF (concentrically braced frames) gusset plates are detailed to develop. In CBFs, gusset plate hinging is part of the brace buckling mechanism, but in BRB frames, the design objective is to limit the inelastic deformation to the BRB cores [16] . Thus, in BRB frames, bracing connections must not yield at force levels corresponding to the yielding of the steel core; they are therefore designed for 1.1 times the adjusted brace strength in compression [29].

2.2.5 Alternative external solutions

The above-mentioned damping system is traditionally installed within a newly designed, as well as existing buildings, in either diagonal or chevron brace configurations connecting adjacent storeys (Figure 2-4). Although multiple studies demonstrated the effectiveness of retrofitting existing structures with BRBs (*e.g.*, [38]), as well as other damping systems, the use of these dissipative devices is often precluded by the long business interruption associated with their installation and related high indirect losses. In fact, the installation of these devices in the exterior frames of multi-storey buildings necessarily entails the removal of the infills and the consequent use interruption of the construction. To overcome this issue, several innovative configurations have been investigated in the last few years, *e.g.*, devices utilized within an "exo-skeleton" or connecting the structure to "external dissipative bracings" [22].

"Exoskeletons" represent a global retrofit intervention type consisting of adding an additional structural system linked sideways to the existing building and optionally provided with an independent foundation system [39]. The aim of this intervention is to link the existing structure (primary structural system), designed for gravity

loads only, to a different structure (secondary system) capable of dissipating the seismic input energy. When properly designed, this system allows the primary structure to remain in the elastic range under an earthquake, while the secondary structure goes into the plastic range. Thus, the global response of the structural system can be assumed as the sum of the structural responses of the individual systems (Figure 2-11). When exoskeletons are equipped with dissipative devices, the latter are introduced within the diagonals along with the outer frames of the structure.

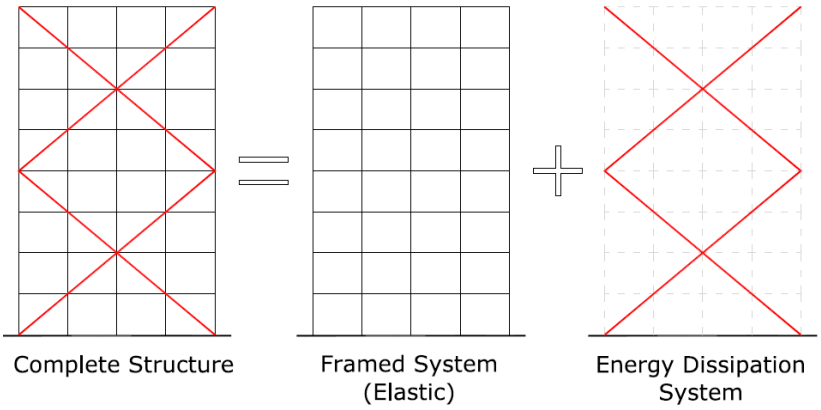

Figure 2-11 *Typical framed structures with dissipative diagonal braces placed externally (exo-skeleton). (from Di Sarno et al.[38])*

"External dissipative bracings", as well as exoskeletons, are structural systems connected to the structure but always provided with their own foundations. This type of intervention provides a very flexible family of solutions that can be grouped into three main categories characterized by different kinematic behaviour (Figure 2-12).

In the first arrangement (Figure 2-12a), the dampers are placed horizontally at floor level, and the links are activated by the relative displacements between the frame and the external structure. An alternative arrangement consists of coupling the frame with an external shear deformable bracing structure (Figure 2-12b). The new and existing structures are connected at the storey level, and the dissipative devices, incorporated in the diagonal braces of the new structure, are activated by the relative displacements between adjacent floors, as in the more traditional case of dissipative braces placed within the existing structure. A third arrangement, denoted as 'dissipative tower', consists of external stiff bracings linked to the frame at the storey level and connected to the foundations by a hinge (Figure 2-12c). The energy dissipation is provided by dampers placed at the external frame base and activated by rocking motion.

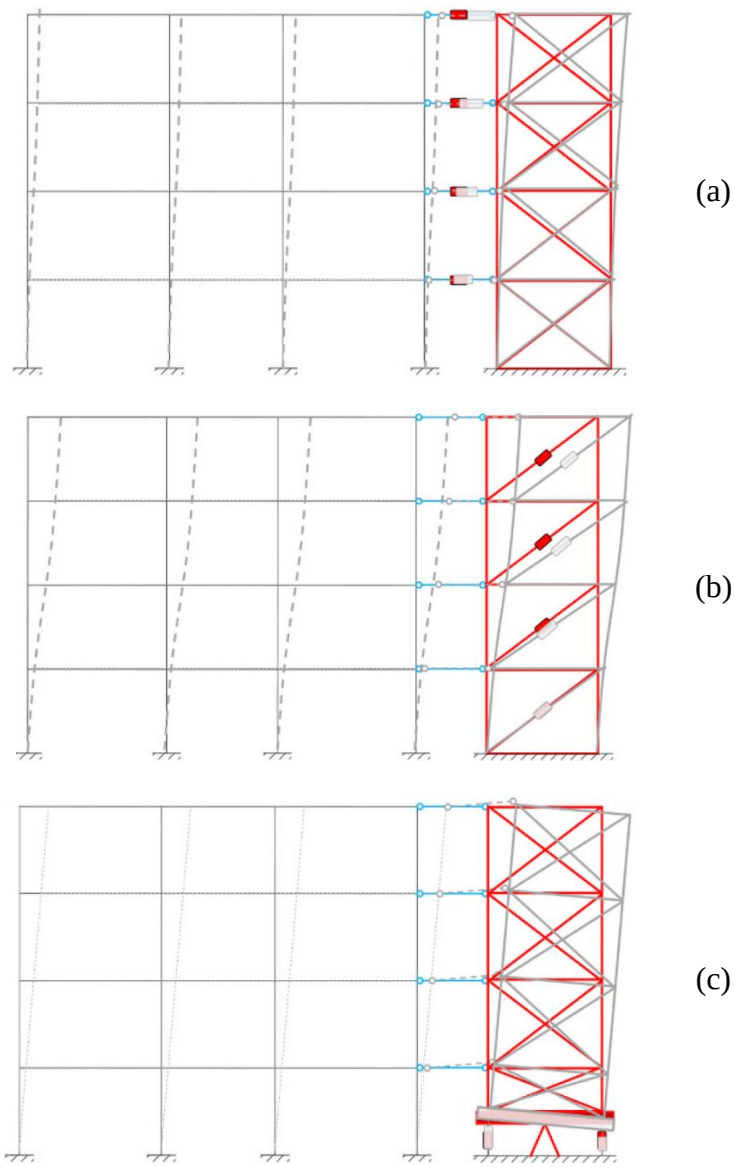

Figure 2-12 *Illustration of three categories of external dissipative systems: (a) dampers placed horizontally at the storey level between the frame and an external stiff contrasting structure; (b) dampers incorporated within a new shear deformable structure; (c) pinned rocking bracing with dampers located at the base (from Gioiella et al.[40]).*

Concerning retrofit interventions with exoskeletons and external dissipative bracings, several critical aspects may compromise the effectiveness of the intervention and thus require further investigation. Among others, it is worth mentioning the importance of the connection between the two resistant systems.

Within this research work, the feasibility of a retrofit intervention by means of the BRBs incorporation into the diagonals of an exoskeleton is investigated, paying particular attention to the effects caused by the connection type used.

3 Case study and Experimental Test

The present research study is based on the experimental work that was carried out within the *HybrId Testing of an Existing Steel FRAme with Infills under Multiple EarthquakeS* (HITFRAMES) research project funded by the European Union as part of the *Seismology and Earthquake Engineering Research Infrastructure Alliance for Europe* (SERA) project.

3.1 Sera Project

The Seismology and Earthquake Engineering Research Infrastructure Alliance for Europe (SERA) aims to reduce the risk posed by natural and anthropogenic earthquakes based on innovative research and development projects. Specifically, the SERA project:

- collaborated with researchers involved in previous seismology and earthquake engineering projects like EPOS, NERA, SHARE, SERIES, NERIES, and SYNER-G;
- facilitated access to ten high-class experimental facilities such as shaking tables and reaction walls;
- offered access to data and products in seismology and anthropogenic seismicity in Europe;
- promoted multi-disciplinary science across the domains of seismology, anthropogenic seismicity, near-fault observatories, and deep underground laboratories to achieve an improved understanding of earthquake occurrence;
- facilitated collaboration and innovations in the fields of deep seismic sounding, experimental earthquake engineering, and site characterization. This objective is pursued by expanding the access to seismological observations and infrastructures as well as by strengthening exchange within the expert community.

SERA was a Horizon 2020-supported programme and involved in the Transnational Access (TA) framework 44 user groups composed of 261 EU and extra-EU talented researchers.

3.1.1 HITFRAMES Project

The HITFRAMES research project is one of the proposals chosen to be part of the SERA project. (L. di Sarno[1], R. Landolfo[2], M. D'Aniello[2], F. Freddi[3], M. Dolsek[4], O-S. Kwon[5], S. Bousias[6], J. Wu[1], F. Gutierrez-Urzua[3], E. Strepelias[6], X.Palios[6], N. Stathas[6]).

Given that current provisions in Europe for the seismic performance assessment of existing steel structures are scarce and do not take into account the presence of masonry infill, it appeared necessary to provide effective methods for the seismic assessment and retrofit of existing non-compliant steel structures. To this end, the HITFRAMES project aimed at four major objectives:

- To develop reliable methods for the seismic assessment of existing steel frames, especially under earthquake sequences;
- To develop design procedures for buckling restrained braces (BRBs) considering the contribution of masonry infills to the lateral load resisting system;
- To evaluate the effectiveness of BRBs as a seismic retrofitting measure;
- To derive fragility curves for existing steel frames with infills and systems retrofitted with BRBs and infills, also considering the effects of earthquake sequences.

In order to pursue these objectives, a two-storey steel MRF designed primarily for gravity loads with insufficient seismic detailing was assessed through pseudo-dynamic (PsD) tests at the Structures Laboratory (STRULAB) of the University of Patras, Greece, which is one of the few European laboratories employing the PsD testing method with sub-structuring hybrid simulations.

Based on the characteristics observed in the existing steel frames in Amatrice [41] [42], the selected case study building was considered representative of non-seismically designed steel frames. Within the HITFRAMS project, two case study building configurations were considered, the prototype and the tested mockup. The prototype building is comprised of two storey, three bays and one bay in the longitudinal and transverse directions, respectively. On the other hand, the tested building was a two-storey one-bay substructure obtained scaling the prototype building. Three configurations of the test specimen were involved in this project, namely bare frame, infilled frame and retrofitted frame. The bare frame and infilled frame were tested as 3D frames, while the retrofitted frame, which comprised of the bare frame and the retrofitted frame with BRBs, was tested as a 2D frame. The

[1] University of Liverpool, UK
[2] University of Naples, Federico II, Italy
[3] University College London, UK
[4] University of Ljubljana, Slovenia
[5] University of Toronto, Canada
[6] Structures Laboratory, University of Patras, Greece

present study is based on the experimental results obtained by testing the retrofitted frame. Therefore, only this test will be described in the following.

3.2 Experimental Test

3.2.1 Test prototype building

The prototype building, identified as a representative of a non-seismically designed, low-ductility, low-rise steel building, is a two-storey, three-bays by one-bay MRF steel frame. In accordance with Eurocode 3 (EC3), the building was designed for gravity loads only and without sufficient seismic details. Given that the EC3 does not prescribe accounting for wind loads in low-rise steel structures design, the case study steel frame completely lacks a lateral loading resisting system. The gravity design was conducted considering a non-structural permanent load, *i.e.*, walls and other finishing, including internal partitions, equal to 2.58 kN/m^{2,} while the considered use category was "offices area" and hence the characteristic value of the imposed load was assumed equal to 3 kN/m^2.

The storey height of the prototype building is 3.4 m, with slight variations between the two stories. The bay is 8.65 m and 4.65 m in the longitudinal and transverse directions, respectively. Figure 3-1 shows an overview of the structural system both in plan and in elevation, including the main geometric parameters and section members. The steel profiles are HE 220 A, IPE 240 and IPE 160, respectively, for columns, primary and secondary beams. The steel grade is S355 (f_y = 355 MPa) for all beams and columns. All external beams are connected to columns through full penetration welds. It is worth mentioning that fully rigid beam-column connections are considered in this study. The floor system was designed as a composite slab with a cold-rolled steel sheet base (t = 1.25 mm) and a 200-mm-deep concrete slab with M19 shear studs at each valley or 300 mm, depending on the steel sheet rib orientation. Concerning masonry infills, it consists of two parallel layers of perforated bricks separated by insulation materials, each of which has a thickness of 58 mm. According to the final design and considering the EC8–1 [2] seismic combination, the building's storey mass is equal to 117.0 and 95.0 tons, respectively, for the first and second storey.

In order to investigate the performance of the structure in its weaker and more deformable direction, the steel frame was tested under a horizontal load in the x-direction, as indicated in Figure 3-1, where the columns are oriented with their weak axis.

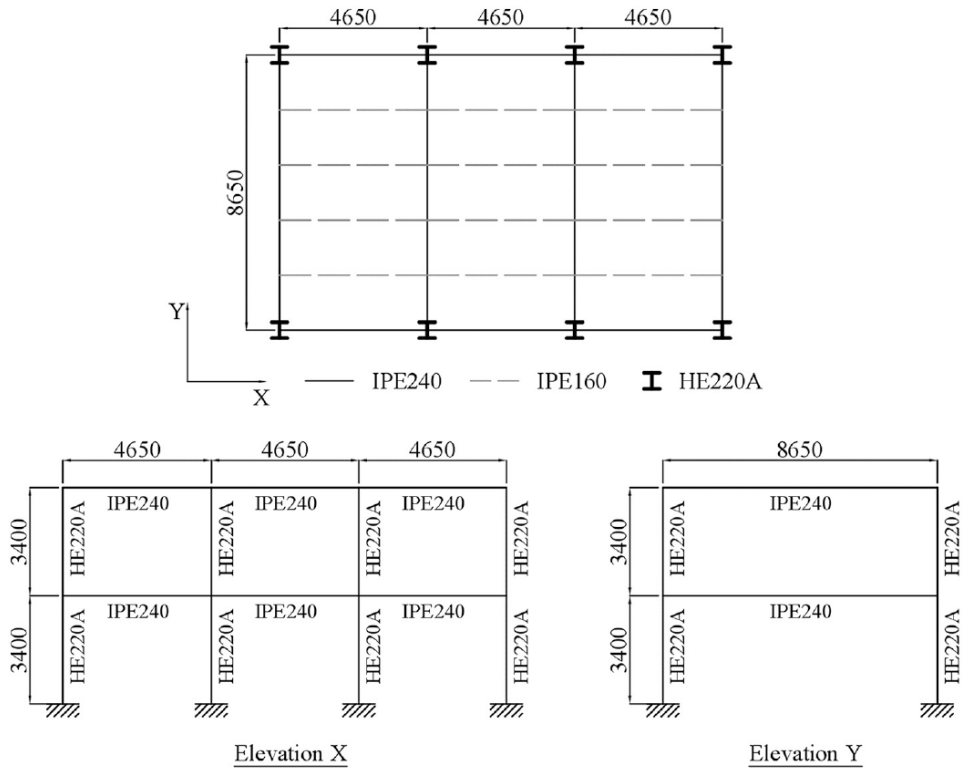

Figure 3-1 *Global geometry of the prototype building: plan view and elevations (unit: mm) (from Di Sarno et al. [1])*

3.2.2 The test specimen

The tested structures were designed and built based on the typical construction techniques of European construction companies. Therefore, the steel frames were welded and prepared in the manufacturer's workshop, brought to the site and assembled directly in the lab.

3.2.2.1 Bare frame

The test specimen represents a single span of the prototype building's outer frame scaled by 75% (*i.e.*, scaling factor $\lambda = 0.75$). The modelling scaling is based on the material and acceleration scaling identity [43]. The scale factor adopted was selected on the basis of laboratory constraints and considering that typically a scale factor greater than 0.6 appears to be adequate to allow the test to correctly reproduce the seismic response of steel frames. Regarding material stress, a unite scale factor was adopted; this represents a common and convenient choice as it allows overcoming the difficulties in replicating the mechanical properties of the prototype building (*e.g.*, Poisson ratio, stress-strain relationships, etc.). The list of the scaling factors for the similitude between the prototype building and test frame is shown in Table 3-1.

Table 3-1 *Similitude scaling factors with $\lambda = 0.75$*

Parameter	Scaling factor
Density	$\lambda^{-1} = 1.33$
Stress, strain, angular deformation and acceleration	$\lambda^{0} = 1$
Period, time and velocity	$\lambda^{1/2} = 0.87$
Length, linear deformation and stiffness	$\lambda^{1} = 0.75$
Force, weight, mass and area	$\lambda^{2} = 0.56$
Volume, section moduli and moment	$\lambda^{3} = 0.42$
Moment of inertia	$\lambda^{4} = 0.32$

The correlation between the prototype building and the test specimen is shown in Figure 3-2. The test mockup has a storey height of 2.5 m and a span of 3.5 m. Geometric properties of the case study frame before and after scaling are summarised in Table 3-2. Profiles HE 180A and IPE 200 were used for columns and primary beams, respectively. The test specimen, together with the shear wall and the actuator, is shown in Figure 3-3. The external beams were connected to columns through full penetration welds, and stiffeners were used to increase the connection rigidity, as shown in Figure 3-4a.

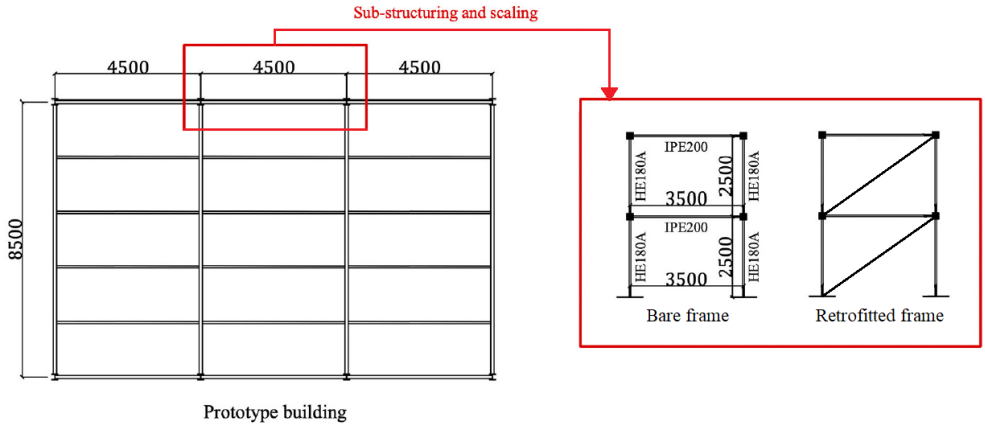

Figure 3-2 *Plan and side views of the test specimens (unit: mm) (Adapted from Di Sarno et al.[1])*

Table 3-2 *Geometric properties of the case study frame before and after scaling.*

	Unite	Prototype building	Lab specimen
Storey height	[m]	3.4	2.5
Span	[m]	4.65	3.5
Column	[-]	HE 220A	HE180A
Main beam	[-]	IPE 240	IPE 200

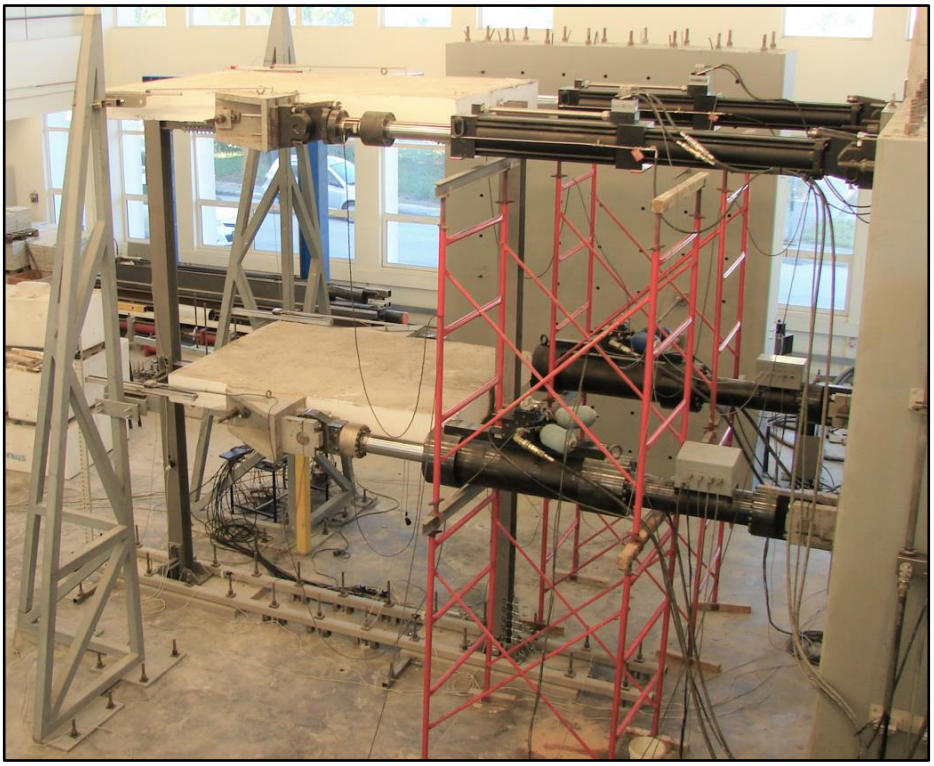

(a)

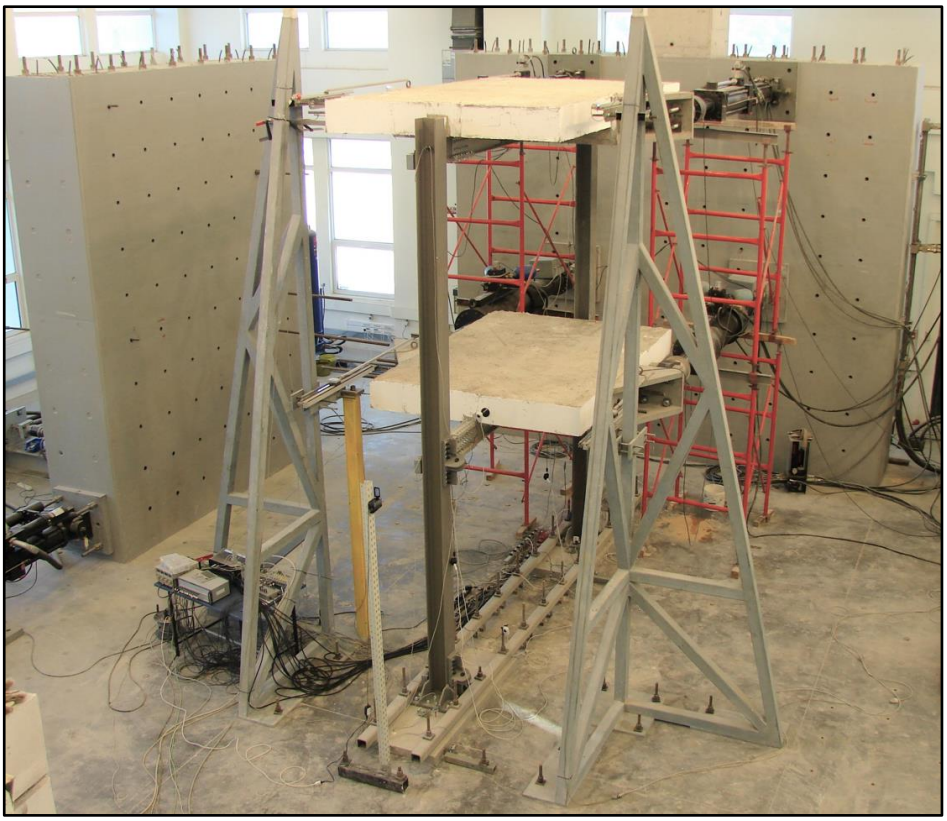

(b)

Figure 3-3 *Test Specimen: (a) frontal view; (b) lateral view*

Figure 3-4 *Position of stiffeners at the beam-column connection*

3.2.2.2 Retrofitted frame

The retrofitted frame represents the second test specimen assessed within this project. The bare frame previously described was retrofitted through BRBs. The retrofit design was done in accordance with a simplified code-based design approach. To this aim, the structure was considered to be located in Central Italy, and therefore the retrofit design was carried out following the recommendations of the Eurocode 8-Part 1 (EC8-1) [2] and Eurocode 3 Part 1-1 (EC3-1-1) [44]. The design is performed for the Ultimate Limit State (*i.e.*, probability of exceedance of 10% in 50 years), considering a Type 1 spectrum, with soil Type B, and Peak Ground Acceleration (PGA) equal to 0.25g. The structure is designed by considering a basic behaviour factor $q_0 = 3$. Compared with commercial catalogues, the design requests led to the choice of a BRB device whose characteristics are shown in Figure 3-5 and Table 3-3.

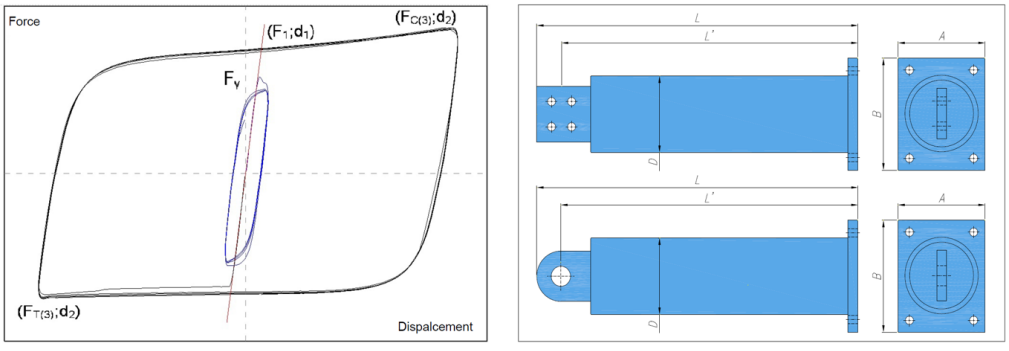

Figure 3-5 *BRB device properties: (a) cyclic behaviour; (b) geometric characteristics*

***Table 3-3** BRB device properties*

Device [-]	**F_1** [kN]	**K_e** [kN/mm]	**d_1** [mm]	**F_2** [kN]	**d_2** [mm]	**$F_{C(3)}$** [kN]	**$F_{C(max)}$** [kN]	**F_y** [kN]
BRAD	178	88	2.02	194	20	210	235	143

***Table 3-4** BRB device properties*

Device [-]	**L_{BRAD}** [mm]	**L'_{BRAD}** [mm]	**Φ_{BRAD}** [mm]	**A** [mm]	**B** [mm]	**P_{BRAD}** [kg]
BRAD	1585	1535	168	190	230	132

Where:

- F_1: yield strength (T/C) at 3rd cycle at displacement d_2;
- K_e: elastic branch stiffness;
- d_1: yield displacement;
- F_2: average maximum force (T/C) at displacement d_2;
- d_2: maximum design displacement;
- $F_{C\,(3)}$: compressive force at 3rd cycle at displacement d_2;
- $F_{C\,(max)}$: maximum compressive force at displacement d_2;
- F_y: first yield strength;
- L_{BRAD}: device length BRAD;
- L'_{BRAD}: device length BRAD to bolt centre of gravity;
- Φ_{BRAD}: retaining pipe diameter;
- A: smaller side of anchor flange;
- B: larger side of anchor flange;
- P_{BRAD}: device weight;

It is worth mentioning that the yield strength at 3rd cycle (F_1) is calculated as the average value between tension force (T) and compression force (C) corresponding to the maximum design displacement d_2. As introduced in 2.2.4.2, there is a difference between the tensile and compressive force values due to the buckling constraint, which results in an "apparent" hardening. In this case, the ultimate tensile force appears to be about 30% greater than the ultimate compressive force.

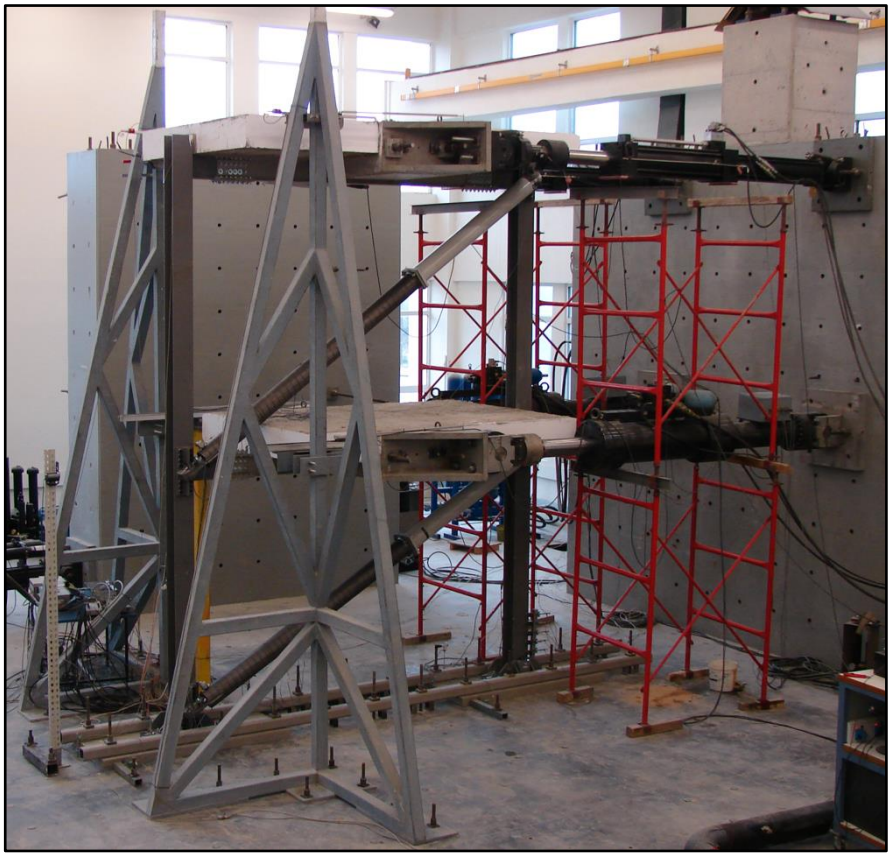

(a)

(b)

Figure 3-6 *Test Specimen: (a) frontal view; (b) lateral view*

The BRB device is connected in series to a steel tubular section (Φ_{est} = 150 mm, t = 10 mm). In order to reduce the invasiveness of the intervention, the BRB device and the connected elastic brace were placed outside the frame plane. To this aim, a special connection was designed (Figure 3-7). The connection type includes a pin to release the moments acting outside the frame plane.

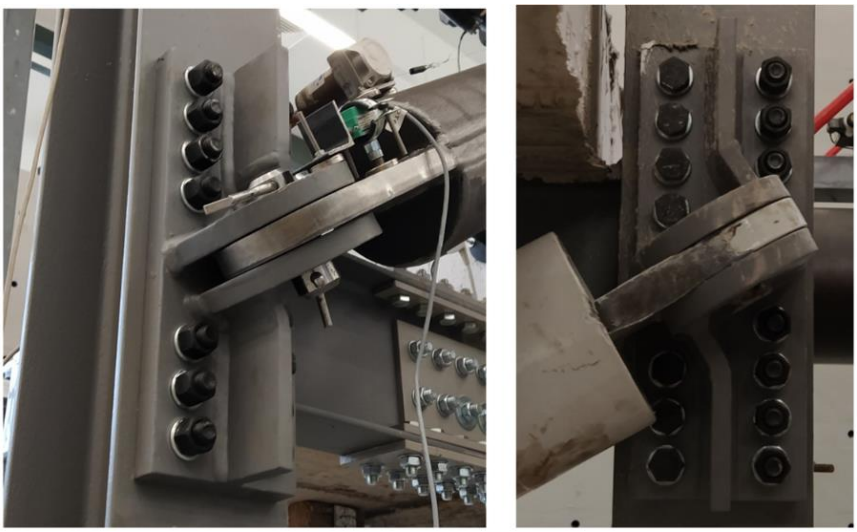

Figure 3-7 *BRB to column connection*

3.2.3 Material properties

Several coupon tests were conducted to inform the numerical modelling of the tested steel frame. To this aim, the steel coupons were obtained directly from the tested frame, both from web and flanges of beams and columns, and were tested according to the BS EN ISO 6892-1 [45]. The results of the coupon tests are summarised in Table 3-5, Table 3-6 and Table 3-7.

Table 3-5 *Yield and ultimate stress (μ: mean value; σ: standard deviation; CoV: coefficient of variation)*

Profile		Quantity	Yield stress			Ultimate stress		
			μ (MPa)	σ (MPa)	CoV (%)	μ (MPa)	σ (MPa)	CoV (%)
Beam (IPE200)	Flange	8	408.94	17.22	4.21	561.92	17.70	3.15
	Web	4	426.38	11.43	2.68	558.47	9.61	1.72
Column (HE180A)	Flange	8	424.06	8.99	2.12	592.21	9.27	1.57
	Web	4	450.32	12.53	2.78	583.42	7.94	1.36

Table 3-6 *Yield and ultimate strain (μ: mean value; σ: standard deviation; CoV: coefficient of variation)*

Profile		Quantity	Strain at yielding			Strain at ultimate stress		
			μ (-)	σ (-)	CoV (%)	μ (-)	σ (-)	CoV (%)
Beam	Flange	8	0.0023	0.0005	21.74	0.1370	0.0038	2.77
(IPE200)	Web	4	0.0020	0.0002	10.00	0.1306	0.0067	5.13
Column	Flange	8	0.0031	0.0007	22.58	0.1355	0.0076	5.61
(HE180A)	Web	4	0.0026	0.0003	11.54	0.1419	0.0067	4.72

Table 3-7 *Overstrenght and ductility (μ: mean value; σ: standard deviation; CoV: coefficient of variation)*

Profile		Quantity	Overstrenght			Ductility at ultimate stress		
			μ (-)	σ (-)	CoV (%)	μ (-)	σ (-)	CoV (%)
Beam	Flange	8	1.13	0.02	1.77	61.77	15.61	25.27
(IPE200)	Web	4	1.31	0.02	1.53	64.59	4.50	6.97
Column	Flange	8	1.40	0.02	1.43	45.73	11.89	26.00
(HE180A)	Web	4	1.30	0.03	2.31	54.79	7.93	14.14

3.2.4 Pseudo-dynamic (PsD) tests

3.2.4.1 Introduction

The inelastic cyclic behaviour of structures is generally quite sensitive to the imposed histories of displacement. Thus, the selection of loading techniques and histories is a key part of the planning for any seismic performance test [46]. Despite their limited availability, shaking tables represent the most efficient way to simulate seismic effects in the laboratory. On the other hand, pseudo-dynamic tests represent alternative methods that allow seismic effects to be reproduced by combining quasi-static experimental techniques with numerical simulation procedures. This testing procedure requires 'conventional' laboratory facilities (*e.g.*, actuators and reaction walls), and hence it is often preferred to the more complex and expensive shake table tests.

The pseudo-dynamic method represents an integrated experimental-numerical procedure. Similar to non-linear dynamic analyses, the controlling computer software discretises the response of the structure in a series of time steps. The governing equations of motion are solved numerically for the incremental structural deformations within each step. As in conventional dynamic analysis, the ground motion, as well as the structure's inertial and damping characteristics, are specified numerically. However, rather than using a mathematical model to determine the structure's restoring force characteristics, these are measured directly from the specimen as the test procedure progresses [47]. As dynamic effects are taken into account through the equations of motion, displacements are imposed in a quasi-

static way on the test specimen. Therefore, this technique enables testing specimens that are too large, massive or strong to be tested through shaking tables.

Despite the advantages of PsD tests, this method cannot accurately model the rate-dependent behaviour of structural elements, such as viscous dampers, compared to the shake table test or the more recently developed real-time PsD test [48] [49]. In typical steel, concrete, or masonry structures, the cyclic response of the structural elements does not depend on the rate of loading imposed by earthquake events [50], and the stress relaxation due to a slow loading rate is negligible [51].

3.2.4.2 Case study

To accurately evaluate the seismic response of a steel retrofitted frame with externally placed BRBs, the PsD test method was adopted in this study. Mass and damping structure's properties were modelled numerically, while the restoring force from the steel frame was obtained experimentally. In the adopted PsD test, the numerical integration scheme predicts the displacements imposed by the actuators to the lab specimen [52][53][54], and hence, it allows simulating the dynamic response of a structure by imposing the displacements in a quasi-static manner.

The tested frame represents the central outer span of the 75% scaled prototype building. The test matrix is summarised in Table 3-8. To facilitate the calibration of the numerical model, the bare frame was first subjected to a modal characterisation process through snap-back free vibration tests. Subsequently, the bare frame was successfully subjected to an incremental PsD test under one ground motion records, considering three scaling factors for the ground motion intensity (SF), respectively equal to 0.35, 0.75 and 1.0. In a similar way, the retrofitted frame was subjected to PsD tests considering the same ground motion with a scale factor of 1 and 1.5.

For the retrofitted frame, during the first test (SF = 1), no severe damage was observed on the frame, and the BRBs were working smoothly. On the other hand, due to safety issues, the second test (SF = 1.5) was stopped when significant torsion and instability problems were observed.

After each ground motion of the sequence for the different seismic intensities, small harmonic excitations were applied to the structure in order to evaluate the variation of the vibration periods, *i.e.*, period elongation, along with the test.

Table 3-8 *Test matrix for the 2D bare frame and retrofitted frame in the laboratory*

Test	Description
1	Snap-back free-vibration test of the bare frame
2	PsD test of the bare frame (SF = 0.35)
3	PsD test of the bare frame (SF = 0.75)
4	PsD test of the bare frame (SF = 1)
5	PsD test of the BRB frame (SF = 1)
6	PsD test of the BRB frame (SF = 1.5)

3.2.4.3 Selection of ground motion sequence

The seismic sequence considered during the tests was derived by selecting one ground motion that could reflect the moderate-to-high seismicity of some areas of Southern Europe and, at the same time, characterised by a large spectral acceleration in the range of natural period of the case-study frame in the different configurations, *i.e.*, 0.1 to 0.5 s, respectively for the BRB frame and the bare frame. Table 3-9 summarises the basic information of the selected earthquake, including the date, moment magnitude (M_w) and epicentral distance (R_{epi}) of the seismic event and the peak ground acceleration (PGA) of the recorded acceleration time-histories. The selected ground motion considered in this study referred to the 2016 Central Italy earthquakes recorded at the Station in Norcia (NRC) in the East-West component. The acceleration time history was available from the Engineering Strong-Motion database (ESM) [55]. The selected ground motion has a PGA of 0.35 g.

Table 3-9*Selected ground motion record*

Event	Date & Hour	M_w [-]	R_{epi} [km]	PGA [g]	ID[a]
GM1	24/08/2016 at 1.36	6.0	15.3	0.35	EMSC - 20160824_0000006

[a] Station in Norcia, Italy (NRC) and East-West component of the ground motion.
Source: https://esm.mi.ingv.it/

As shown in Table 3-1, to account for the variations in dynamic properties due to model scaling, the time step of the ground motion sequence, which was originally 0.02 s (Figure 3-8a), was scaled by a factor of 0.87 (the square root of 0.75) to 0.0173 s (Figure 3-8b), while the amplitudes remained the same as no scaling was required for the acceleration (see Table 3-1). Figure 3-9a shows the response spectra of the selected ground motion (unscaled in time step) as well as the elastic response spectrum defined by EC8-3 at the SD limit state. It is possible to see that, within the range from 0.2 times the fundamental period of the infilled frame to two times the fundamental period of the bare frame, the response spectra of the unscaled ground motion is close to the elastic response spectrum of the SD limit state.. As mentioned in the previous sections (3.2.4.2), in order to assess the structure under a higher earthquake, in the second PsD test the selected ground motion was scaled in amplitude by 1.5 times. Figure 3-9b shows the response spectra of the considered

ground motion scaled by a factor of 1.5 compared with the response spectrum defined by the EC8-3 at the NC limit state.

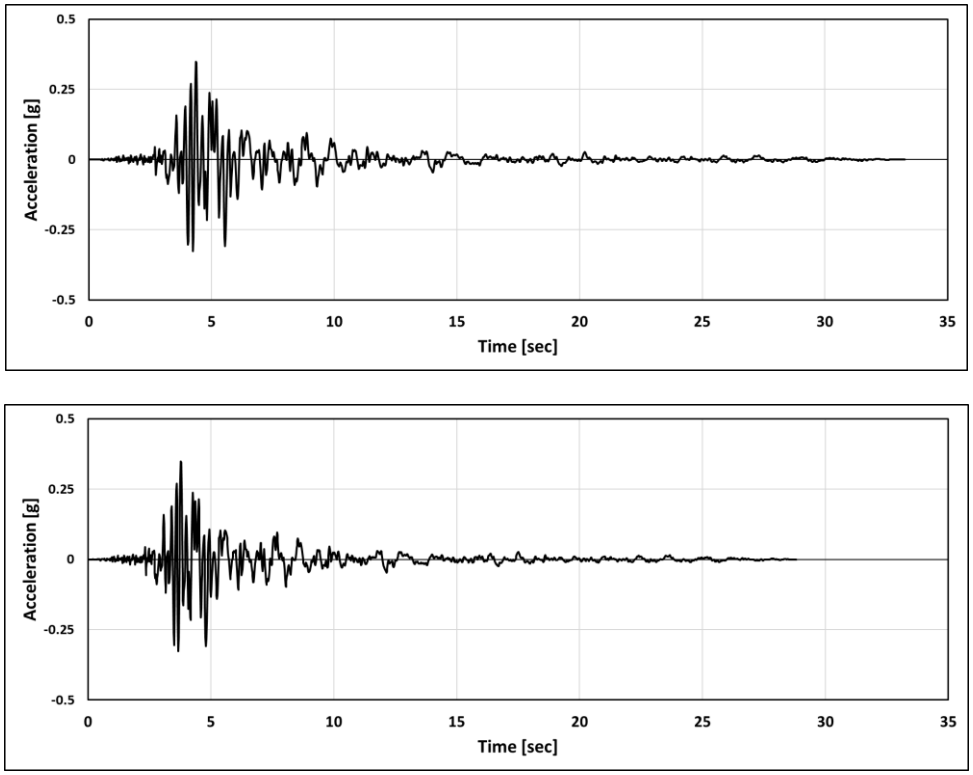

Figure 3-8 *Time history of the seismic sequence: (a) original record; (b) scaled record*

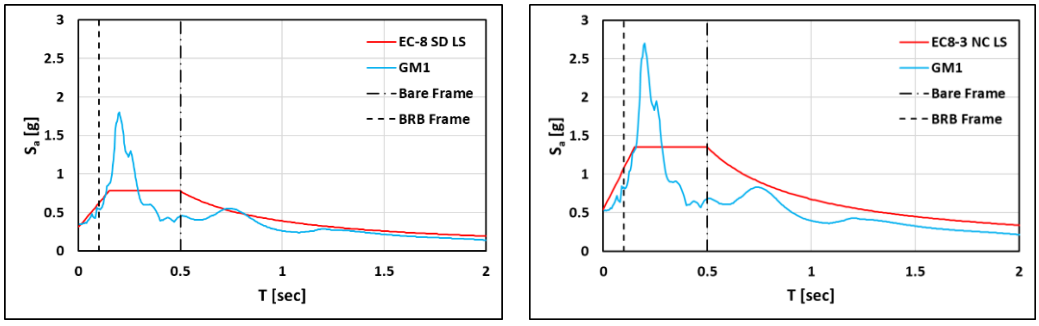

Figure 3-9 *Response spectra of the selected ground motion compared with the elastic response spectrum suggested in EC8-3: (a) unscaled ground motions at significant damage limit state; (b) Scaled ground motion at near collapse limit state.*

3.2.5 Test setup and instrumentation

Unlike real structures, the tested specimens were connected to the lab's strong floor rather than to a typical pad concrete foundation. To reduce the possibility of base plate sliding and provide enough base shear capacity in the shear connectors, the frame's base plates were connected to 80 mm thick steel base plates, which distributed the lateral loads to a larger number of floor anchors. In addition, a tubular support beam was placed on top of the thick base plates to reduce the lateral deformation and avoid significant plate bending due to moment transfer from the structure. Figure 3-10 shows the typical base plate configuration for the experiments. In addition, a composite slab of 250 mm thick concrete was connected to the beam through M19 shear studs at 150 mm spacing in order to ensure the transfer of actuator-applied horizontal loading and simulate the stiffness of the composite beam. It is worth mentioning that, to reduce any out of plane displacements and torsional effects, the storey displacement history was applied through two actuators per storey connected at both sides of the frame. The slab length is 2700 mm and 3260 mm at the first and second levels, respectively. This difference in size is a consequence of the need to place the BRB in the subsequent phases of the test. Shear studs were omitted in a 0.5 m-wide region around each joint as commonly adopted to avoid the development of composite actions in the joints. The general setup of the 2D structure can be observed in Figure 3-11.

Figure 3-10 *Typical configuration of the structures' foundation*

Figure 3-11 *General setup of the 2D structure*

The instrumentation for the PsD tests was designed to monitor the response of several structural components. All of the instrumentations are described here and are summarised in Table 3-10. As shown in Figure 3-12a four accelerometers (ACC1-4) and four displacement-measuring optical devices (OPT1-4) were used in the test free vibration test in order to monitor story displacements. Moreover, two potentiometers (DTB1-2) were placed to monitor any storey transversal displacement (Figure 3-14). A total of four inclinometers (INC1-4), whose locations are shown in Figure 3-12b, were used to monitor the column's joints rotation in the frame plane (Figure 3-15). To monitor the relative vertical, horizontal and rotational deformation of the column base plate, as well as the column deformation along with the height of the expected plastic hinge zone, fourteen potentiometers (DTC1-14) were placed in accordance with Figure 3-12b. Three potentiometers were placed to measure the diagonal elongation of the first (DTA1-2) and second (DTB7) floor, as demonstrated in Figure 3-12b and Figure 3-16. Furthermore, twelve strain gauges (SG1-12) were considered and placed to measure the strains induced in a selected column, as shown in Figure 3-12b and Figure 3-17. It is worth mentioning that the strain gauges were placed only through one column because of the number of available channels.

Regarding the tests conducted on the retrofitted frame, in addition to the instrumentation described above, further eight potentiometers (DTA5-10 and DTB3-4) and six strain gauges (SG13-18) were added in order to monitor the BRB devices and the elastic diagonal brace (Figure 3-13). In particular, the devices DTA5-8 were placed to measure the BRB slippage caused by the different sizes

between the pin and the connection hole (Figure 3-18). On the other hand, the devices DTB3-4 (Figure 3-19) and DTA9-10 (Figure 3-20) were used to monitor the elongation of the elastic brace and the BRB core, respectively. It is worth mentioning that DTA9-10 were only used in the test with a scaled ground motion (Scale Factor: 1.5).

Table 3-10 *List of sensors and devices used for the PsD tests*

Label	Device	Description	Quantity
ACC	Accelerometer (10g)	ACC1-2: first storey acceleration (free vibration test only). ACC3-4: top storey acceleration (free vibration test only).	4
OPT	Optical device	OPT1-2: displacements of the first storey in the test direction. OPT3-4: displacements of top storey in the test direction.	4
INC	Inclinometer	INC1 and INC4: column panel zones rotation (base). INC2: column panel zone rotation (first storey). INC3: column panel zone rotation (top storey).	4
DTA	Linear Variable Displacement Transducer (String potentiometer) 343 mm.	DTA 1-2: diagonal first storey elongation. DTA 5-6: BRB slippage (second storey); DTA 7-8: BRB slippage (first storey); DTA 9-10: BRB core elongation (SF 1.5 only)	8
DTB	Linear Variable Displacement Transducer (Potentiometer) 50 mm.	DTB1-2: transversal storey displacement. DTB3-4: elastic diagonal brace elongation. DTB7: top storey diagonal elongation.	5
DTC	Linear Variable Displacement Transducer (Potentiometer) 25 mm.	DTC1-6: relative vertical, horizontal and rotational deformation of a selected column base plate. DTC7-9: relative vertical, horizontal and rotational deformation of a selected column base plate. DTC10-14: column deformation along the height of the expected plastic hinge zone	14
SG	Strain gauge	SG1-12: strain in column. SG13-15: strain in diagonal elastic brace (fist storey). SG16-18: strain in diagonal elastic brace (second storey).	18

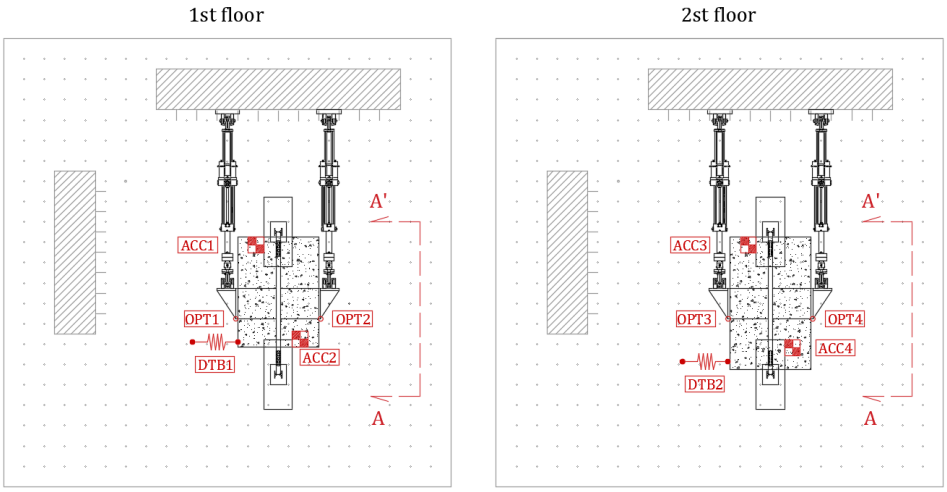

(a)

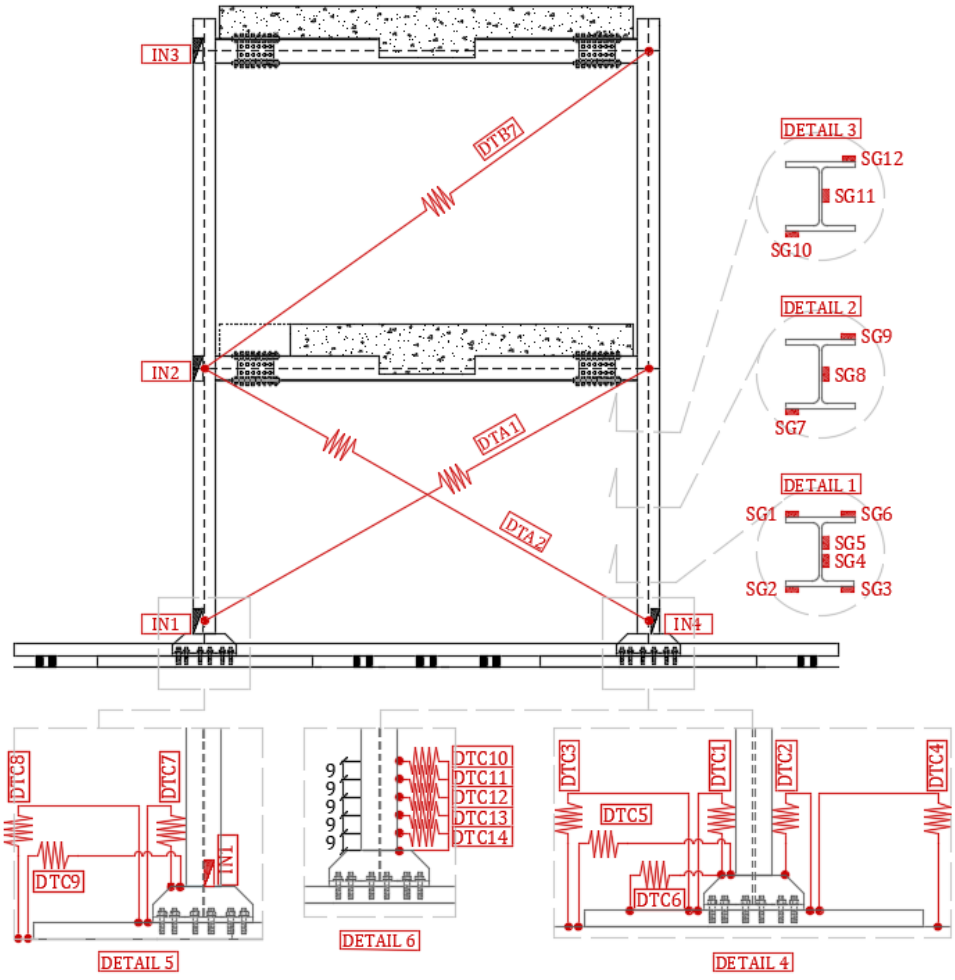

(b)

Figure 3-12 *Locations of actuators and sensors: (a) Test mock-up plan view; (b) Section A-A' bare frame without actuators;*

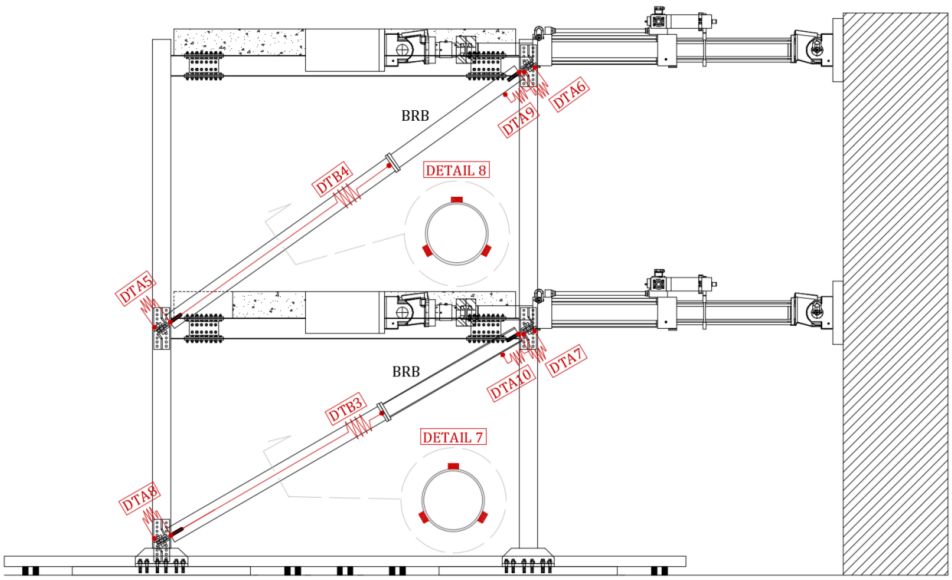

Figure 3-13 *Locations of actuators and sensors: section A-A' BRB frame with actuators*

(a) (b)

Figure 3-14 *Linear Variable Displacement Transducer to measure the transversal storey displacement: (a) DTB1; (b) DTB2*

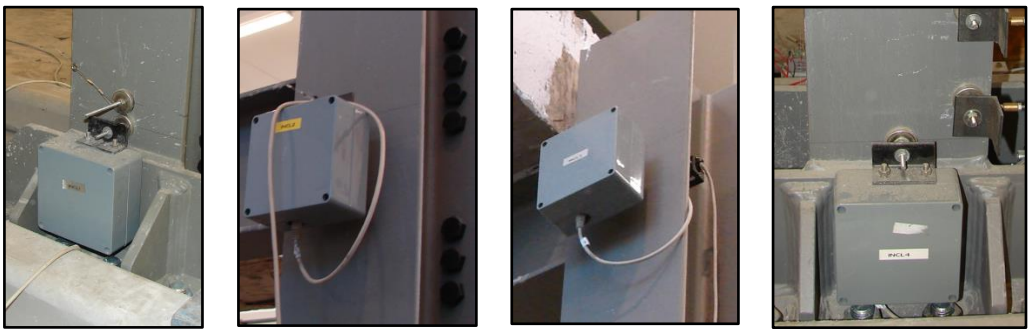

(a) (b) (c) (d)

Figure 3-15 *Inclinometers placed to monitor the nodal rotation: (a) IN1; (b) IN2; (c) IN3; (d) IN4*

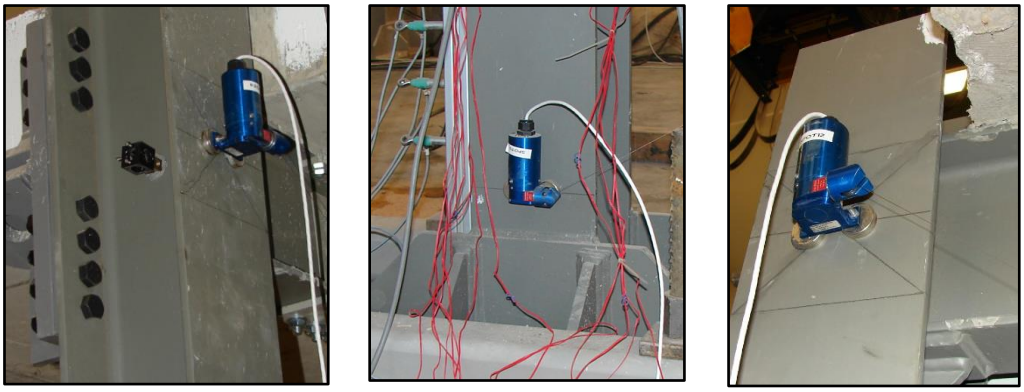

(a) (b) (c)

Figure 3-16 *Linear Variable Displacement Transducer placed to monitor the diagonal elongation:(a) DTA1; (b) DTA2; (c) DTB7*

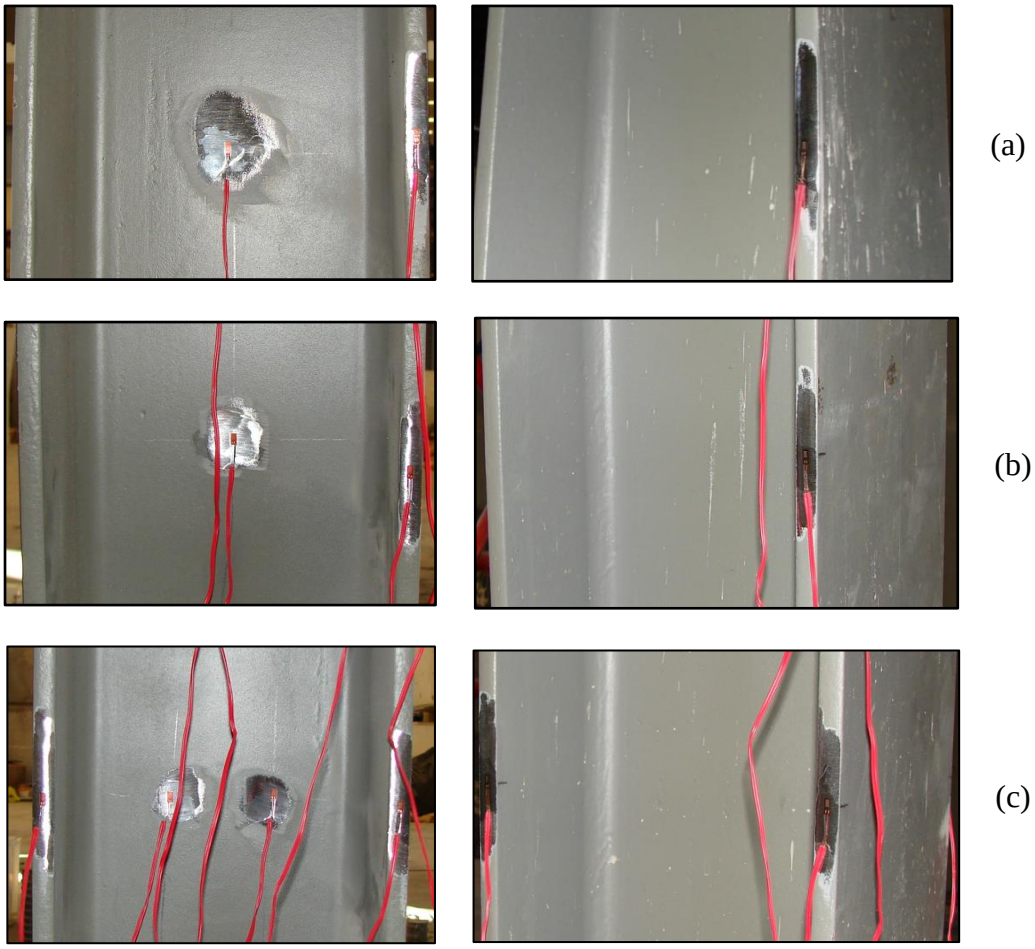

(a)

(b)

(c)

Figure 3-17 *Column strain gauges (from sx to dx): (a) DETAIL 3: SG11, SG12, SG10; (b) DETAIL 2: SG8, SG9, SG7;*
(c) DETAIL 1: SG3, SG4, SG5, SG6, SG1, SG2

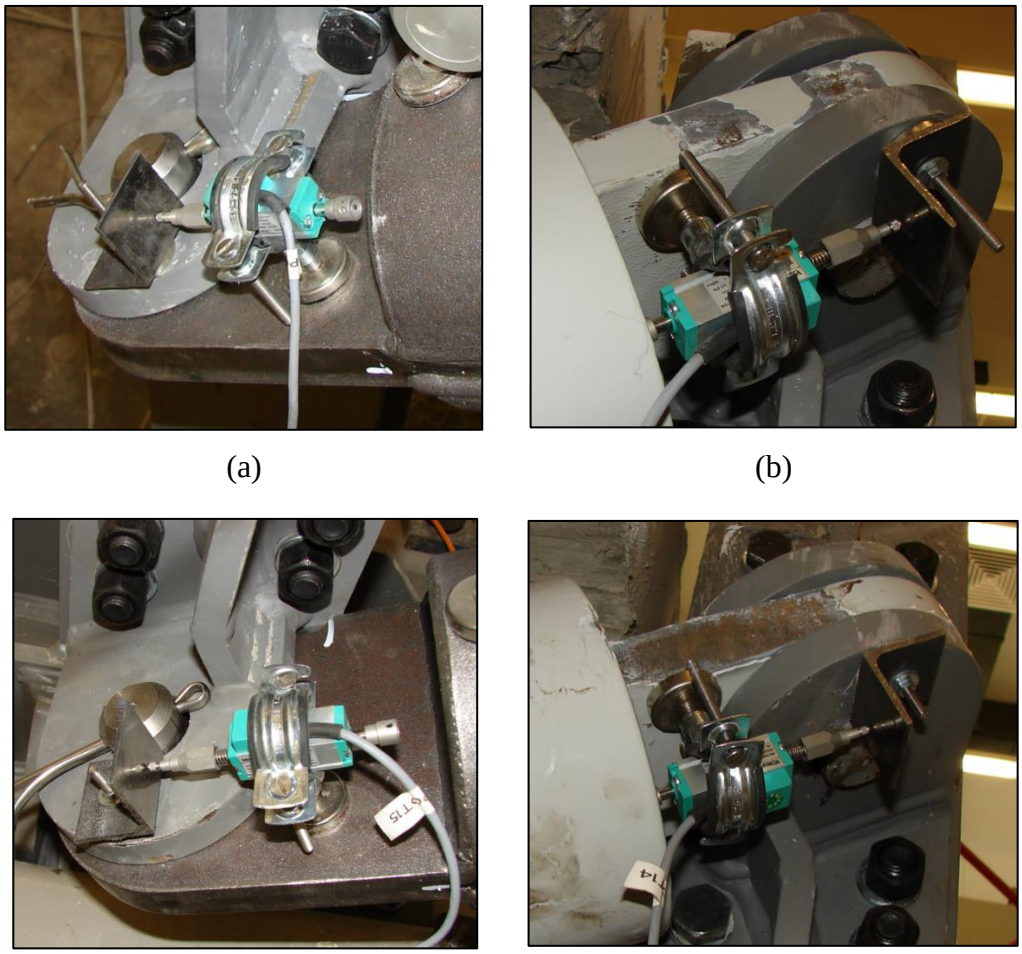

(a) (b)

(c) (d)

Figure 3-18 *Linear Variable Displacement Transducer placed to measure the BRB slippage: (a) DTA5, (b) DTA6; (c) DTA8; (d) DTA7*

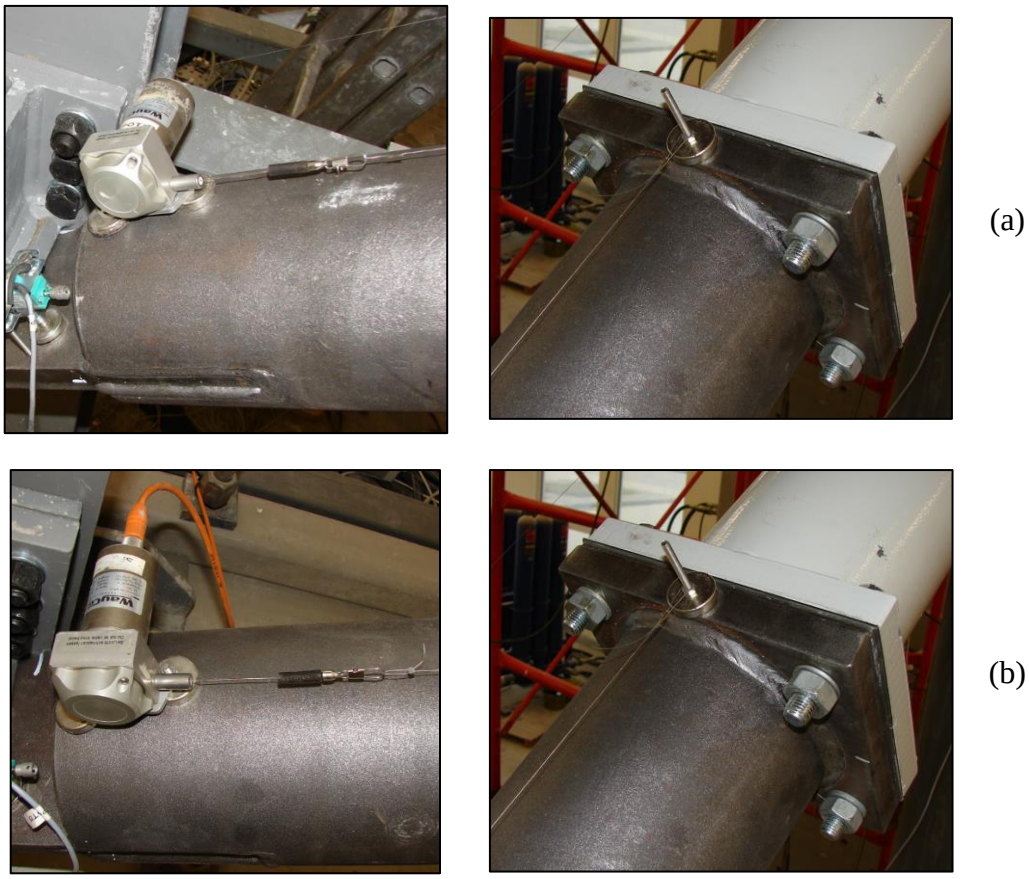

(a)

(b)

Figure 3-19 *Linear Variable Displacement Transducer placed to measure the elastic diagonal brace elongation:*
(a) DTBA 4; (b) DTBA 3

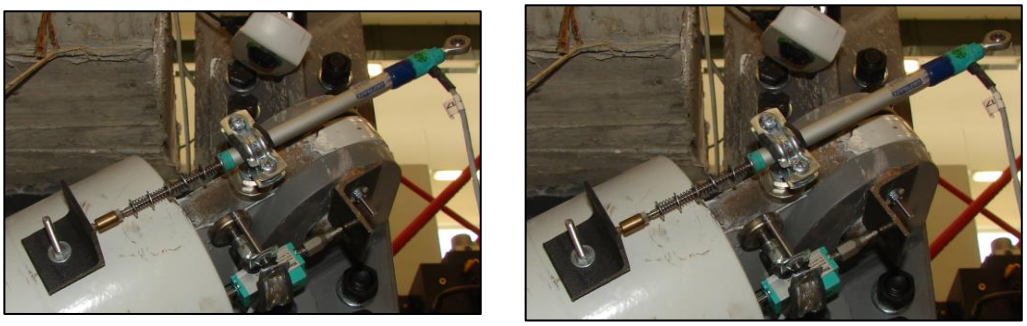

(a) (b)

Figure 3-20 *Linear Variable Displacement Transducer placed to measure the BRB core elongation (SF 1.5 only):*
(a) DTA9; (b) DTA10

3.2.6 Final observations

The experimental tests allowed the following conclusions to be drawn. As shown in the following sections (4.2.5), the retrofit strategy investigated turns out to be characterised by some limitations that reduce the effectiveness of the intervention.

The main issue is that the introduction of BRBs has only increased the strength and stiffness of the frame, leaving the dissipative capacity unaffected. This behaviour can be attributed to the torsional and distortional deformability of the column. In fact, given any inter-storey displacement, these two phenomena reduce the axial displacements imposed on the BRB, thus delaying its entrance into the non-linear range. However, the experimental campaign showed that to ensure the proposed retrofit strategy to be effective, attention must be paid to specific aspects. In the following sections (4-5) these aspects are discussed in greater depth while trying to provide solutions aimed at eliminating or reducing these phenomena.

On the other hand, the BRBs eccentricity turns out to be a fundamental factor when assessing the intervention feasibility. In fact, the PsD test on the BRB frame considering the earthquake sequence with higher intensity (*i.e.*, scaling factor of 1.5), had to be stopped when reaching an inter-story drift of about 2.30% due to excessive out-of-plane displacements other than damages observed in the column web (Figure 3-21c). In addition, it is worth mentioning that contacts between the BRBs and the columns emerged during the test (Figure 3-21a, b),

(a) (b) (c)

Figure 3-21 *Failure modes: (a) Crack in the column web; (b), (c) Contact between BRBs and columns*

4 Numerical Modelling and Validation

The test specimen described in the previous section was modelled as a 3D finite element (FE) model in Abaqus [56]. Several FE models have been created and validated against the experimental results. Firstly, the model of the bare frame was created and validated. Successively, the BRB device was modelled by calibrating the hardening parameters according to the response from cyclic experimental tests provided by the manufacturer. The FE model of the retrofitted frame was created by incorporating the calibrated BRB devices within the validated model of the bare frame. Finally, the global response of the FE model of the retrofitted frame was validated against the experimental results. These steps are described in detail in the following sections.

4.1 Bare Frame

4.1.1 Modelling

4.1.1.1 Material Model

In order to improve the numerical model accuracy, the material properties assigned to the steel elements were upgraded.

Constructional steel material exhibits ductile behaviour as it is capable of developing large inelastic strains. Since large strain plasticity is undertaken in the analysis, material properties for finite-strain calculations are used: “stress” means “true” (Cauchy) stress and “strain” means logarithmic strain. Material data for all steel definitions were, therefore, given in the true stress-logarithmic plastic strain relationship, as required by Abaqus.

As mentioned in 3.2.3, several coupon tests were conducted on both web and flanges specimens taken from both beams and columns. Therefore, before presenting the outcomes, a brief description of the coupon test is reported.

4.1.1.1.1 Coupon Test

The uniaxial coupon tests (UNI EN ISO 6892-1 and ASTM 370-10) are performed on a specimen of standard dimensions (UNI EN ISO 377), which has in the central part a smaller cross-section compared to the ones at the ends (Figure 4-1). The specimen is shaped so that fracture occurs in the central section of the specimen, which is subject to a uniaxial stress state. The aim of the test is to determine the stress (σ) - strain (ε) curve and to characterise the material response by means of several parameters, such as modulus of elasticity, yield stress, rupture stress and the corresponding deformations (Figure 4-2). During the test, the values of the tensile

force (F) and relative displacement (ΔL) between two reference points located at a distance (L_0) are measured. From this test, is it possible to derive two different stress (σ) - strain (ε) curves:

- Engineering stress (σ_E) – engineering strain (ε_E);
- True (or Cauchy) stress (σ_T) –logarithmic true strain (ε_T);

The engineering stress (σ_E) is evaluated by dividing the tensile force (F) for the initial nominal area (S_0) of the specimen, while the engineering strain (ε_E) is obtained by dividing the change in length (ΔL) by the original length (L_0). On the other hand, the true stress (σ_T) is calculated by dividing the tensile force (F) by the current area (S), while the true strain (ε_E) is considered as the natural logarithm of the ratio of the current length (L) to the original length (L_0). Engineering stress and strain can be shown to be equal to Eqs. (4-1) and (4-2), respectively[57].

$$\sigma_{eng} = \frac{F}{S_0} \tag{4-1}$$

$$\varepsilon_{eng} = \frac{L - L_0}{L_0} = \frac{\Delta L}{L_0} \tag{4-2}$$

On the other hand, true stress and true strain can be calculated in accordance with Eqs. (4-3) and (4-4), respectively[57].

$$\sigma_{true} = \frac{F}{S} = \sigma_{eng}\left(1 + \varepsilon_{eng}\right) \tag{4-3}$$

$$\varepsilon_{true} = \int_{L_0}^{L} \frac{dL}{L} = ln\left(1 + \varepsilon_{eng}\right) \tag{4-4}$$

It is worth mentioning that these equations are valid only until uniform deformation, viz., before the onset of necking[58]. An analytic solution[59] is widely used for trues stress correction in the necked region of a tensile specimen with a round cross-section. However, the Bridgman equation is not applicable for correction of average trues stress-logarithmic true strain curve of a tensile specimen with a rectangular cross-section. Although different studies focused on this topic[58,60–63], there is no firmly and explicitly established method or formula to correct true stress after necking of a flat specimen. However, the following represent the three most common conversion methods:

- *Straight line*

When calculating the true stress – logarithmic true strain curve, it is possible to connect the necking point to the failure point through a straight line. In cases in which the cross-sectional area of the specimen is measured when rupture occurs

(S_f), the coordinates of the failure point can be calculated in accordance with Eqs. (4-5) and (4-6):

$$\sigma_{f,true} = \frac{F_f}{S_f} \tag{4-5}$$

$$\varepsilon_{f,true} = ln\left(1 + \varepsilon_{f,eng}\right) \tag{4-6}$$

On the other hand, when the measurement of the cross-sectional area at the breaking point is not available, it is possible to extend the stress-strain curve through a straight-line tangent to the necking point by means of the following equation (4-7):

$$\sigma_{true} = a \cdot \varepsilon + b \tag{4-7}$$

Where the parameters (a and b) can be calculated in accordance with Eqs. (4-8) and (4-9). In this case, the logarithmic true strain at the breaking point ($\varepsilon_{f,true}$) can be calculated according to the equation (4-6).

$$a = \sigma_{u,true} \tag{4-8}$$

$$b = \sigma_{u,true}\left(1 + \varepsilon_{u,true}\right) \tag{4-9}$$

- *Nonlinear power relation* [62]

Alternatively, it is possible to connect the necking point to the failure point through a nonlinear power relation (4-10):

$$\sigma_{true} = K \cdot \varepsilon^n \tag{4-10}$$

Where the parameters (K and n) can be calculated in accordance with Eqs. (4-11) and (4-12).

$$K = \sigma_{u,true}/n^n \tag{4-11}$$

$$n = \varepsilon_{u,true} \tag{4-12}$$

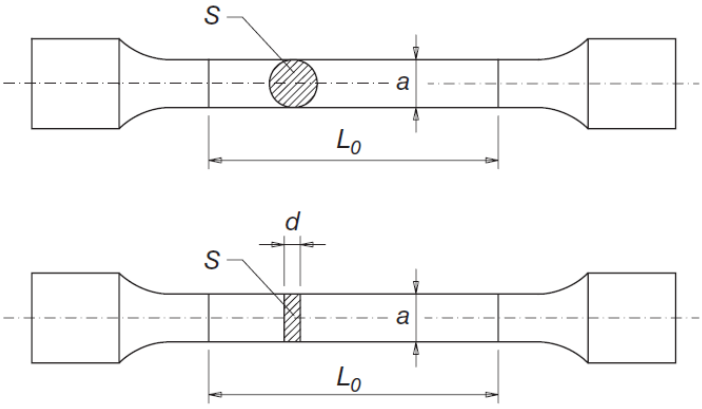

Figure 4-1 *Typical sample for rolled products (from Bernuzzi et al.[64])*

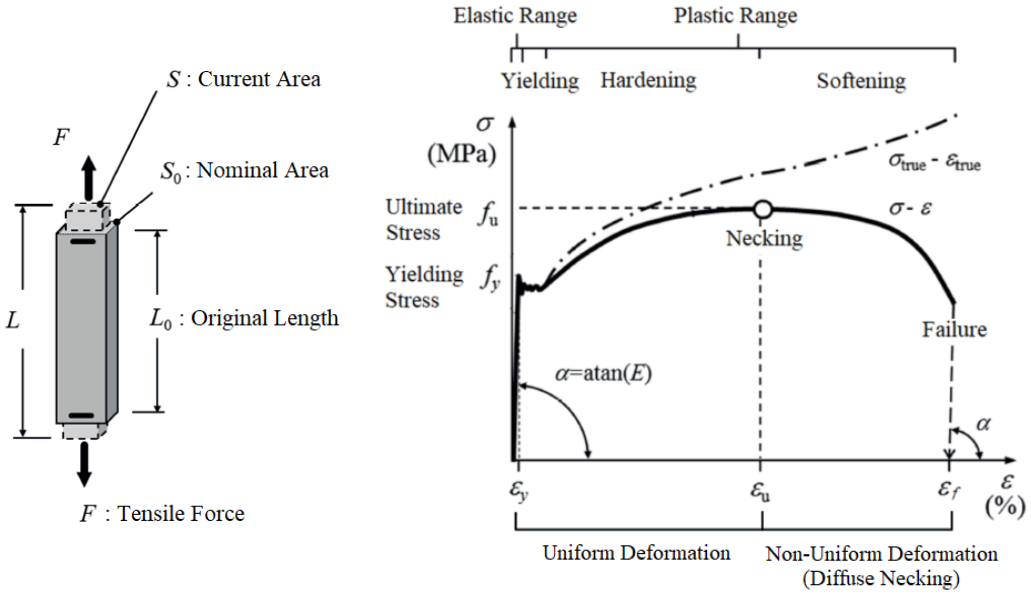

(a) (b)

Figure 4-2 *Coupon test: (a) Test scheme and measured values, (b) Stress (σ) - strain (ε) curve obtained from the test*

4.1.1.1.2 Test Data

As mentioned in 3.2.3, several coupon tests were conducted on steel coupons taken from different components (*i.e.*, webs and flanges of beam and column profiles). Table 4-1 reports all the characteristics related to the specimens considered for the coupon tests. In this case, the laboratory provided both stress-strain curves (engineering and true). Figure 4-3 shows the true stress – logarithmic true strain provided by the laboratory.

Table 4-1 *Coupon Test*

Test	ID	El. Type	El. Num.	El. Part	Part Num.	Mat.
1	C1	Beam	3	Flange	1	612
2	C1	Beam	3	Flange	1	613
3	C2	Beam	3	Flange	2	614
4	C2	Beam	3	Flange	2	615
5	C3	Beam	3	Web	-	616
6	C3	Beam	3	Web	-	617
7	C4	Beam	5	Flange	1	618
8	C4	Beam	5	Flange	1	619
9	C5	Beam	5	Flange	2	620
10	C5	Beam	5	Flange	2	621
11	C6	Beam	5	Web	-	622
12	C6	Beam	5	Web	-	623
13	C7	Col	4	Flange	1	624
14	C7	Col	4	Flange	1	625
15	C8	Col	4	Flange	2	626
16	C8	Col	4	Flange	2	627
17	C9	Col	4	Web	-	628
18	C9	Col	4	Web	-	629
19	C10	Col	1	Flange	1	630
20	C10	Col	1	Flange	1	631
21	C11	Col	1	Flange	2	632
22	C11	Col	1	Flange	2	633
23	C12	Col	1	Web	-	634
24	C12	Col	1	Web	-	635

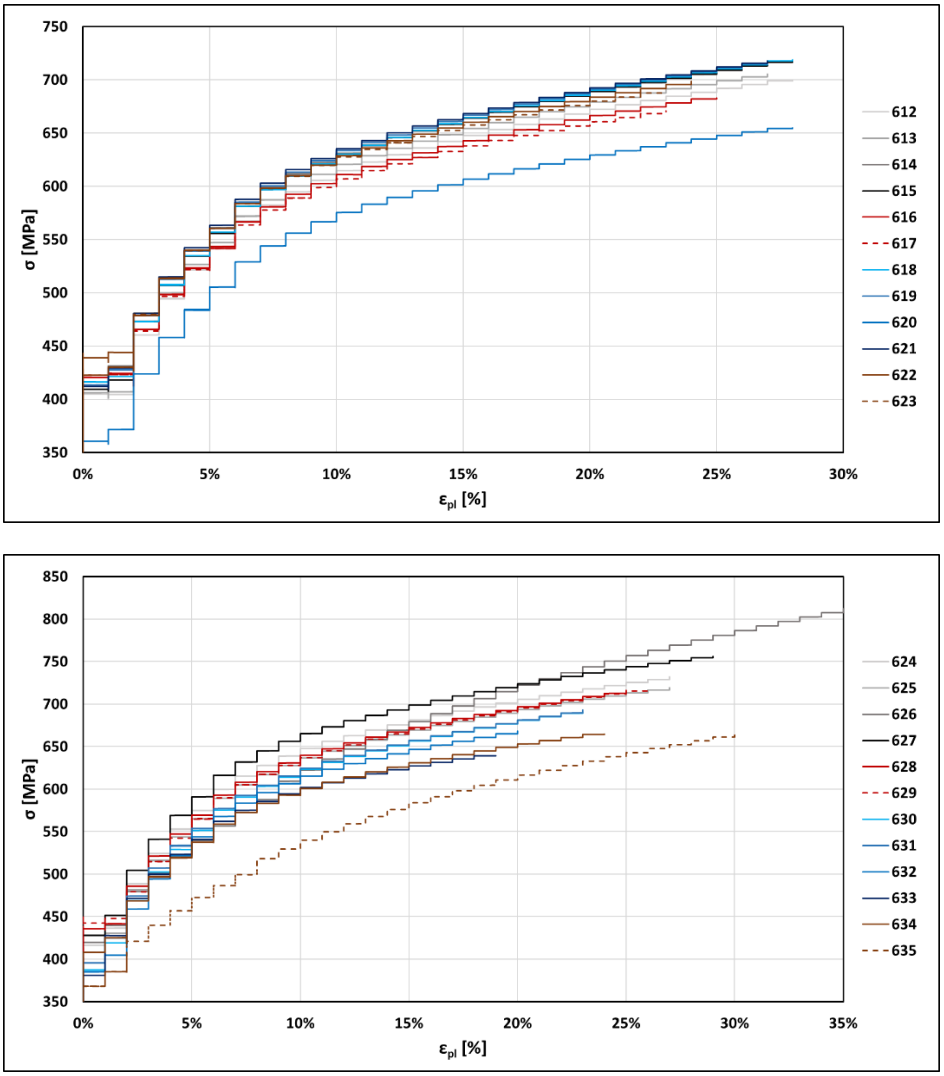

Figure 4-3 *True stress - logarithmic true strain from coupon tests: (a) Beam specimen, (c) Column specimen*

4.1.1.1.3 Abaqus Model

Considering the true stress – logarithmic true strain reported in Figure 4-3, an average behaviour between those curves was first derived, and then a bilinear model was used to define the steel material behaviour in Abaqus. These properties are reported in Table 4-2 and Table 4-3, and illustrated in Figure 4-4.

Table 4-2 *Abaqus Steel Properties - Beam*

	ε_{true} [%]	$\varepsilon_{true,pl}$ [%]	σ_{true} [MPa]
Yielding	0.2	0	415
Failure	0.163	0.161	662

Table 4-3 *Abaqus Steel Properties - Column*

	ε_{true} [%]	$\varepsilon_{true,pl}$ [%]	σ_{true} [MPa]
Yielding	0.2	0	433
Failure	0.165	0.163	662

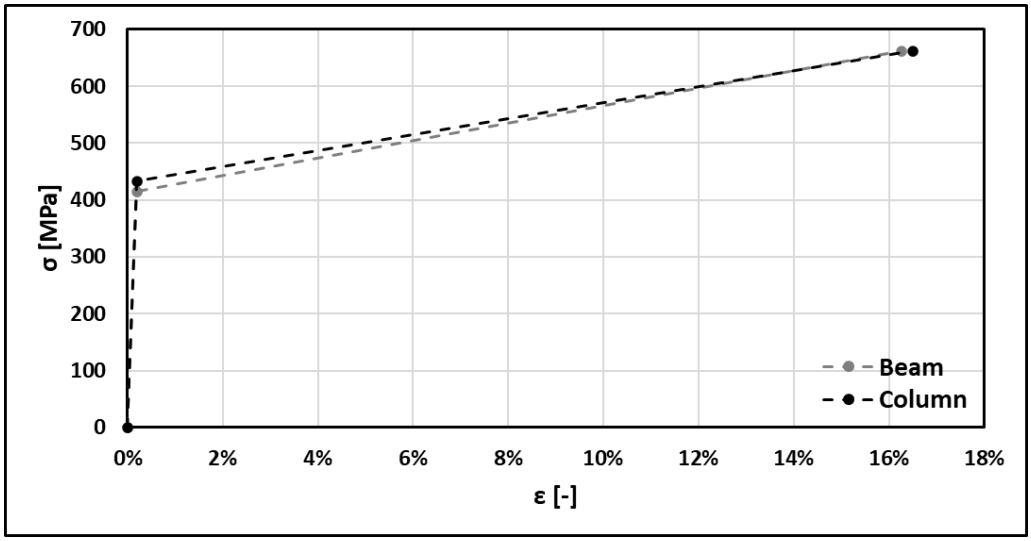

Figure 4-4 *Abaqus Steel material behaviour*

4.1.1.2 3D Model

As illustrated in Figure 4-5, all steel components (*i.e.*, beams, columns and stiffeners) were modelled as solid elements (C3D8R). The material properties were assigned in accordance with 4.1.1.1.3. Full penetration welds were simulated by connecting beams, columns, and stiffeners through tie constraints. Aside from the steel members, the reinforced concrete slabs in the FE model were modelled using solid elements (C3D8R) as well. A simplified model consisting of homogeneous concrete blocks with an equivalent Young's modulus was used to simulate the higher rigidity of the slab. Plastic behaviour was not defined for concrete in the present study since no cracking was observed in the concrete components of the case study building during the PsD test. The slab was connected to the top flange of beams through tie constraints in the region where shear studs were present. In regions without shear studs, contact was defined between the slab and beam, including tangential behaviour with a friction coefficient of 0.7 and 'Hard' normal behaviour. Fixed boundary conditions were imposed on the bottom of columns.

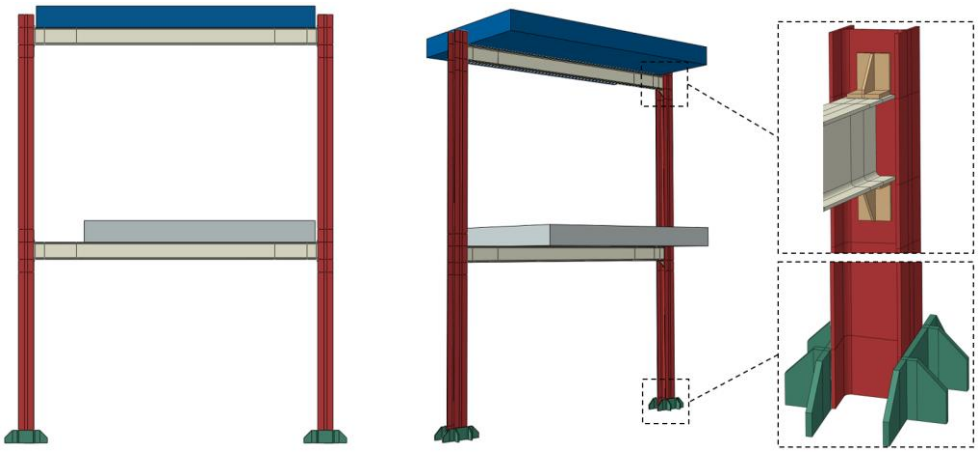

Figure 4-5 *Description of the 3D bare frame Abaqus model*

All steel elements were meshed using elements with an average size of 20 mm. It is worth mentioning that the mesh size has been reduced in the connection zones between beams and columns to better capture the distribution of forces and deformations in such zones. Figure 4-6 shows in detail how the aforementioned elements were meshed.

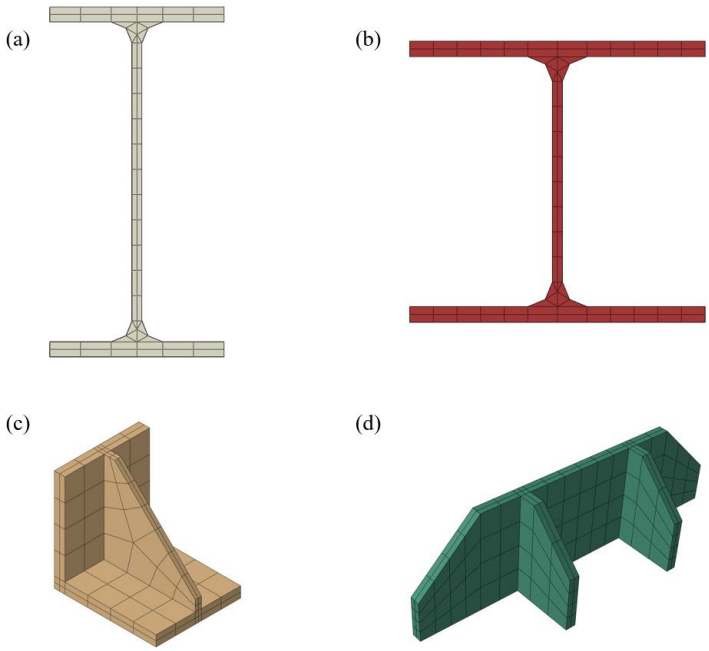

Figure 4-6 *Mesh detail: (a) beam; (b) column; (c) stiffener; (d) base stiffener*

4.1.2 Validation

The numerical simulations were performed through two steps: the Gravity and the Pseudo Dynamic analysis. The Pseudo Dynamic analysis was conducted by imposing the same horizontal floors displacements applied during the tests. In particular, the displacements were imposed to two different control points, belongings to the top surface of the slab. The control points enforced the top surface

of the slab to undergo the same horizontal displacement through *coupling* constraint. *Quasi-static* analysis in the *implicit dynamic* analysis category was selected for the Pushover analysis. As mentioned in the previous paragraph (313.2.4.2), the bare frame was subjected to three PsD tests in which the same ground motion was scaled through three different scale factors: 0.35, 0.75 and 1, respectively. The following section presents the validation of the model considering the ground motion scaled to SF = 0.35. The comparison between the Abaqus model and test results regarding the other two scale factors are presented in Appendix A.

In order to validate the FE model, comparisons were made in terms of actuator forces, floor stiffness and local stress. In the following paragraphs, the test measurements, together with the Abaqus results, are shown.

4.1.2.1 Scaled Ground Motion (SF = 0.35)

Figure 4-7 shows the displacement history imposed on the first and second floor during both the test and the numerical simulation. The first comparison between the test specimen and the FE model was made in terms of actuator forces, *i.e.*, comparing the forces required to impose the predefined displacement. Figure 4-8 shows the actuator force applied during the test compared with the one obtained through Abaqus. It can be seen that the error between these two values is always lower than 10%. It is worth mentioning that in order to highlight the differences, the most relevant steps only are shown. As shown in Figure 4-9, the second comparison was made in terms of floor stiffness. Once again, it can be seen that the Abaqus model successfully captures the experimental results. Figure 4-10 and Figure 4-11 show the comparison between the values obtained from the strain gauges placed on the column (Detail 1 of Figure 3-13a) and the corresponding values obtained from Abaqus. An almost perfect match between the two values is also achieved in this case. However, it is worth emphasising that, although the measurements obtained from the strain gauges positioned on the column web are affected by a significant noise, the Abaqus model manages to appropriately capture the general trend of the acting stresses. The considerations made regarding the measurements obtained from the strain gauges positioned in the first section of the column (Detail 1 of Figure 3-13a) are also valid for the other two sections of the column (Details 2 and 3 of Figure 3-13a), which are shown respectively in Figure 4-12 and Figure 4-13.

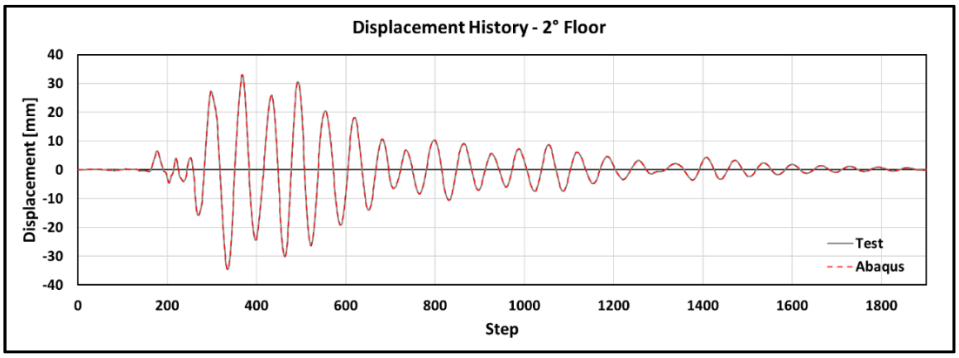

(a)

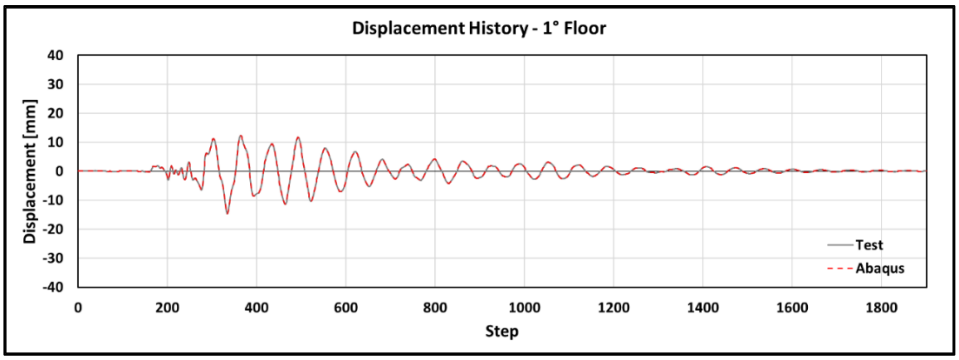

(b)

Figure 4-7 *Displacement History: (a) Second Floor; (b) First Floor.*

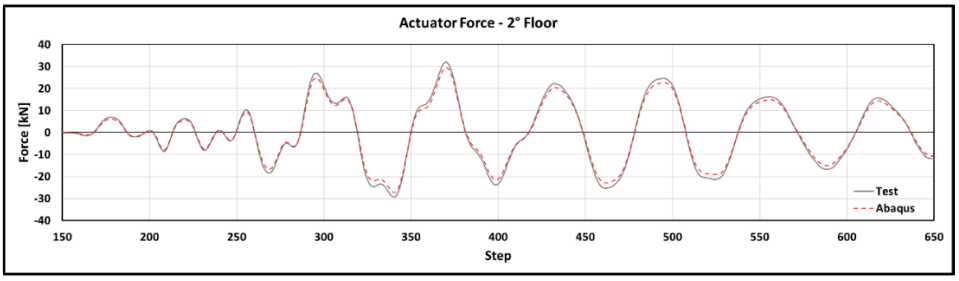

(a)

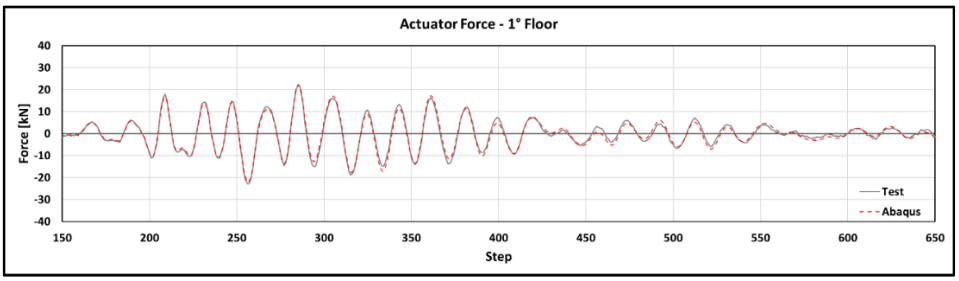

(b)

Figure 4-8 *Actuator Force: (a) Second Floor; (b) First Floor*

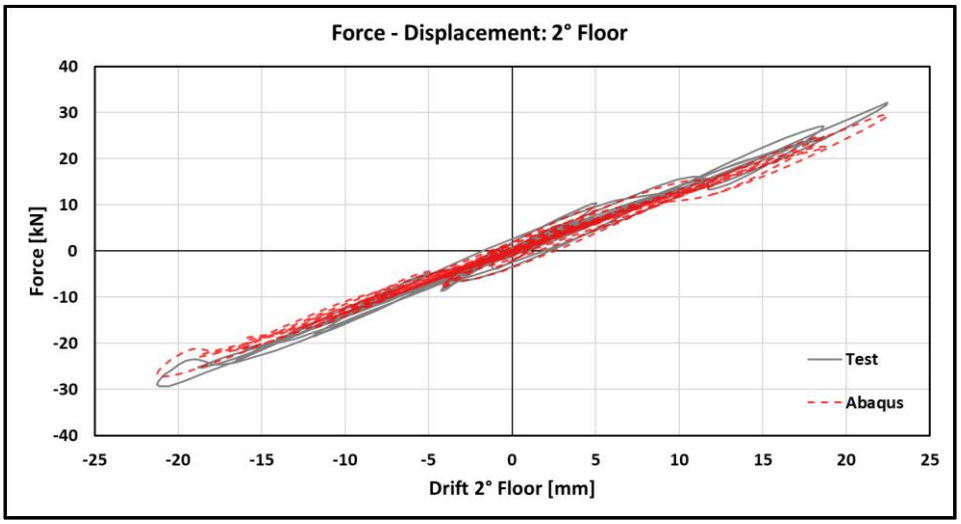

(a)

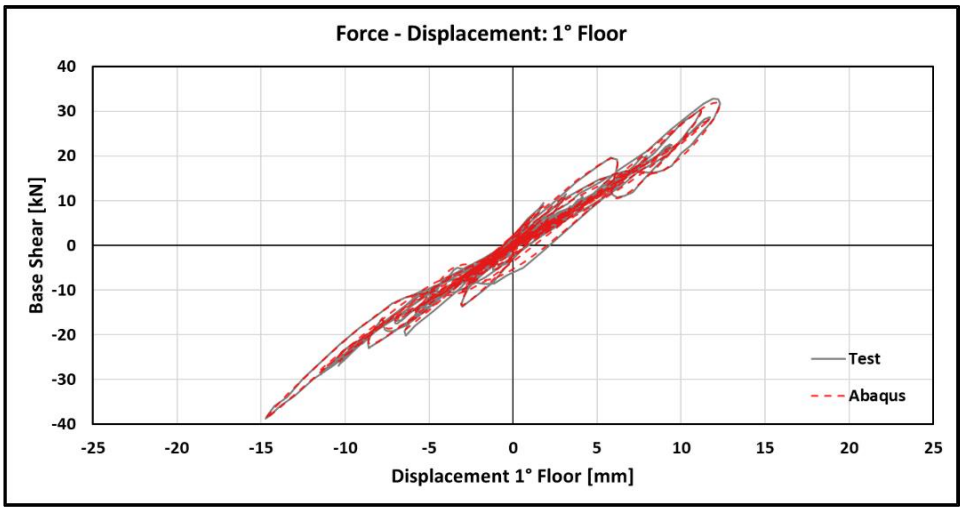

(b)

Figure 4-9 *Floor Stiffeness: (a) Second Floor; (b) First Floor.*

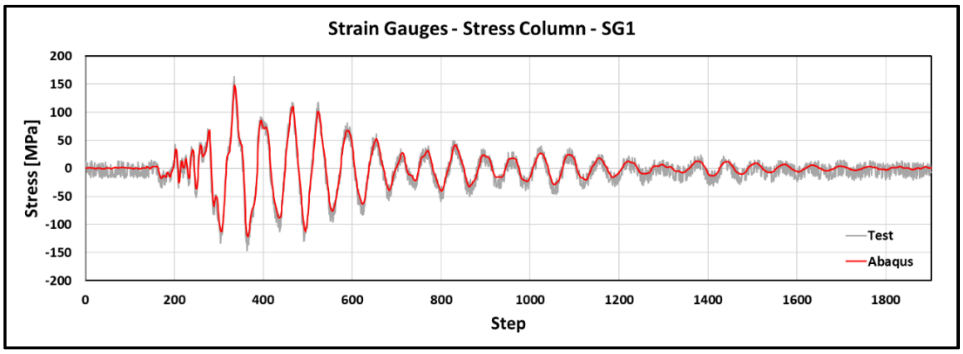

(a)

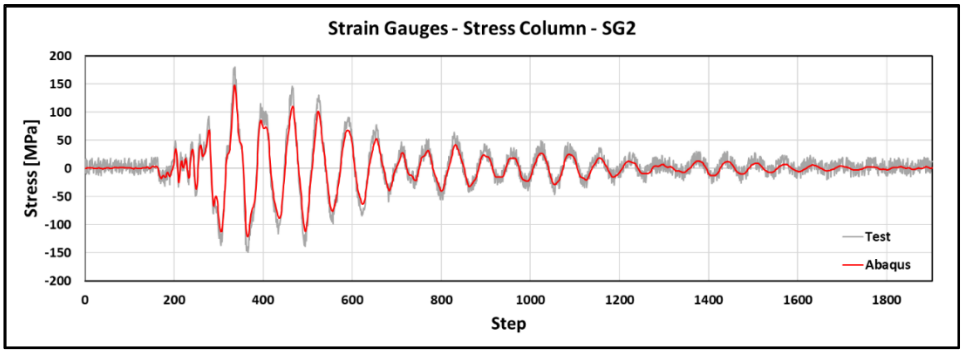

(b)

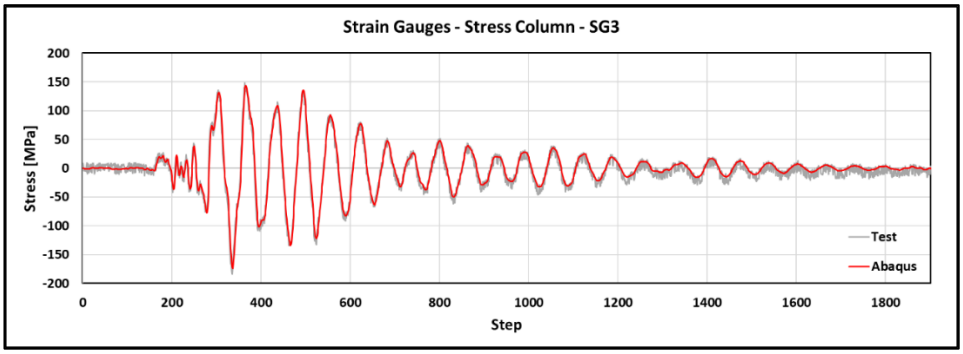

(c)

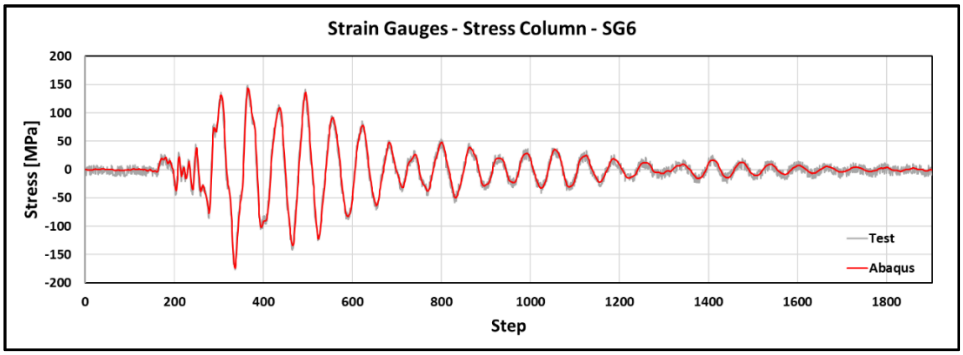

(d)

Figure 4-10 *Column Flange Strain Gauges - Detail 1: (a) SG1, (b) SG2, (c) SG3, (d) SG6*

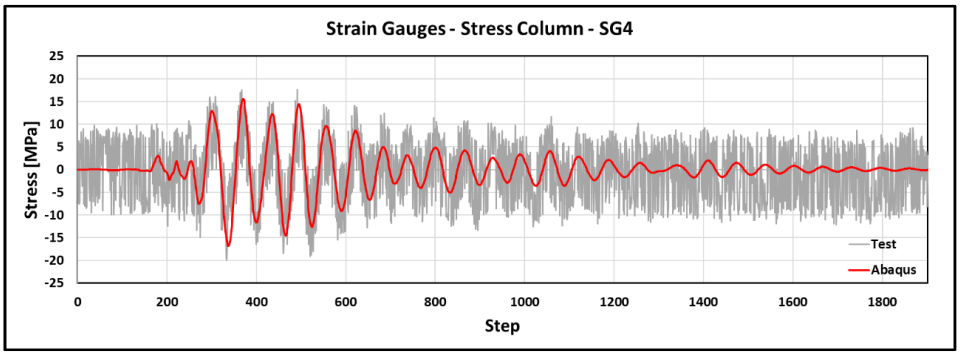

(a)

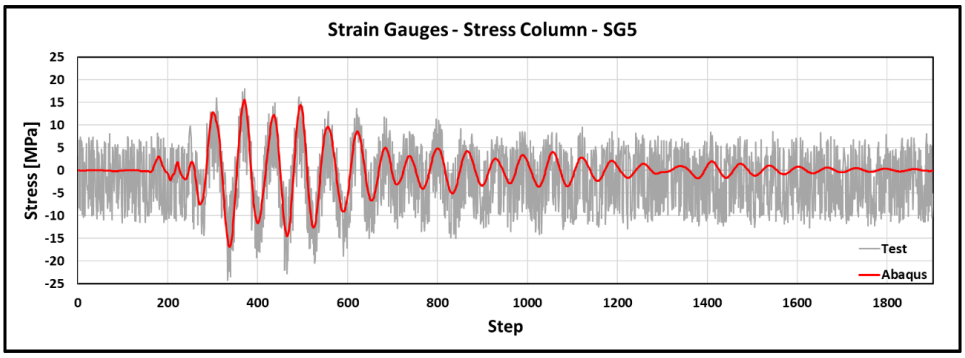

(b)

Figure 4-11 *Column Web Strain Gauges - Detail 1: (a) SG4, (b) SG5*

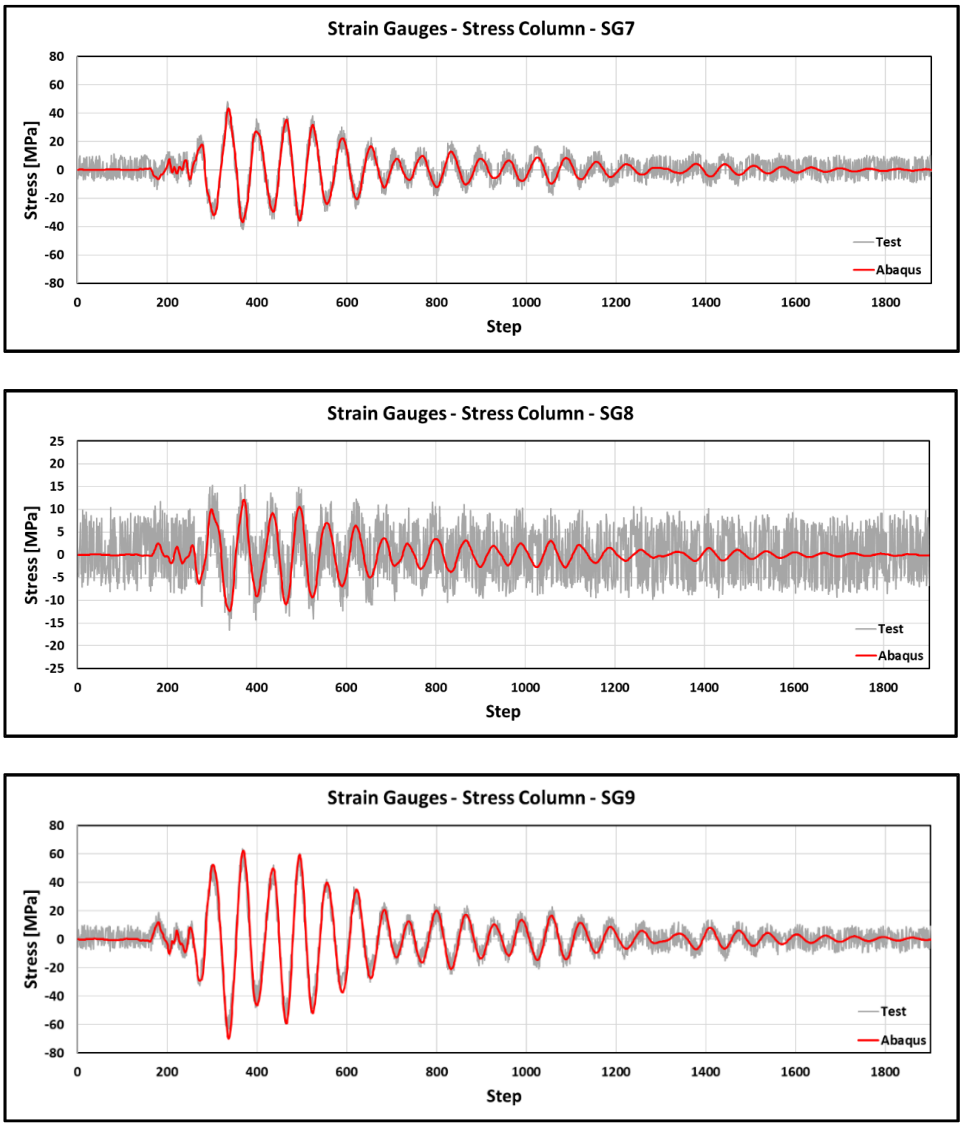

Figure 4-12 *Column Flange Strain Gauges - Detail 2: (a) SG7, (b) SG8, (c) SG9*

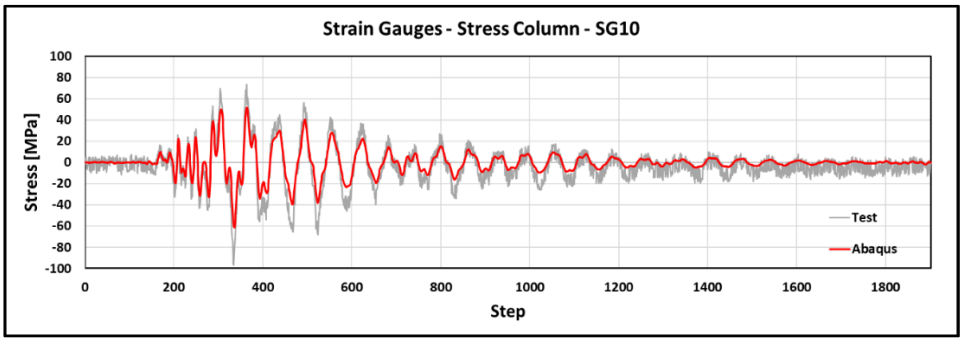

(a)

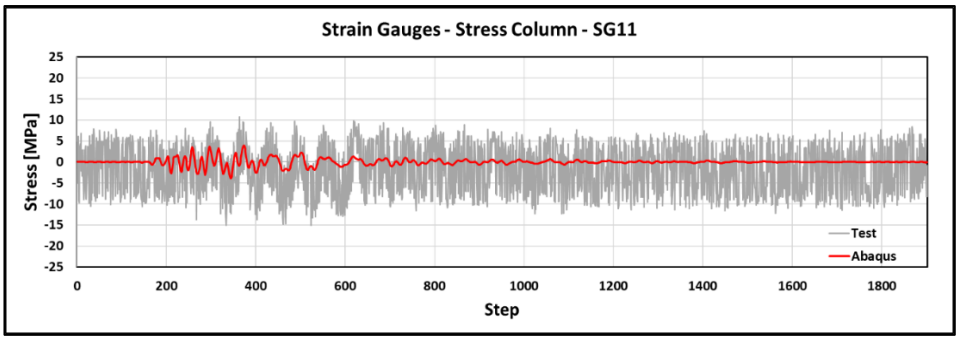

(b)

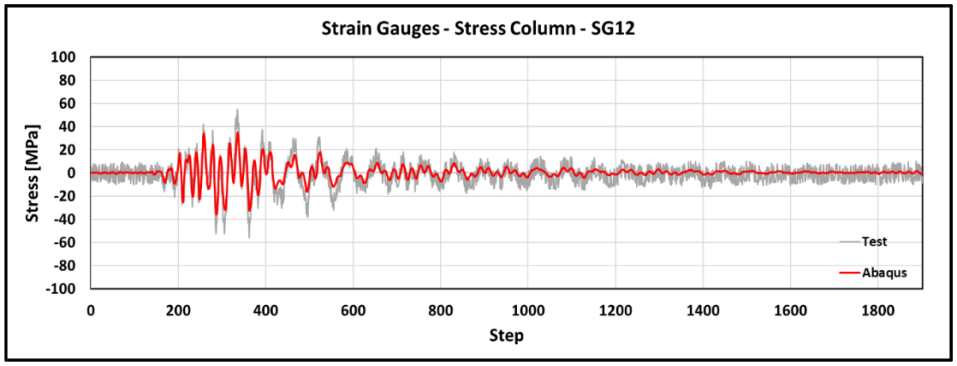

(c)

Figure 4-13 *Column Flange Strain Gauges - Detail 3: (a) SG10, (b) SG11, (c) SG12*

4.2 BRB Frame

As mentioned in the previous section (3.2.2.2), after the first set of tests, the bare frame was retrofitted with Buckling Restrained Braces (BRBs) placed outside the frame plane through a specially designed connection. Therefore, before building and validating the retrofitted frame model, it was necessary to model and validate the dissipative device only (BRB). In the following sections, the procedure is described.

Before presenting the modelling strategy adopted, a number of essential notions for understanding what follows are given below.

4.2.1 Material non-linearity in Cyclic loading

Modelling the cyclic response of structural steel plays an important role in the design and performance assessment of steel structures. During a seismic event, the structural steel elements (*e.g.*, Buckling Restrained Braces, shear links/panels) undergo cyclic deformations. Therefore, a material model able to properly simulate the cyclic behaviour of structural steel must be experimentally validated. The calibrated material model can be further used to simulate the structural elements for cyclic numerical analyses.

In order to describe how a material behaves under cyclic loading with different stress or strain amplitudes before reaching stabilised state, a constitutive model of cyclic plasticity is needed. The theory of cyclic plasticity provides a mathematical description of a material stress-strain response in plastically deformed (time-independent plasticity) solids under cyclic loading [65].

Within this thesis, the “built in” combined isotropic/kinematic hardening model is used to model metal plasticity under cyclic loading regime. This represents a time-independent constitutive model for cyclic plasticity of metals implemented in the nonlinear finite element software Abaqus, which is based on the work of Lemaitre and Chaboche [66]. In this model, the von Mises yield criterion and associative flow rule are assumed. The evolution law in the model consists of a kinematic hardening component which describes the translation of the yield surface in the stress space. An isotropic component, which describes the change of the elastic range, is added for the nonlinear isotropic/kinematic hardening model.

A brief description of the constitutive model, capable of capturing the main features of response of the steel material for proportional, and non-proportional cyclic loading paths in engineering sense, are given.

4.2.1.1 Nonlinear isotropic/kinematic hardening model

Nonlinear isotropic/kinematic hardening model with multiple backstresses in combination with the von Mises yield surface (isotropic yield plasticity) represents an Abaqus integrated material model for metals subjected to cyclic loading. The

assumption of associated plastic flow is acceptable for metals subjected to cyclic loading as long as microscopic details, such as localization of plastic flow occurring as a metal component ruptures due to cyclic fatigue loads, are not of interest [56].

The nonlinear isotropic/kinematic hardening model has both nonlinear kinematic and nonlinear isotropic hardening components. The evolution law of this model consists of two components: a nonlinear kinematic hardening component, which describes the translation of the yield surface in stress space through the backstress α, and an isotropic hardening component, which describes the change of the equivalent stress defining the size of the yield surface σ_0 as a function of plastic deformation. The combined isotropic/kinematic hardening model is schematically presented in Figure 4-14.

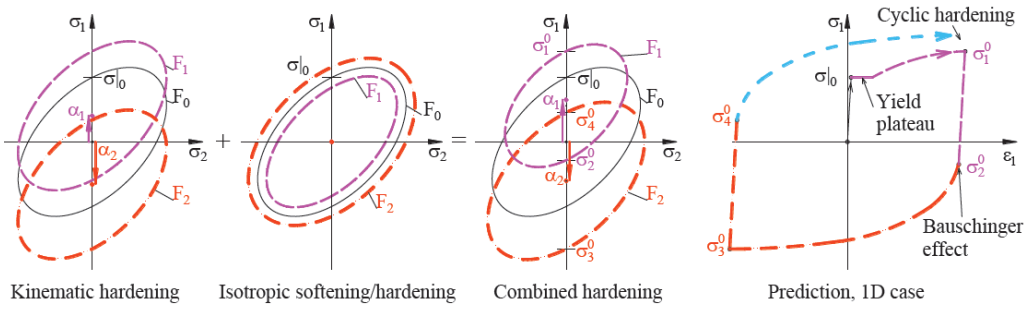

Figure 4-14 *Combined isotropic/kinematic hardening model (from Zub et al. [67])*

The following constitutive equations and hypotheses are considered in this material model [56]:

- *Total strain tensor* (ε): decomposed into elastic (ε_{el}) and plastic (ε_{pl}) parts:

$$\varepsilon = \varepsilon^{el} + \varepsilon^{pl} \qquad \textit{(Eq. 4.1)}$$

- *Yield surface* (F): defined as a function of equivalent stress ($f(\sigma - \alpha)$) and yield stress (σ^0), where α represents the backstress tensor:

$$F = f(\sigma - \alpha) - \sigma^0 = 0 \qquad \text{(Eq. 4.2)}$$

It is worth mentioning that when $F < 0$, an elastic stress state is obtained, while $F = 0$ represents a plastic stress state; moreover, $F > 0$ is not admissible.

- *Von Mises yield criterion* ($f(\sigma - \alpha)$): defined as a function of the deviatoric stress tensor (S) and deviatoric part of the backstress tensor (α^{dev}):

$$f(\sigma - \alpha) = \left[\frac{3}{2}(S - \alpha^{dev}) : (S - \alpha^{dev})\right]^{0.5} \qquad \textit{(Eq. 4.3)}$$

- *Associated plastic flow rule*:

$$\dot{\varepsilon}^{pl} = \dot{\bar{\varepsilon}}^{pl} \frac{\partial F}{\partial \sigma} \qquad \textit{(Eq. 4.4)}$$

where $\dot{\varepsilon}^{pl}$ is the rate of plastic flow and $\dot{\bar{\varepsilon}}^{pl}$ is the equivalent plastic strain rate, which, for isotropic von Mises plasticity, is calculated as:

$$\dot{\bar{\varepsilon}}^{pl} = \sqrt{\frac{2}{3}\dot{\varepsilon}^{pl} : \dot{\varepsilon}^{pl}} \qquad \textit{(Eq. 4.5)}$$

- *Nonlinear isotropic/kinematic hardening rule*. The evolution law of this model consists of two components: a *nonlinear kinematic hardening* component, which describes the translation of the yield surface in stress space through the backstress (α); and an *isotropic hardening* component, which describes the change of the equivalent stress defining the size of the yield surface (σ^0) as a function of plastic deformation.

The *kinematic hardening component* is defined to be an additive combination of a purely kinematic term (linear Ziegler hardening law) and a relaxation term (the recall term), which introduces the nonlinearity. In addition, several kinematic hardening components (backstresses) can be superposed, which may considerably improve results in some cases. When temperature and field variable dependencies are omitted, the hardening laws for each backstress are:

$$\dot{\alpha}_k = C_k \cdot \frac{1}{\sigma_0} \cdot (\sigma - \alpha) \cdot \dot{\bar{\varepsilon}}^{pl} - \gamma_k \cdot \alpha_k \cdot \dot{\bar{\varepsilon}}^{pl} \qquad \textit{(Eq. 4.6)}$$

and the overall backstress is computed from the relation:

$$\alpha = \sum_{k=1}^{N} \alpha_k \qquad \textit{(Eq. 4.7)}$$

where N is the number of backstresses, and C_k and γ_k are material parameters that must be calibrated from cyclic test data. C_k are the initial kinematic hardening moduli, and γ_k determine the rate at which the kinematic hardening moduli decrease with increasing plastic deformation. The kinematic hardening law can be separated into a deviatoric part and a hydrostatic part; only the deviatoric part has an effect on the material behaviour. When C_k and γ_k are zero, the model reduces to an isotropic hardening model. When all γ_k equal zero, the linear Ziegler hardening law is recovered. It is worth mentioning that whenever using different backstresses, each of them usually covers a different range of strains, and the linear hardening law is commonly retained for large strains.

The *isotropic hardening behaviour* of the model defines the evolution of the yield surface size (σ^0) as a function of the equivalent plastic strain ($\bar{\varepsilon}^{pl}$). This evolution law can be represented by the following exponential law:

$$\sigma^0 = \sigma|_0 + Q_\infty \left(1 - e^{-b\bar{\varepsilon}^{pl}}\right) \qquad (Eq.\ 4.8)$$

where $\sigma|_0$ is the yield stress at zero plastic strain, while Q_∞ and b are material parameters. Q_∞ represents the maximum change in the size of the yield surface, while b defines the rate at which the size of the yield surface changes as plastic straining develops. When the equivalent stress defining the size of the yield surface remains constant ($\sigma^0 = \sigma|_0$), the model reduces to a nonlinear kinematic hardening model.

The notions introduced in this section are essential for the calibration of the parameters through which the non-linear cyclic behaviour of the BRB device was modelled.

4.2.2 Connector

The analyst is often faced with modelling problems in which two different parts are connected in some way. Whenever the connection may impose complicated constraints, *connector* elements in Abaqus provide an easy and versatile way to model different types of physical mechanisms [56].

Connector modelling consists of choosing and defining the appropriate *connector elements* and defining the *connector behaviour*.

4.2.2.1 Connector element

Connector elements:

- are available for two-dimensional, axisymmetric, and three-dimensional analyses;
- can define a connection between two nodes (each node can be connected to a rigid part, a deformable part, or not connected to any part);
- can define a connection between a node and ground;
- have relative displacements and rotations that are local to the element, which are referred to as components of relative motion;
- are functionally defined by specifying the connector attributes;
- have comprehensive kinematic and kinetic output;
- can be used to monitor kinematics in local coordinate systems.

4.2.2.1.1 Choosing an appropriate element

Two connector elements are provided. The element type to be chosen depends on the dimensionality of the analysis: CONN2D2 for two-dimensional and

axisymmetric analyses and CONN3D2 for three-dimensional analyses. Both connector elements have at most two nodes. The position and motion of the second node on the connector element are measured relative to the first node.

4.2.2.1.2 Components of relative motion

Connector elements have relative displacements and rotations that are local to the element. These relative displacements and rotations are referred to as components of relative motion. In the three-dimensional case, connector elements use twelve nodal degrees of freedom to define six relative motion components: three displacements and three rotations in element local directions. In two dimensions, six nodal degrees of freedom define three relative motion components: two displacements and one rotation. The components of relative motion are either constrained or unconstrained ("available"), depending upon the definition of the connector element.

Constrained components of relative motion are displacements and rotations that are fixed by the connector element. In connector elements with constrained components of relative motion, Abaqus/Standard uses Lagrange multipliers to enforce the kinematic constraints. Accordingly, in Abaqus/Standard, the constraint forces and moments carried by the element appear as additional solution variables. The number of additional solution variables is equal to the number of constrained components of relative motion. In Abaqus/Explicit, the constraints are enforced using an augmented Lagrangian technique for which no additional solution variables are needed.

Available components of relative motion are displacements and rotations that are not constrained kinematically and, hence, remain available for defining material-like behaviour, specifying time-dependent motion, applying loading, or assigning complex interactions, such as contact or friction.

4.2.2.1.3 Defining the connection attributes

The connection attributes define the connector element's function. In the most general case, the following attributes are specified:

- the connection type or types,
- the local directions associated with the connector's nodes,
- additional data for certain connection types and the connector behaviour.

Abaqus provides a comprehensive library of *connection types* that are divided into three categories: basic connection components, assembled connections, and complex connections. The basic connection components affect either translations or rotations on the second node. A connector element may include one translational basic connection component and/or one rotational basic connection component. The assembled connections are constructed from the basic connection components.

They are provided for convenience and cannot be combined in the same connector element definition with a basic connection component or other assembled connections. Complex connections affect a combination of degrees of freedom at the nodes in the connection and cannot be combined with other connection components.

4.2.2.2 Connector behaviour

Connector behaviours allow for modelling of the following types of effects:

- spring-like elastic behaviour;
- rigid-like elastic behaviour;
- dashpot-like (damping) behaviour;
- friction;
- plasticity;
- damage;
- stops;
- locks;
- failure;
- uniaxial behaviour.

Kinetic behaviour can be specified only in available components of relative motion. A connector behaviour can be specified in any of the following ways:

- *uncoupled*: the behaviour is specified separately in individual available components of relative motion;
- *coupled*: all or several of the available components of relative motion are used simultaneously in a coupled manner to define the behaviour; or
- *combined*: a combination of both uncoupled and coupled definitions are used simultaneously.

A conceptual model illustrating how connector behaviours interact with each other is shown in Figure 4-15. Most behaviours (elasticity, damping, stops, locks, friction) act in parallel. Plasticity models are always defined in conjunction with spring-like or rigid-like elasticity definitions. Degradation due to damage can be specified either for the elastic-plastic or rigid-plastic response alone or for the entire kinetic response in the connector. The failure behaviour apply to the entire connector response.

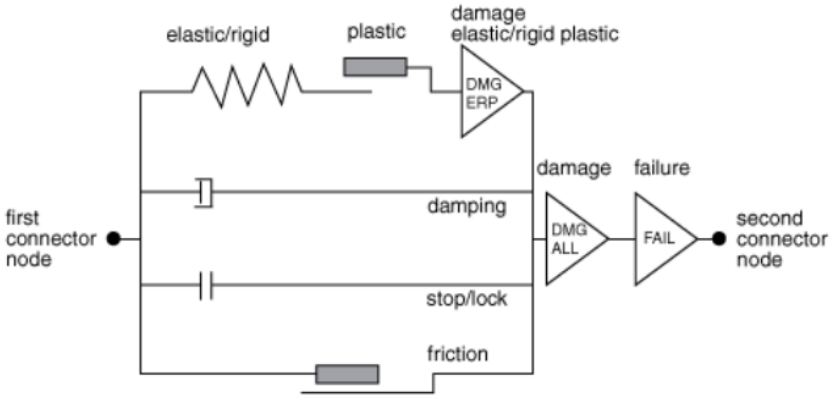

Figure 4-15 *Conceptual illustration of connector behaviours (from Smith et al.[56])*

Multiple definitions for the same behaviour type are permitted. For example, if connector elasticity (or damping) is defined several times in an uncoupled fashion for the same available component of relative motion, in a coupled fashion, or in both fashions, the spring-like (or dashpot-like) responses are added together. Multiple definitions of friction, plasticity, and damage behaviours are permitted as long as the rules outlined in the corresponding behaviour sections are followed. Multiple uncoupled stop and lock definitions for the same component are permitted, but only one will be enforced at a time.

Connector element behaviours allow for proper modelling of most physical connection behaviours within a single connector element. However, in rare circumstances more complex connection behaviours may require multiple connector elements to be used in *parallel* or in *series*. Is it possible to place connector elements in parallel by defining two or more connector elements between the same nodes. Similarly, it is possible to place connectors in series by specifying additional nodes (most often in the same location as the nodes of interest) and then stringing connector elements between these nodes.

4.2.2.2.1 Defining connector behaviour using tabular data

Tabular data are often used to define connector behaviours, such as nonlinear elasticity, isotropic hardening, etc. As shown in Figure 4-16, the data points make up a nonlinear curve in the constitutive space.

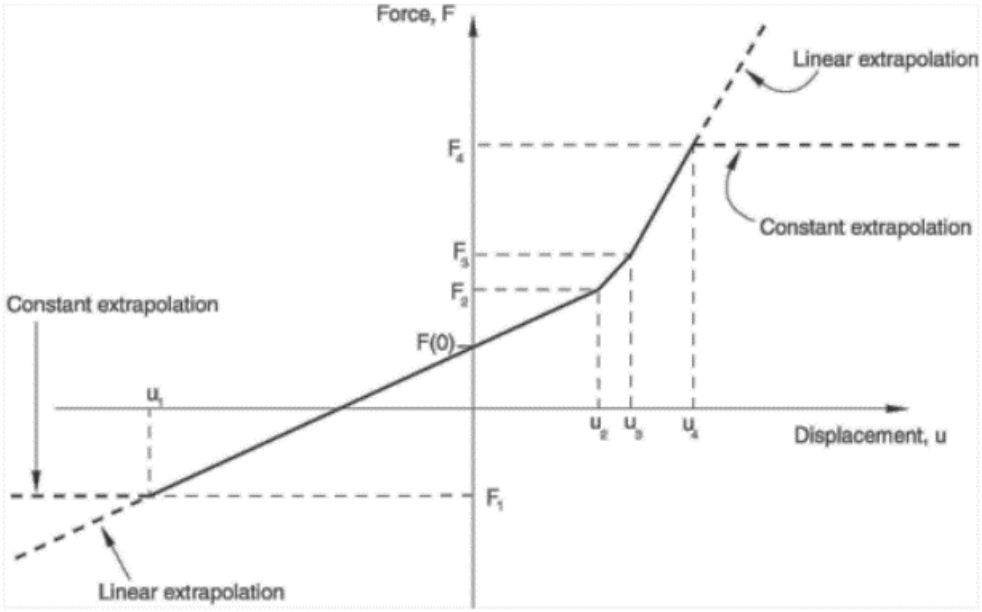

Figure 4-16 *Nonlinear connector behaviours defined as tabular data (from Smith et al.[56])*

By default, the dependent variables are extrapolated as a constant (with a value corresponding to the endpoints of the curve) outside the specified range of the independent variables. This choice may cause a zero-stiffness response, which may lead to convergence problems. Is it possible to specify linear extrapolation to extrapolate the dependent variables outside the specified range of the independent variables assuming that the slope given by the end points of the curve remains constant. The extrapolation behaviour is illustrated in Figure 4-16.

4.2.2.2.2 Connector plastic behaviour

Connector plasticity in Abaqus can be used to model plastic (irreversible) deformations of parts forming an actual connection device.

The plasticity formulation in connectors is similar to the plasticity formulation in metal plasticity described in section 4.2.1. In connectors the stress (σ) corresponds to the force (f), while the strain (ε) corresponds to the constitutive motion (u). Moreover, the plastic strain (ε^{pl}) corresponds to the plastic relative motion (u^{pl}), while the equivalent plastic strain ($\bar{\varepsilon}^{pl}$) corresponds to the equivalent plastic relative motion ($\bar{u}^{pl}$). The yield function (Φ) is defined as:

$$\Phi(\mathrm{f}, \bar{u}^{pl}) = P(\mathrm{f}) - F^0 \leq 0 \qquad \textit{(Eq. 4.9)}$$

where "f" represents the collection of forces and moments in the available components of relative motion that ultimately contribute to the yield function. The connector potential ($P(\mathrm{f})$) defines a magnitude of connector tractions similar to defining an equivalent state of stress in Mises plasticity and is either automatically defined by Abaqus or user-defined. Moreover, F^0 is the yield force/moment. The

connector relative motions (u) remain elastic as long as $\Phi < 0$. On the other hand, when plastic flow occurs, $\Phi = 0$.

If yielding occurs, the plastic flow rule is assumed to be associated; thus, the plastic relative motions are defined by:

$$\dot{u}^{pl} = \bar{u}^{pl} \frac{\partial \Phi}{\partial \mathrm{f}} \qquad \textit{(Eq. 4.10)}$$

where $\dot{u}^{pl}$ represents the rate of plastic relative motion and $\bar{u}^{pl}$ is the equivalent plastic relative motion rate.

Abaqus provides a number of *hardening models* varying from simple perfect plasticity to nonlinear isotropic/kinematic hardening. Connector hardening is analogous to the hardening models used in Abaqus for metals subjected to cyclic loading.

Isotropic hardening behaviour defines the evolution of the yield surface size (F^0) as a function of the equivalent plastic relative motion ($\bar{u}^{pl}$). This evolution can be introduced by specifying F^0 directly as a function of $\bar{u}^{pl}$ in tabular form or by using the simple exponential law:

$$F^0 = F|_0 + Q_\infty \left(1 - e^{-b\bar{u}^{pl}}\right) \qquad \textit{(Eq. 4.11)}$$

where $F|_0$ represents the yield value at zero plastic relative motion, while Q_∞ and b are material parameters. Q_∞ is the maximum change in the size of the yield surface, and b defines the rate at which the size of the yield surface changes as plastic deformation develops. When the equivalent force defining the size of the yield surface remains constant ($F^0 = F|_0$), there is no isotropic hardening.

When *nonlinear kinematic hardening* is specified, the centre of the yield surface is allowed to translate in the force space. The backforce (α) is the current centre of the yield surface. The yield surface is defined by the function:

$$\Phi := P(\mathrm{f} - \alpha) - F^0 \leq 0 \qquad \textit{(Eq. 4.12)}$$

where F^0 is the yield value and $P(\mathrm{f} - \alpha)$ is the potential with respect to the backforce α. The kinematic hardening component is defined to be an additive combination of a purely kinematic term (the linear Ziegler hardening law) and a relaxation term (the recall term) that introduces the nonlinearity. When temperature and field variable dependencies are omitted, the hardening law is

$$\alpha_k = C \cdot \frac{1}{F_0} \cdot (\mathrm{f} - \alpha) \cdot \dot{\bar{u}}^{pl} - \gamma \cdot \alpha \cdot \dot{\bar{u}}^{pl} \qquad \textit{(Eq. 4.13)}$$

where C and γ are material parameters that must be calibrated from cyclic test data. C is the initial kinematic hardening modulus, and γ determines the rate at which the kinematic hardening modulus decreases with increasing plastic deformation. When C and γ are zero, the model reduces to an isotropic hardening model. When γ is zero, the linear Ziegler hardening law is recovered.

4.2.3 Modelling

The BRB frame 3D Abaqus model is reported in Figure 4-17. Figure 4-18a shows the BRB devices, with a length of 1455 mm, placed in series with braces with a hollow circular section and lengths of 2326 mm and 2586 mm, respectively, for the first and second floor. As shown in Figure 4-18b, the diagonal brace was modelled in Abaqus through four elements in series: an *elastic element with a hollow section*, a *rigid element* and *two connectors* acting in parallel. It is worth mentioning that the first element was modelled elastic as it is overstrength compared to the BRB device, while the rigid element was included to take into account the actual dimensions of the dissipative element. In order to improve the connections between the components, two 25 mm plates were placed at the ends of the circular hollow element. Except for the connectors, all other components have been modelled as *solid elements* (C3D8R). Both the rigid element and the plates have a solid circular cross-section with a radius of 75 mm. On the other hand, the elastic brace cross-section has an external radius equal to 75 mm and a thickness of 10 mm. The material assigned to both the elastic brace and the connection plates was characterized by a Young's modulus of 210 GPa and a Poisson's coefficient equal to 0.3. Moreover, no plastic behaviour was defined since all the non-linearities were assumed to be concentrated in the connectors. On the other hand, a material with higher stiffness was assigned to the rigid element in order to ensure a rigid behaviour. To provide a uniform behaviour, all the diagonal elements have been connected by means of *tie constraints*.

The diagonal brace is linked to the column through a special designed *pinned connection*. Figure 4-19 compares the connection detail used in the test specimen with the one modelled in Abaqus. As above, all elements have been modelled as *solid elements* (C3D8R). The used connection is made up of stiffeners welded to a rectangular plate and connected to the BRB end connection through a pin. A *general contact*, characterized by a friction coefficient of 0.35 in the tangential behaviour and a "hard" contact in the normal behaviour, was defined to model the interaction between the connection stiffeners, the BRB end and the pin, as well as the interaction between the bolts, the rectangular plate and the column. Given that no deformation occurred in these elements during the test, a *perfectly elastic material* with a Young's modulus of 210 GPa and a Poisson's coefficient of 0.3 was assigned to them. Regarding the bolts, a *linear elastic-plastic* model was used to describe the

material behaviour, characterized by a Young's modulus of 200 GPa, a Poisson's coefficient of 0.3, a yield stress of 640 MPa and an ultimate stress of 800 MPa corresponding to an ultimate plastic strain of 0.178.

As in the former model, beams and columns were meshed using elements with an average size of 20 mm. The bolts and all areas with which they are in contact (column and rectangular connection plate) were meshed using an element with a dimension of approximately 5 mm. Figure 4-20 shows the mesh detail of the element involved in the connection between the BRB and the column.

The non-linear behaviour of the BRB device was modelled using a connector element. This element type was chosen because it allows complex relationships to be defined between the relative displacements of two distinct points. Even if connector element behaviours allow for proper modelling of most physical connection behaviours within a single connector element, in rare circumstances, more complex connections may require multiple connector elements to be used in parallel or in series. In this case, each BRB device was modelled through *two connectors in parallel*.

Figure 4-17 *Description of the 3D bare frame Abaqus model*

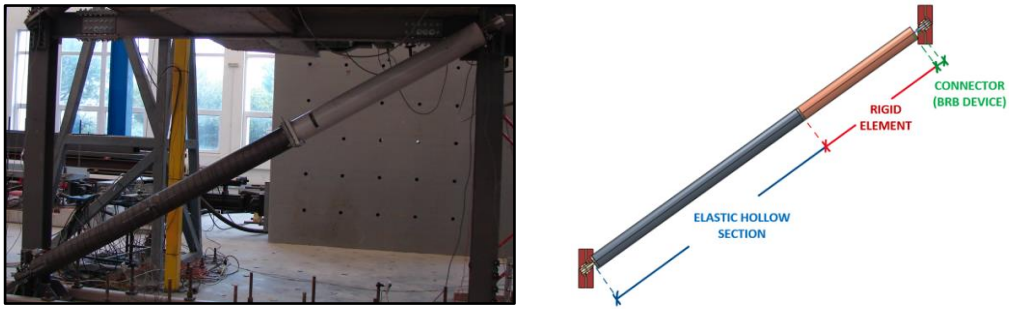

(a) (b)

Figure 4-18 *Diagonal Brace: (a) Test specimen; (b) Abaqus model*

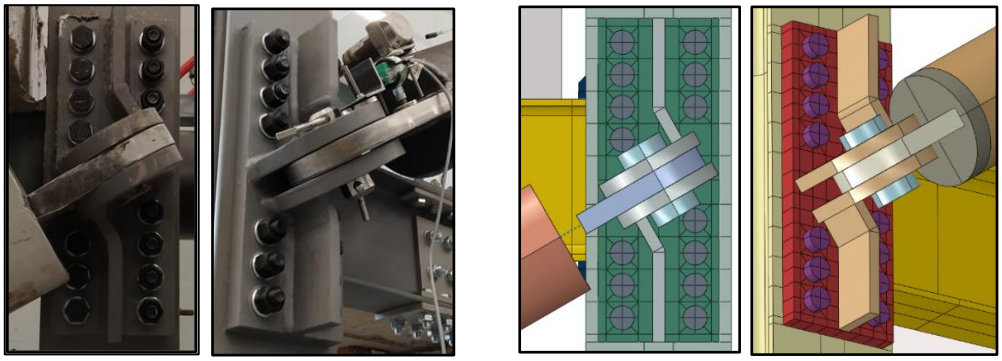

(a) (b)

Figure 4-19 *BRB to Column Connection: (a) Test specimen, (b) Abaqus model*

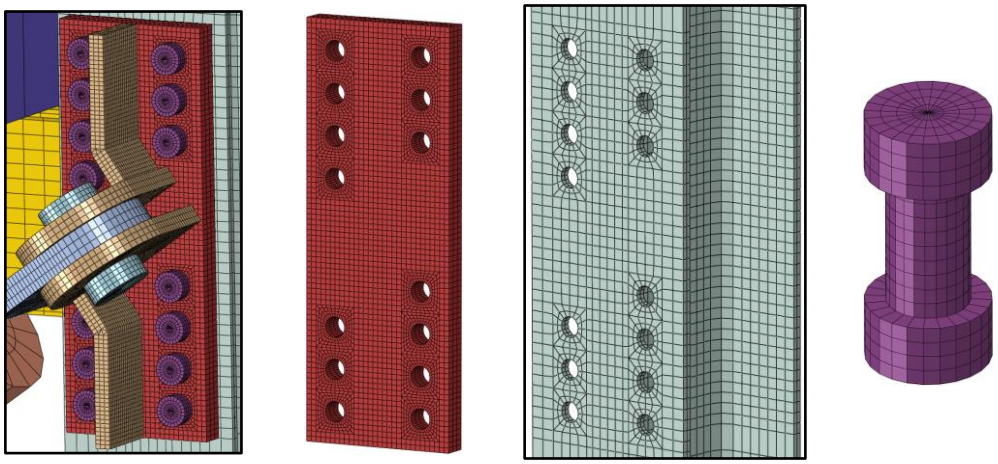

(a) (b) (c) (d)

Figure 4-20 *Mesh detail of BRB to Column Connection: (a) Connection, (b) Plate, (c) Column, (d) Bolt.*

4.2.4 Validation

As in the previous case, the numerical simulations were performed through two steps: the Gravity and the Pseudo Dynamic analysis. The Pseudo Dynamic analysis was conducted by imposing the same horizontal floor displacements applied during the tests. In particular, the displacements were imposed on two different control points belongings to the top surface of the slab. The control points enforced the top surface of the slab to undergo the same horizontal displacement through coupling constraint. Quasi-static analysis in the implicit dynamic analysis category was selected for the Pushover analysis. As mentioned in the previous paragraph (3.2.4.2), the BRB frame was subjected to two PsD tests in which the same ground motion was scaled through two different scale factors: 1.0 and 1.5, respectively. The following section presents the validation of the model considering one scaled ground motion only (SF = 1). The comparison between the Abaqus model and test results regarding the other scale factor is presented in Appendix B.

In order to validate the FE model, comparisons were made in terms of actuator forces, floor stiffness and local stress. In the following paragraphs, before showing the test measurements together with the Abaqus results, the connector calibration and validation are reported.

4.2.4.1 Connector calibration

The connector type and parameters were evaluated to provide a realistic representation of the BRB device. As mentioned before, to improve the accuracy of results, the BRB device was modelled using two connectors placed in series. The choice of including a second connector was guided by the awareness that, although only one pair of kinematic hardening parameters can be assigned to each connector, usually more than one pair of parameters is required to better capture the non-linear cyclic behaviour of the device. For each connector was defined a local rectangular coordinate system (CSYS) having the local z-axis coincident with the BRB axis.

In order to assign the stiffness for all the components of relative motions (CORM), a Cartesian and Rotation type element was assigned to the first connector. A linear and uncoupled behaviour was used to define the elastic response of the connector. The axial stiffness (D33) was calibrated from the characteristics provided by the supplier and shown in Figure 4-21 in grey. On the other hand, the shear (D11, D22), the bending (D44, D55) and the torsional (D66) stiffnesses were defined considering the contribution provided by the encasing mortar and the external steel tube. For the axial behaviour only (D33), a plastic behaviour was defined by directly assigning isotropic and kinematic hardening parameters. All the parameters are shown in Table 4-4.

Considering that the aim was to improve the accuracy of the results by adding more isotropic hardening parameters, a Cartesian type element was assigned to the

second connector. The axial (D33) and shear (D11, D22) stiffness values were evaluated to ensure that the system of two connectors in series could be representative of the actual BRB device behaviour. Due to the previously mentioned reason, a kinematic hardening only was defined for the axial plastic behaviour of the second connector. All the parameters are shown in Table 4-5.

As shown in Figure 4-21, when calibrating the connector parameters, the asymmetrical behaviour of the BRB was neglected. This topic is dealt with in more detail in chapter 4.2.5.

Table 4-4 *Connector section 1*

Elasticity								
Definition	F, M	Coupling	D11	D22	D33	D44	D55	D66
Linear	All	Uncoupled	1.00E+10	1.00E+10	88000	1.95E+09	1.95E+09	4.97E+07
Plasticity								
			Isotropic Hardening			**Kinematic Hardening**		
Definition	Coupling	F, M	Yield F/M	Qinf	b	Yield F/M	C	gamma
Nonlinear	Uncoupled	F3	75000	75000	0.003	75000	55000	1.25

Table 4-5 *Connector section 2*

Elasticity								
Definition	F, M	Coupling	D11	D22	D33	D44	D55	D66
Linear	F1, F2, F3	Uncoupled	1.00E+10	1.00E+10	100	[-]	[-]	[-]
Plasticity								
			Isotropic Hardening			**Kinematic Hardening**		
Definition	Coupling	F, M	Yield F/M	Qinf	b	Yield F/M	C	gamma
Nonlinear	Uncoupled	F3	[-]	[-]	0. [-]	85.2	3000	0.25

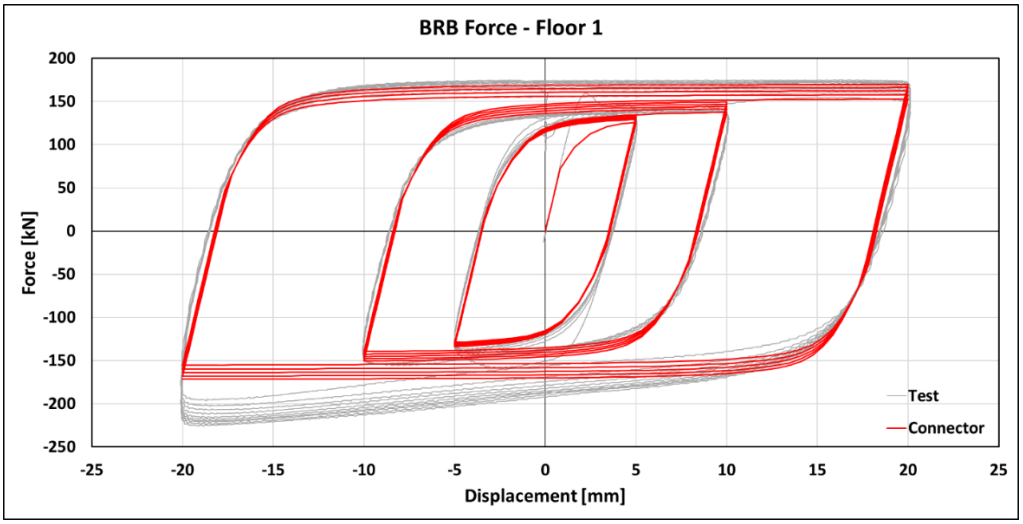

Figure 4-21 *BRB Cyclic Behaviour*

4.2.4.2 Ground Motion (SF=1)

Figure 4-22 shows the displacement history imposed on the first and second floor during both the test and the numerical simulation. The first comparison between the test specimen and the FE model was made in terms of actuator forces, *i.e.*, comparing the forces required to impose the predefined displacement. Figure 4-23 shows the actuator force applied during the test compared with the one obtained through Abaqus. Although a good match can be achieved, it can be seen that at some isolated points, an error of around 40% is observed. Explanations for such behaviour can be related to the limitations of the model as discussed in section 4.2.5. It is worth mentioning that in order to highlight the differences, the most relevant steps only are shown. As shown in Figure 4-24, the second comparison was made in terms of the forces acting within the BRB forces. Once again, even if the error between the two values could reach approximately 50%, it can be seen that the Abaqus model successfully captures the experimental results. It can be seen that the highest error recorded in the actuator forces (i.e. 40%) turned out to be lower than the maximum error recorded in the BRB forces (i.e. 50%). This can be attributed to the gap in the connection, which is discussed in more detail in section 4.2.5. Nevertheless, as shown in Figure 4-25, the comparison in terms of floor stiffness demonstrate an excellent match between the two models. Figure 4-26 shows the BRBs behaviour recorded throughout the Abaqus simulations. Given that the BRB core elongation was not measured throughout the first test (SF=1), no comparison could be made for this parameter. Nonetheless, as discussed in the following sections (4.2.6), these graphs turn out to be crucial when investigating the effectiveness of the intervention. As in the previous cases, Figure 4-27, Figure 4-28, Figure 4-29 and Figure 4-30 show the comparison between the values obtained

from the strain gauges placed on the column and the corresponding values obtained from Abaqus. Once again, a good matching between the two models is shown.

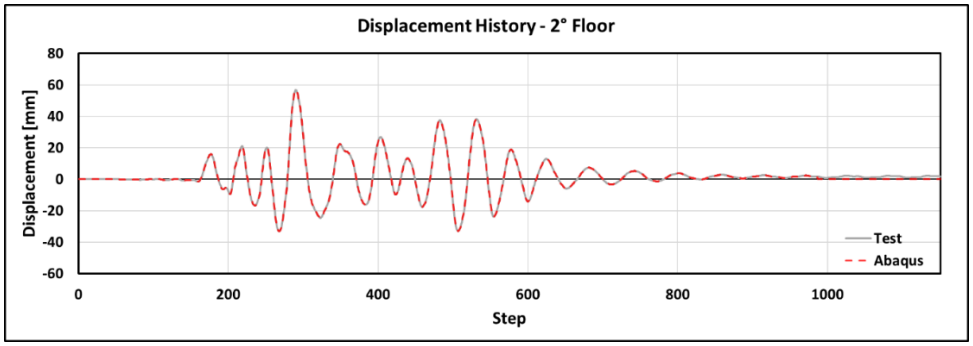

(a)

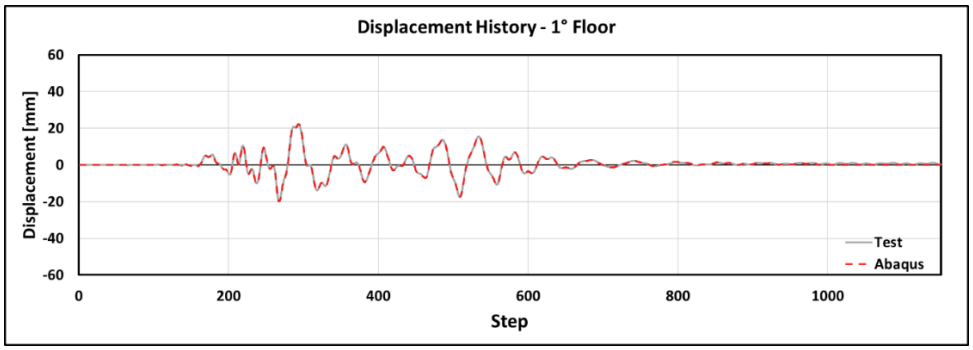

(b)

Figure 4-22 *Displacement History: (a) Second Floor; (b) First Floor.*

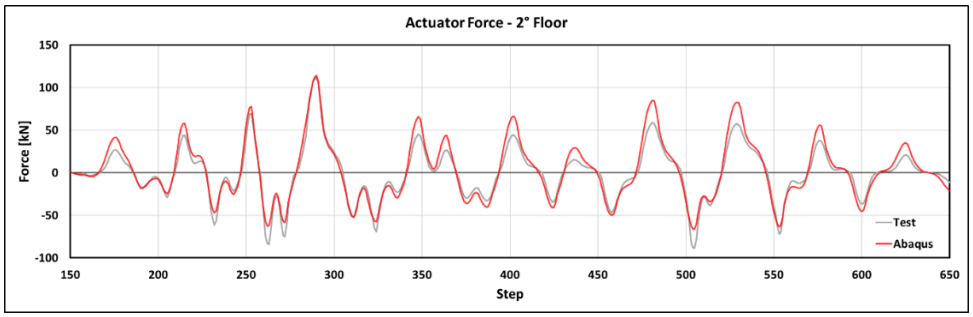

(a)

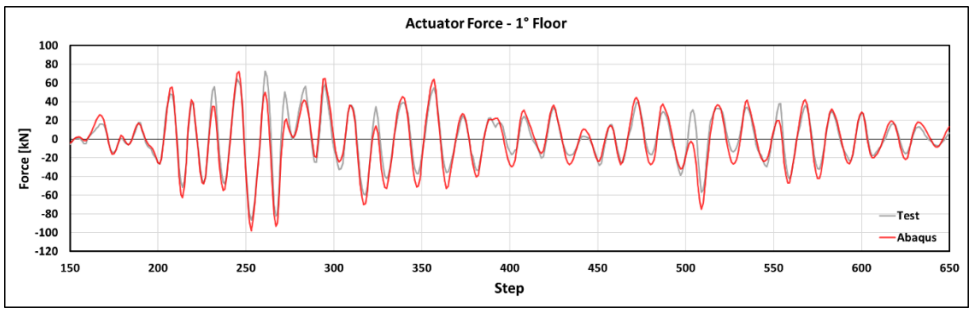

(b)

Figure 4-23 *Actuator Force: (a) Second Floor; (b) First Floor*

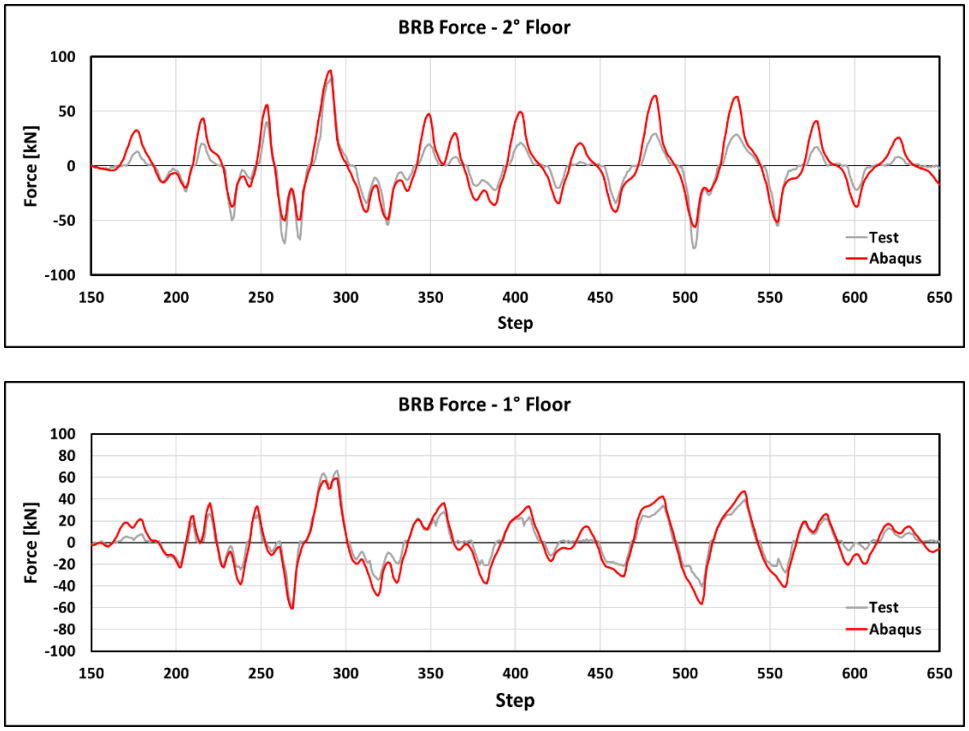

(a)

(b)

Figure 4-24 *BRB Force: (a) Second Floor; (b) First Floor*

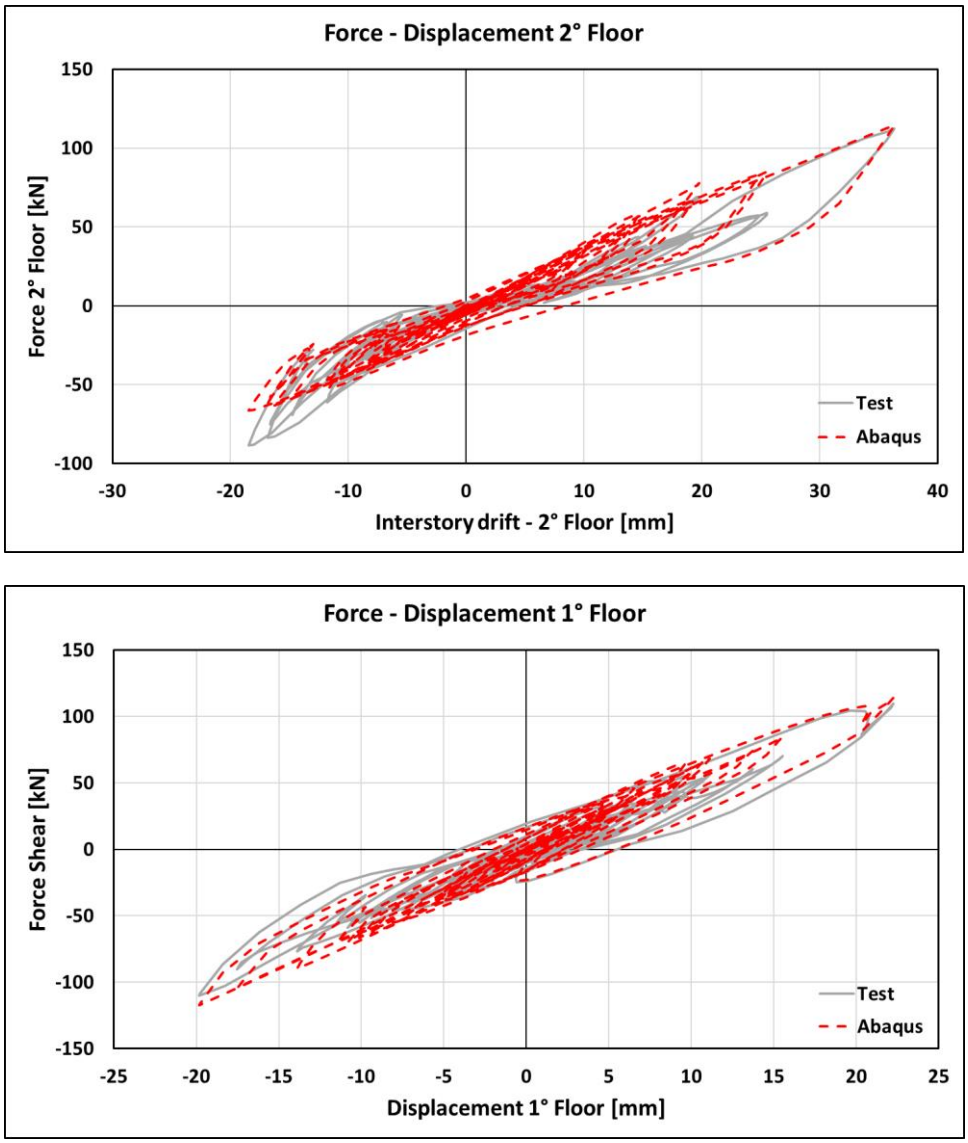

Figure 4-25 *Floor Stiffeness: (a) Second Floor; (b) First Floor.*

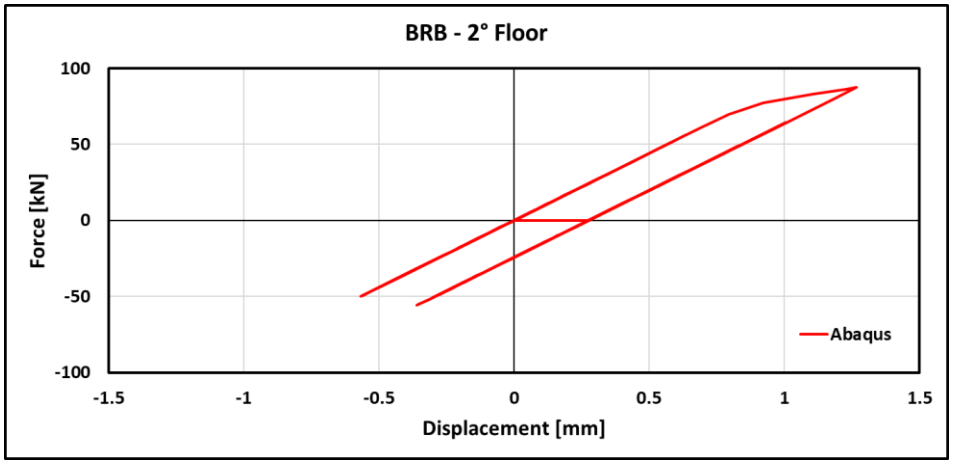

(a)

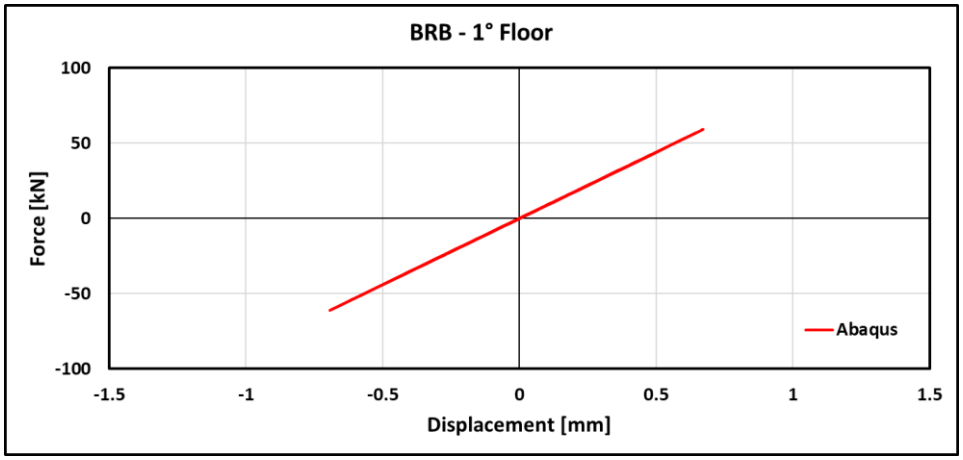

(b)

Figure 4-26 *BRB behaviour: (a) Second Floor; (b) First Floor.*

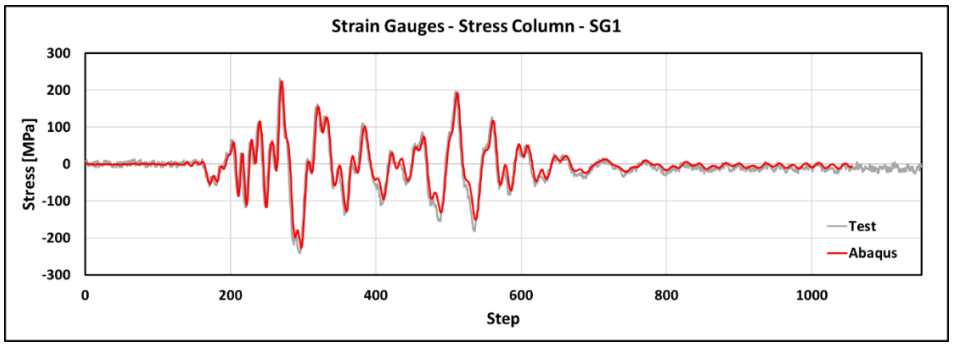

(a)

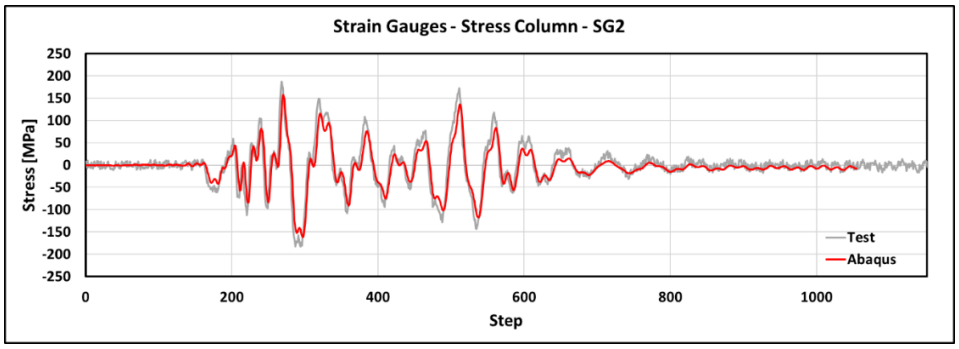

(b)

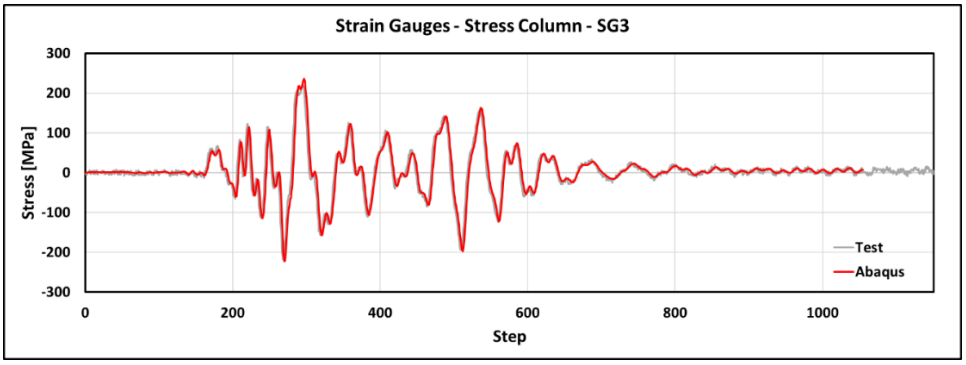

(c)

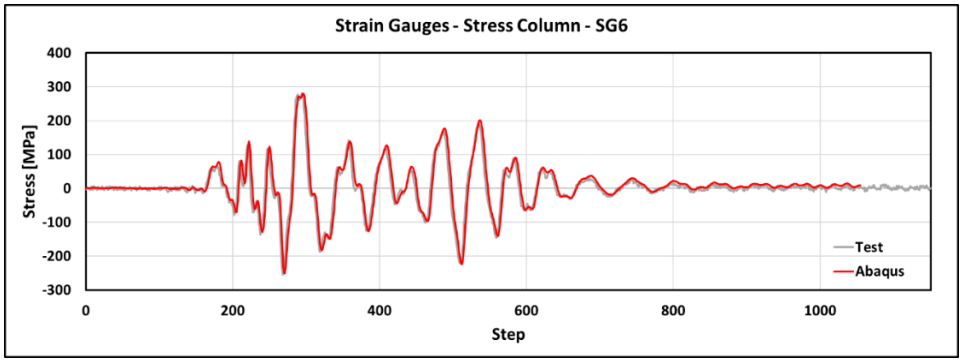

(d)

Figure 4-27 *Column Flange Strain Gauges - Detail 1: (a) SG1, (b) SG2, (c) SG3, (d) SG6*

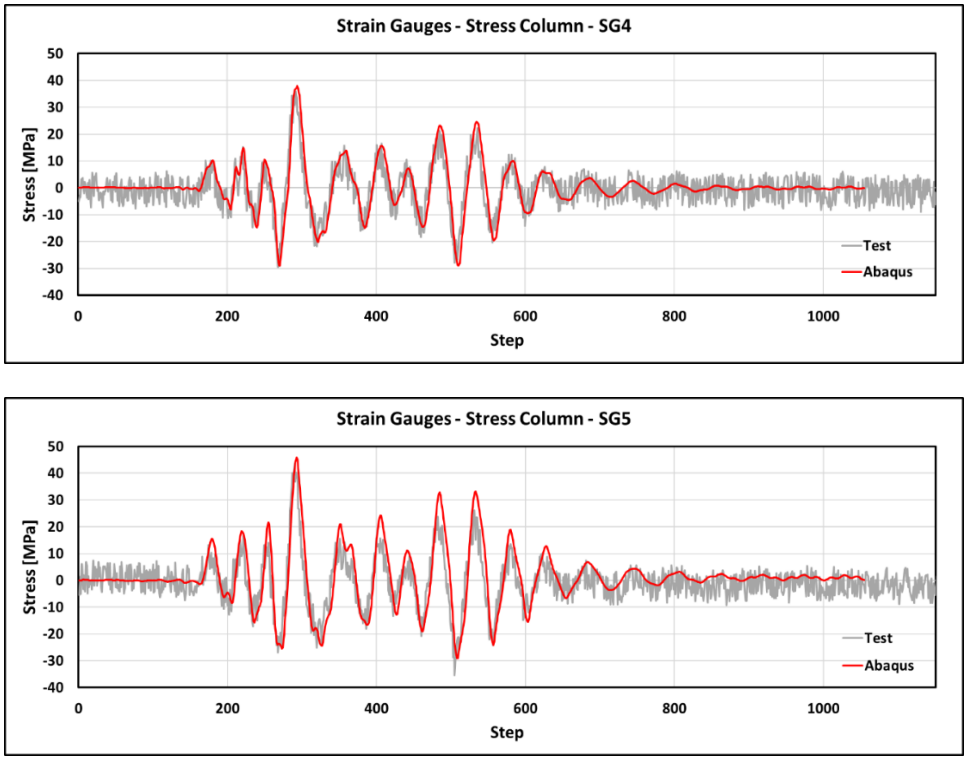

Figure 4-28 *Column Web Strain Gauges - Detail 1: (a) SG4, (b) SG5*

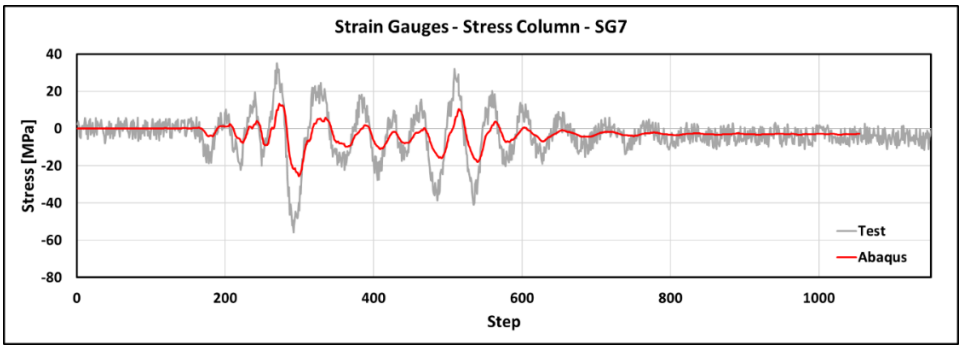

(a)

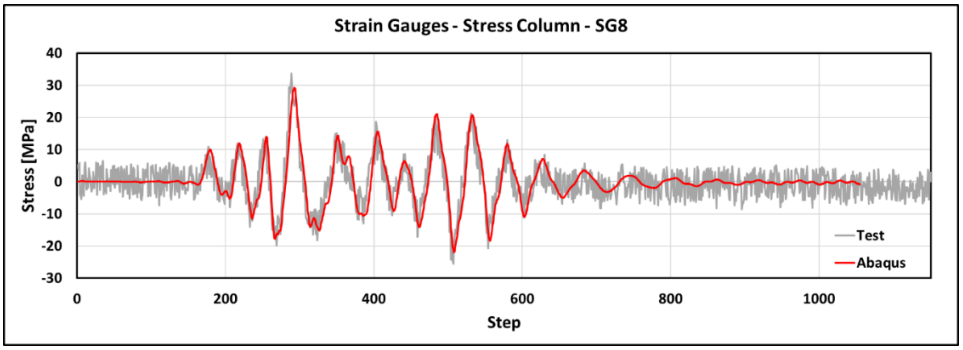

(b)

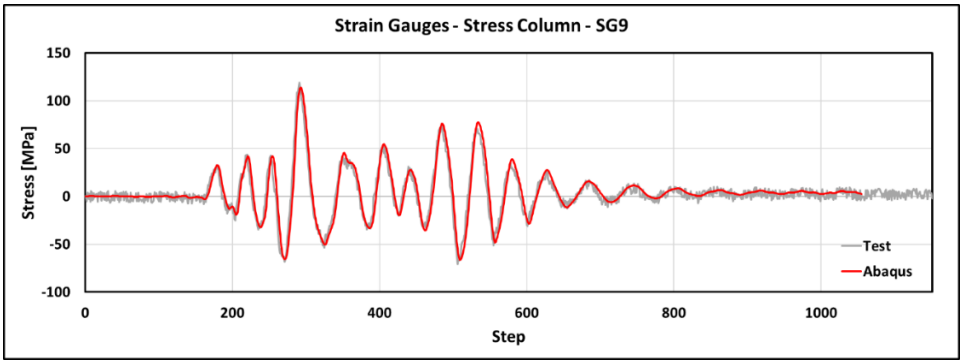

(c)

Figure 4-29 *Column Flange Strain Gauges - Detail 2: (a) SG7, (b) SG8, (c) SG9*

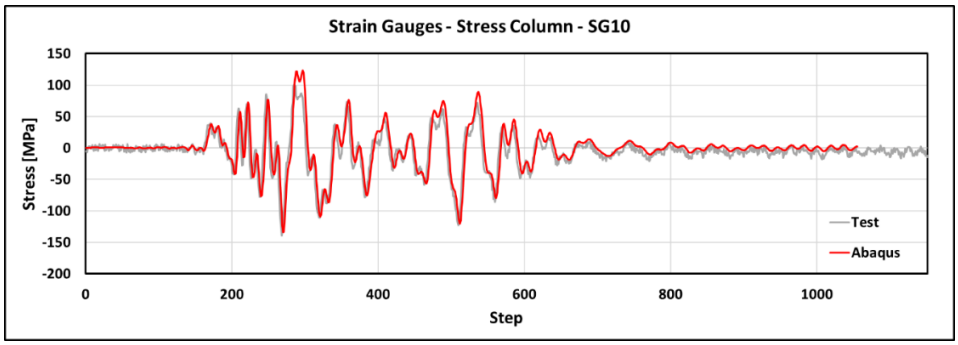

(a)

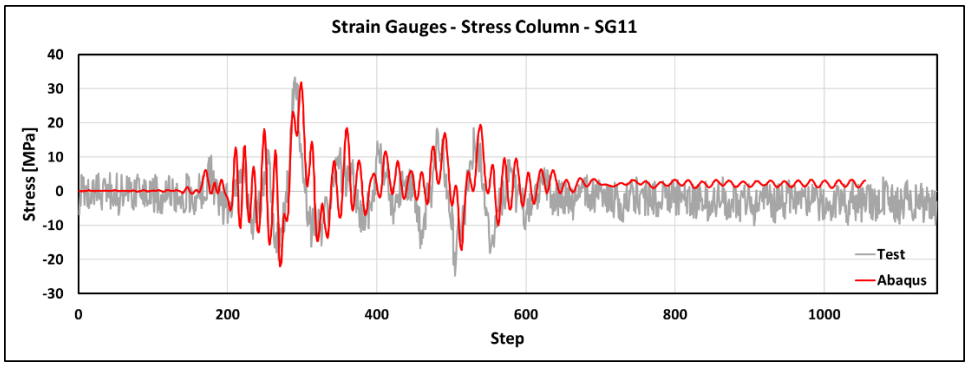

(b)

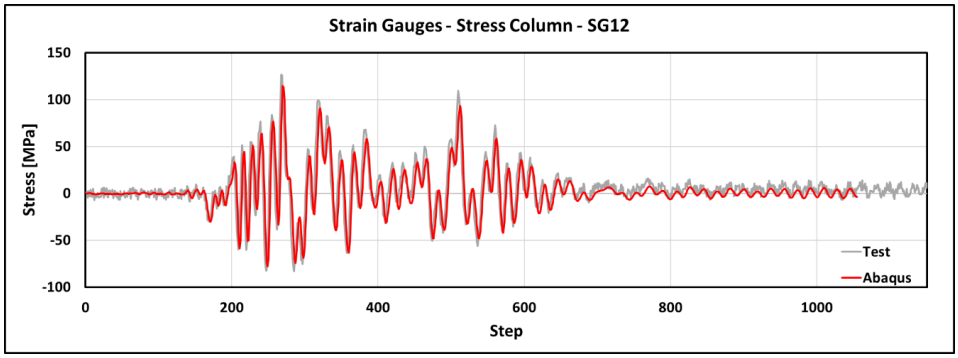

(c)

Figure 4-30 *Column Flange Strain Gauges - Detail 3: (a) SG10, (b) SG11, (c) SG12*

4.2.4.3 Failure modes

The Abaqus model was found to be capable of reproducing the failure mechanisms that affected the tested frame. In particular, Figure 4-31a shows a concentration of stresses in the area where the column web experienced fracture during the test (Figure 4-31b). In addition, Figure 4-32 shows the excessive deformations of a column at two nodal sections and the resulting high out-of-plane displacements observed during the experimental tests (3.2.6). On the other side, considering the modelling strategy adopted for the BRBs, it is clear that the Abaqus model cannot adequately model the contact between the BRBs and the columns (Figure 3-21b, c). In fact, considering that a gap of 30mm has been included in the BRB model, it is expected that the contact between the BRBs and the columns occurs for higher inter-storey drifts than those experienced throughout the test.

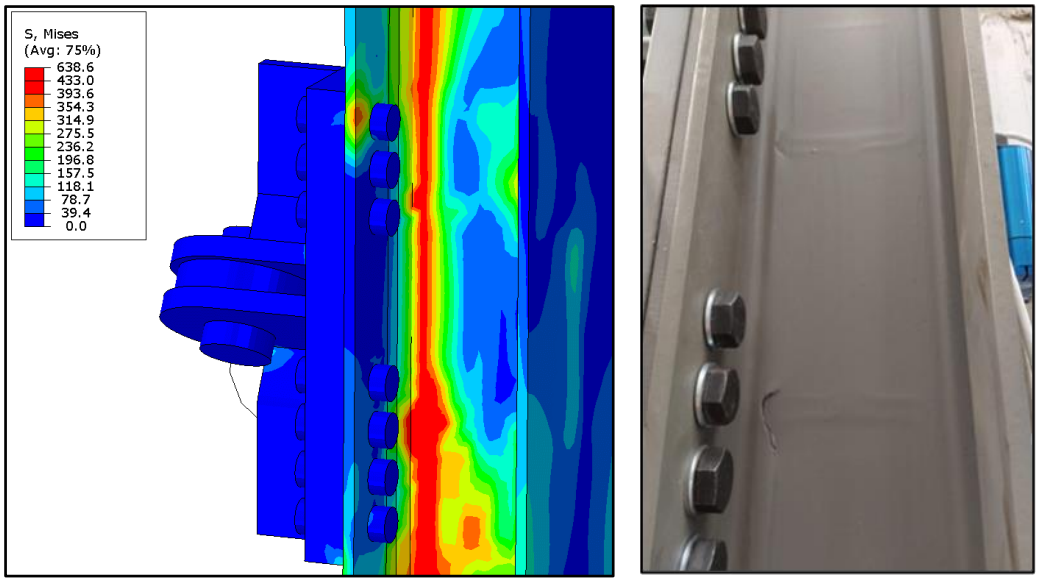

(a) (b)

Figure 4-31 *Column local deformation: (a) Abaqus model; (b) Tested frame*

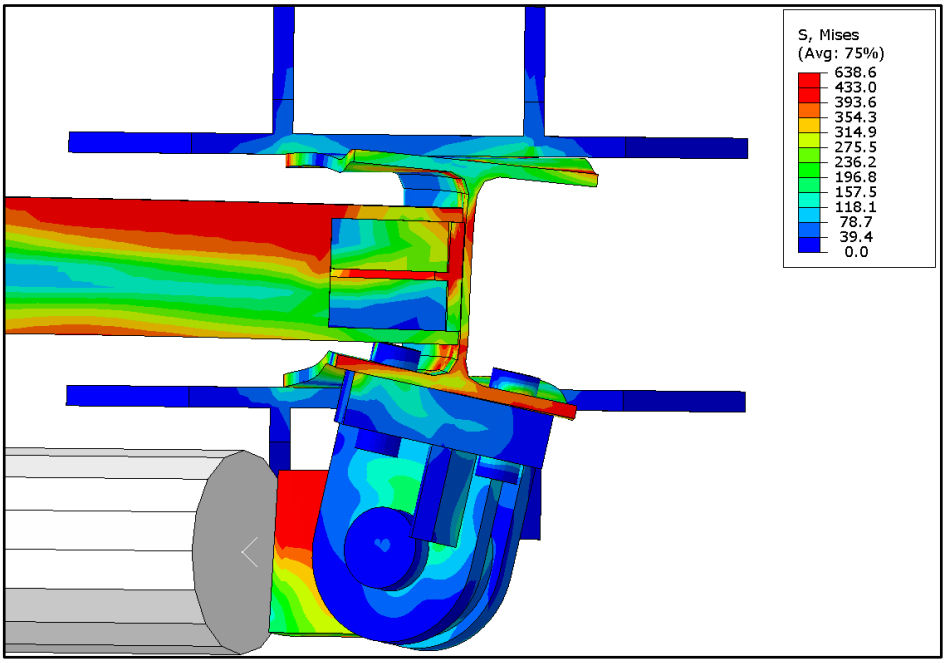

(a)

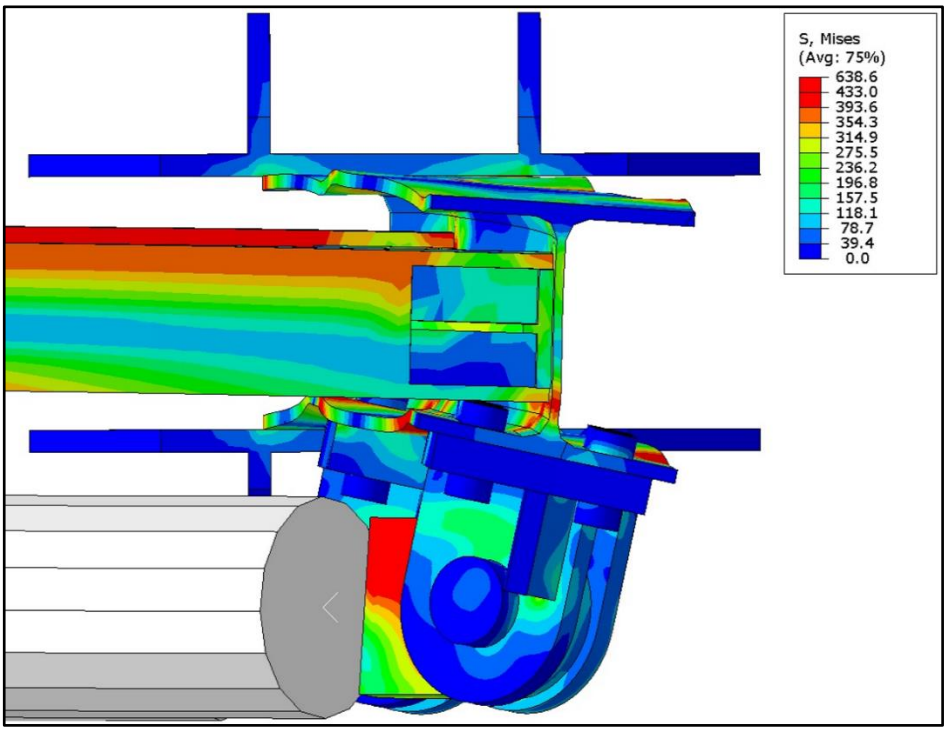

(b)

Figure 4-32 *Column deformation and out of plane displacements: (a) first floor, (b) second floor*

4.2.5 Modelling limitations

The model presented in the previous Sections (4.2.3) is affected by a few limitations that prevent it from completely recreating the test set-up conditions.

As already shown in 4.2.4.1, the most evident limitation consists in BRB cyclic behaviour. In fact, the strength increase of the BRB in compression was neglected, thus assigning to the dissipative element a symmetrical cyclic behaviour.. The choice of not modelling the strength increase of 25% that occurs in compression for high plastic deformations is related to the difficulties in modelling this behaviour through a connector element. The real behaviour of the BRB could have been considered by modelling each part of the BRB in detail and calibrating the different material parameters to assign to the BRB core [68,69]. However, given that the aim of the model is to study the overall behaviour of the frame, detailed modelling of the BRB was ruled out. In the following Sections (5) this limitation will be overcome by performing Pushover analyses where the monotonic behaviour of the BRBs is considered both in tension and compression, accounting for the asymmetry of the devices.

A further limitation consists in the modelling of the pinned connection between the BRB and the column. As shown in Figure 4-33a, in the test specimen, the pin diameter does not coincide with the dimension of the hole. On the contrary, as shown in Figure 4-33b, in the Abaqus model, the pin diameter perfectly fits into the hole of the connecting element. As demonstrated by the graphs shown in Figure 4-34 and Figure 4-35, the different size between the pin and the hole causes slippage of the BRB up to 4 mm. Given that, it is expected that under the same inter-storey drift, the elongations to which the BRB is subjected in Abaqus is greater than the ones recorded during the test. As a result, the numerical model turns out to be more rigid than the real one, thus leading to an increase in the recorded forces.

As already mentioned in 4.2.4.3, the Abaqus model appears to be inadequate to model the contact between the BRBs and the columns. However, considering that this issue can be overcome by modifying the connection system, the retrofit strategy through external BRBs is still considered viable, and its effectiveness is studied in the following sections (5).

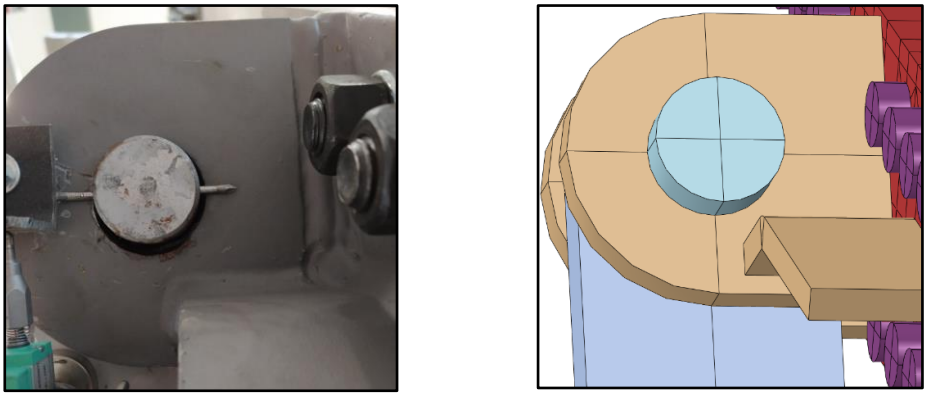

(a) (b)

Figure 4-33 *Detail of the pinned connection between the BRB and the column: (a) Test specimen, (b) Abaqus model*

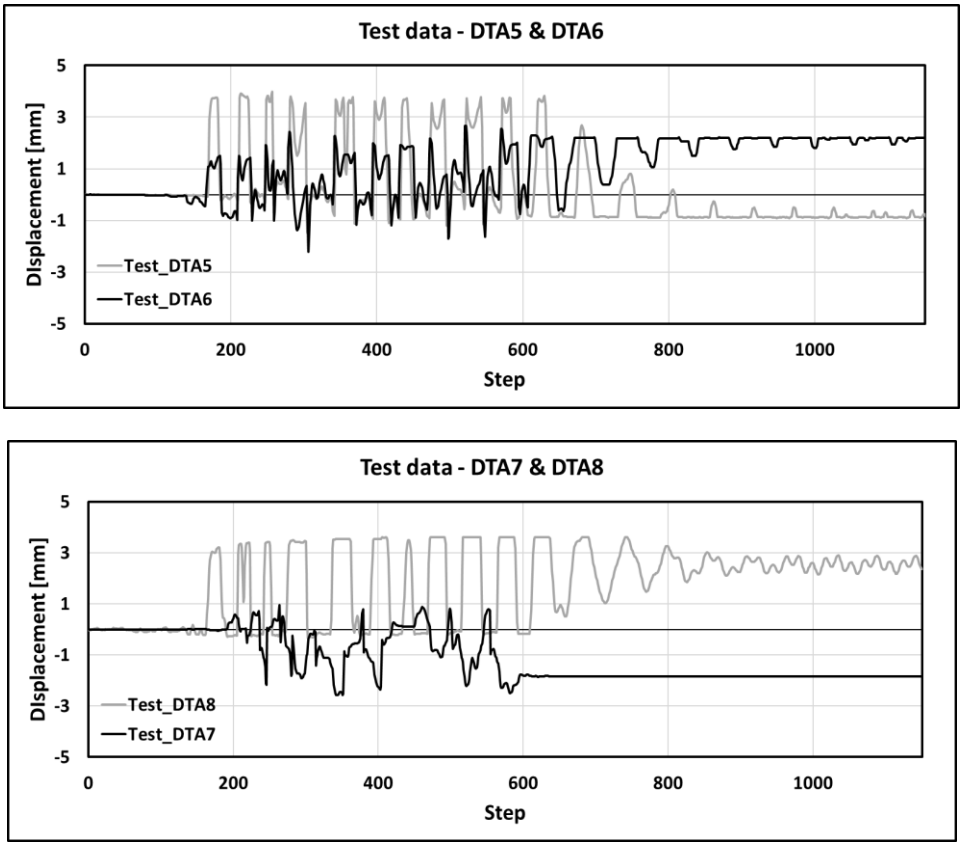

(a)

(b)

Figure 4-34 *BRB slippage (Test with SF 1): (a) Second Floor, (b) First Floor*

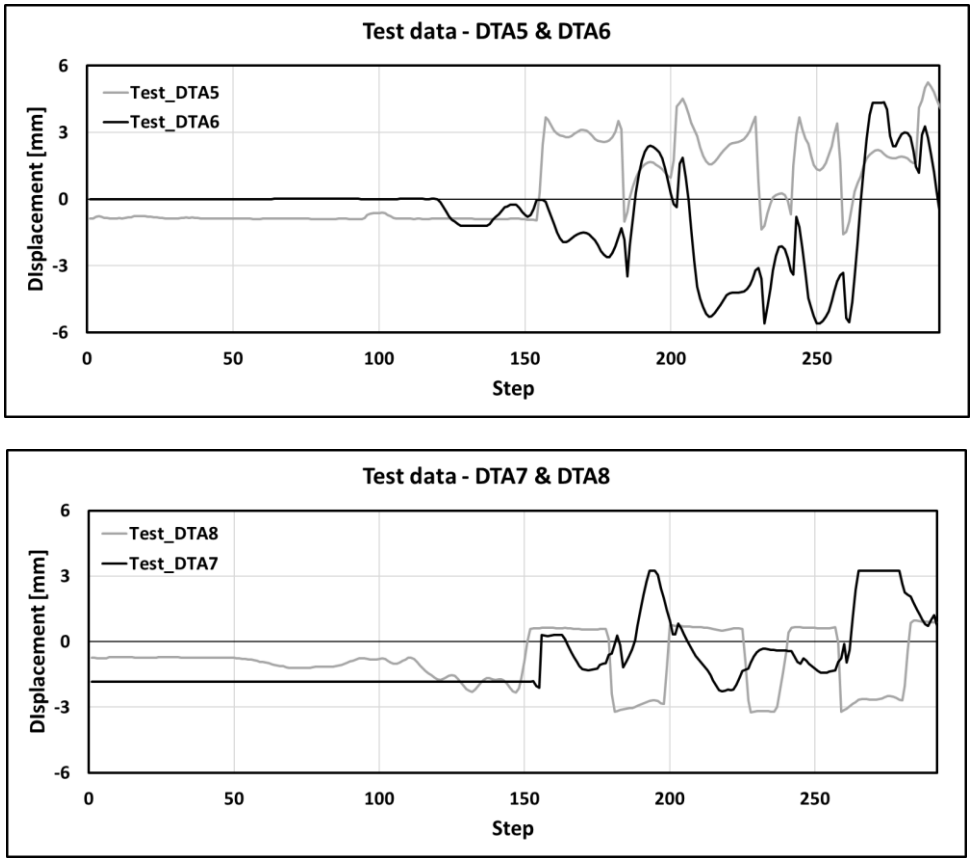

Figure 4-35 *BRB slippage (Test with SF 1.5): (a) Second Floor, (b) First Floor*

4.2.6 Conclusions

When comparing the in-plane stiffnesses of the BRB frame (Figure 4-25) and Bare frame (Figure 4-9), it is evident that the retrofit intervention provided an increase in frame stiffness and strength. Nonetheless, as shown in Figure 4-26, BRBs are found to remain almost entirely in the elastic range, thus resulting in nearly zero increase in the dissipative capacity of the frame. Considering that the main objective of the retrofit intervention consists in increasing the dissipative capacity of the frame other than its strength and stiffness, it can be stated that, under the test conditions, this retrofit intervention appears to be unsatisfactory. The following chapter (5) presents the study conducted to identify the parameters that determine this behaviour and the evaluation of their influence.

Due to the high computational effort resulting from the detailed modelling of connections using mechanical elements, a simplified model is referred to from now on. As shown in Figure 4-36, the introduced simplification consists in modelling the connection between the BRB and the column through tie constraints between the plate and the flange of the column instead of using bolts. This decision is derived from the observation that the introduction of such a simplification does not significantly alter the results and also brings a computational benefit. This can be

observed in Figure 4-37, where the in-plane stiffnesses of the two models are compared.

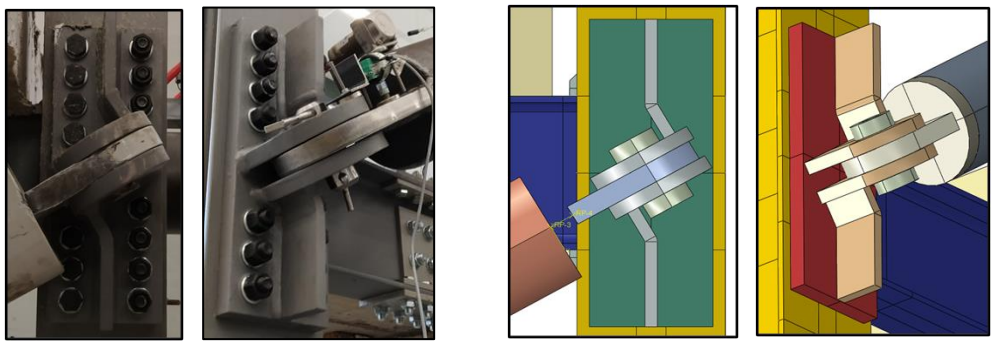

(a) (b)

Figure 4-36 *BRB to Column Connection: (a) Test specimen, (b) Abaqus model*

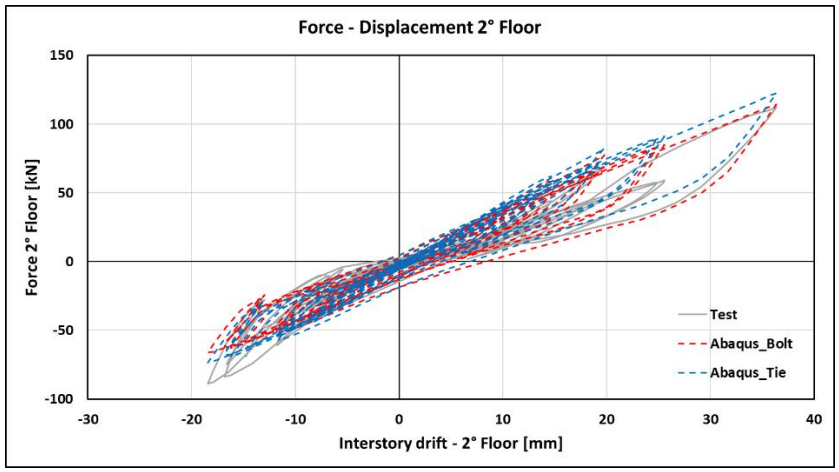

(a)

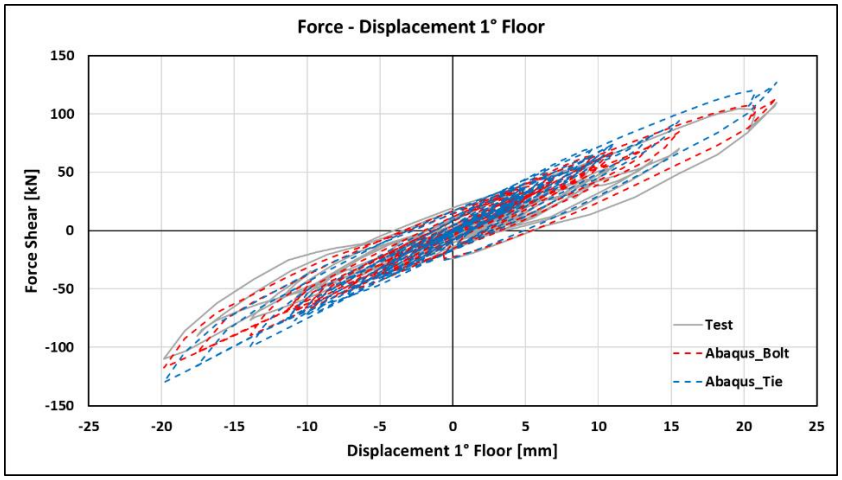

(b)

Figure 4-37 *Comparison between Floor Stiffeness in the model with bolt (Abaqus_Bolt) and the simplified model (Abaqus_Tie): (a) Second Floor; (b) First Floor.*

5 Retrofit Strategies Limitations

5.1 Introduction

5.1.1 Objectives

The outcomes of both test results and numerical analysis illustrated in the previous chapters (3, 4) highlighted the limitation of the retrofit strategy and the need for careful considerations about the connection of the BRBs with the existing structure. As discussed in the present chapter, a critical aspect is the distortional deformability of the column and its torsional stiffness. The following models have been created to further discuss and analyse these aspects:

- An equivalent model with BRBs positioned in-plane with respect to the frame;
- An equivalent model with BRBs positioned externally with respect to the frame aided with torsional and distortional constraints for the columns and the joints.

The comparison between these two models and the validated model from the experimental tests highlighted the influence of the torsional and distortional deformability of the column on the inelastic response and hence on the dissipative capacity of the BRBs.

Subsequently, the influence of the torsional and distortional deformability of the column on the structural behaviour of the frame was investigated by considering the following models:

- A model with external BRBs and torsional constraints only;
- A model with external BRBs and distortional constraints only;

Finally, after demonstrating that a distortional constraint is essential to increase the effectiveness of the retrofit intervention, a parametric analysis is conducted to evaluate the behaviour of the frame for different column torsional stiffnesses. To this aim, the following model was considered:

- Several models with external BRBs and distortional constraints together with torsional springs characterised by different values of the stiffness.

5.1.2 BRB Device Model

To overcome the limitation related to the inaccurate modelling of the BRB cyclic behaviour, pushover analyses were performed. Therefore, an update of the BRB device model was required. As in previous models, the BRB device was modelled through two connectors placed in series. However, different parameters were assigned to accurately model the behaviour in tension and compression differently.

In order to assign the stiffness for all the components of relative motions (CORM), a Cartesian and Rotation type element was assigned to the first connector. A linear and uncoupled behaviour was used to define the elastic response of the connector. The shear (D11, D22), the bending (D44, D55) and the torsional (D66) stiffnesses were defined considering the contribution provided by the encasing mortar and the external steel tube. The smooth transition from the elastic to the plastic range was modelled by assigning to the axial behaviour only (D33) a plastic behaviour through kinematic hardening parameters (Table 5-1 and Table 5-3). Finally, the slope of the hardening branch was modelled through an Axial connector placed in series with the previous one (Table 5-2 and Table 5-4). The axial (D33) stiffness of both connectors was evaluated to ensure that the system of two connectors in series could represent an envelope of the actual BRB device behaviour (Figure 5-1 and Figure 5-2).

Table 5-1 *Elasto-plastic Connector (tension)*

Elasticity								
Def.	F, M	Coupling	D11	D22	D33	D44	D55	D66
Linear	All	Uncoup.	1.00E+10	1.00E+10	85756	1.95E+09	1.95E+09	4.97E+07
Plasticity								
				Kinematic Hardening				
Def.	Coupling	F, M	Yield F/M	C		gamma		
Nonlin.	Uncoup.	F3	68215	65000		1.25		

Table 5-2 *Elastic Connector (tension)*

Def.	F, M	Coupling	D11
Linear	F1	Uncoup.	2243

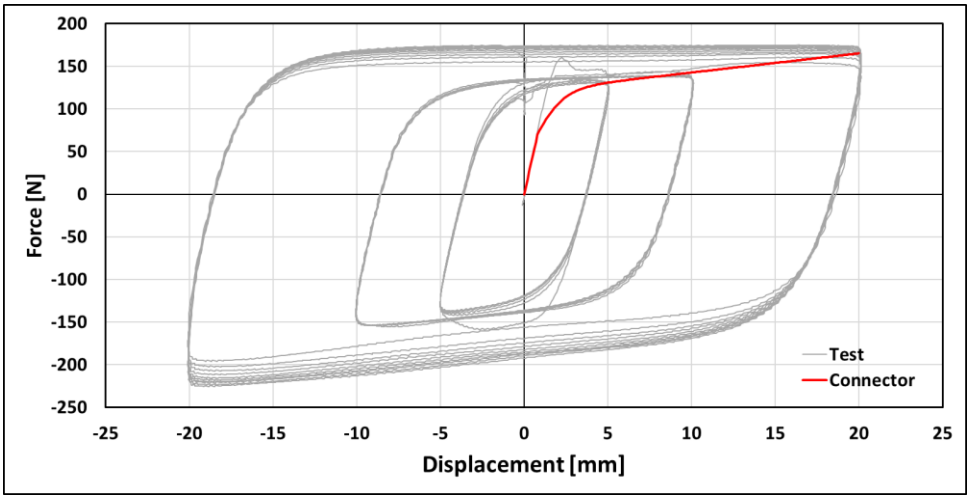

Figure 5-1 *BRB cyclic behaviour vs. Connector monotonic behaviour (tension)*

Table 5-3 *Elasto-plastic Connector (compression)*

Elasticity								
Def.	F, M	Coupling	D11	D22	D33	D44	D55	D66
Linear	All	Uncoup.	1.00E+10	1.00E+10	82851	1.95E+09	1.95E+09	4.97E+07
Plasticity								
					Kinematic Hardening			
Def.	Coupling	F, M	Yield F/M		C		gamma	
Nonlin.	Uncoup.	F3	65904		65000		1.25	

Table 5-4 *Elastic Connector (compression)*

Def.	F, M	Coupling	D11
Linear	F1	Uncoup.	5148

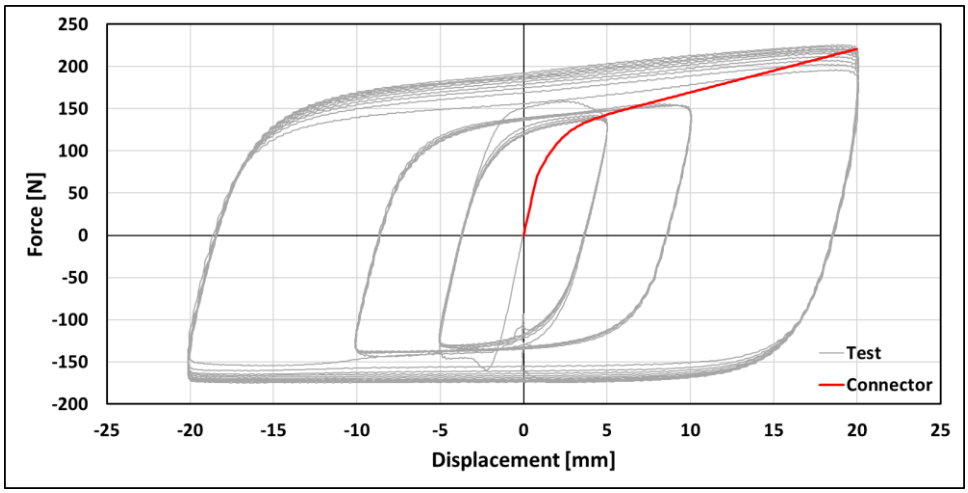

Figure 5-2 *BRB cyclic behaviour vs. Connector monotonic behaviour (compression)*

5.1.3 Nonlinear Static Analysis

As mentioned in a previous chapter (2.1.2), according to both EC8-1 and EC8-3, at least two vertical distributions of lateral loads should be applied: a "uniform" pattern, based on lateral forces that are proportional to mass regardless of elevation (uniform response acceleration) and a "modal" pattern, proportional to lateral forces consistent with the lateral force distribution determined in elastic analysis. However, as a first attempt, the second pattern only was applied. To this end, a modal dynamic analysis was conducted on both the bare frame and the BRB frame. The dynamic properties of the fundamental mode in the direction of interest are reported in Table 5-5 and illustrated in Figure 5-3. Therefore, an inverse triangular pattern consistent with the modal shape of interest was applied. The pushover analysis was conducted up to a top displacement of 285mm, which corresponds to an interstory drift of 6.0% at both storeys.

Table 5-5 *Dynamic properties of fundamental period*

Bare Frame			BRB Frame		
T	[sec]	0.5	T	[sec]	0.1
Modal	[2° Floor]	1	Modal	[2° Floor]	1
Shape	[1° Floor]	0.39	Shape	[1° Floor]	0.49

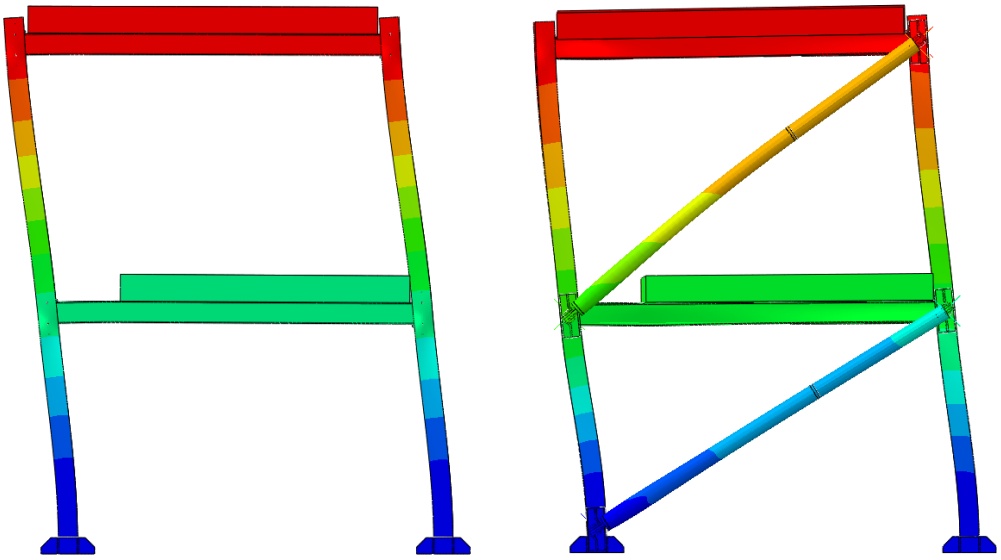

(a) (b)

Figure 5-3 *Fundamental mode shape in the direction of interest: (a) Bare Frame, (b) BRB Frame*

5.2 BRB Frame

The first step undertaken at this stage of the study was to conduct pushover analyses on the following models:

- The Bare Frame model;
- The BRB Frame model (test conditions).

The two models are shown in Figure 5-4. The Bare Frame model (Figure 5-4a) was modelled in accordance with 4.1.1. The BRB Frame model (Figure 5-4b) was modelled in accordance with 4.2.3, and introducing the simplifications defined in 4.2.6. The BRB device was instead modelled in accordance with 5.1.2. In both models, the steel material definition was changed in accordance with 4.1.1.1.

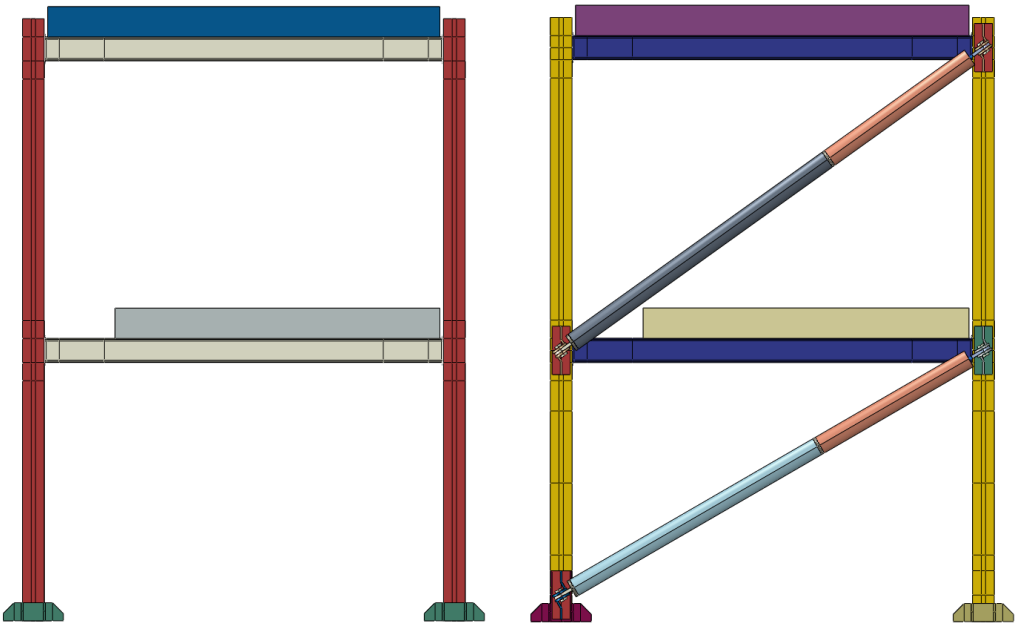

(a) (b)

Figure 5-4 *3D Abaqus Model for PushOver Analysis: (a) Bare Frame; (b) BRB Frame*

It is worth mentioning that, since the model in Abaqus has already proven to be unable to account for the contact between the BRB and the column appropriately (4.2.5), only the pushover analyses results in which BRBs are in tension are reported and discussed. In addition, given that the objective of the present chapter is to identify the limitations of the retrofit intervention, it is sufficient to analyse the frame behaviour in one direction only. In fact, once eliminated the chance of contact between the BRBs and the column, it is expected that the frame pushover curves in the two directions turn out to be similar, presenting a higher resistance in the direction where the BRBs are in compression. This result can be derived having considered the non-symmetrical cyclical behaviour of the BRB (Figure 5-1, Figure 5-2).

As shown in Figure 5-5, it is clear that the placement of BRBs results in an increase of the frame stiffness and strength. However, as already proven in the previous chapter, the dissipative capacity of the frame remains almost unchanged. Although the dissipative capacity of the frame is not directly assessable through pushover analysis, indirect information about it can still be obtained. For instance, by monitoring the BRB elongation in relation to storey drift, indirect information on the dissipative capacity of the frame can be derived. To this end, Figure 5-6 shows the first floor BRB elongation against storey drift (*i.e.*, first floor displacement). In this case, it can be seen that the ultimate elongation of the BRB (20 mm) is reached for an interestory drift of about 3.5%. Figure 5-7 shows the column's cross-sectional deformation for an interstory drift of 3%. This picture will be essential in 5.3.3 when trying to identify the parameters affecting the retrofit effectiveness.

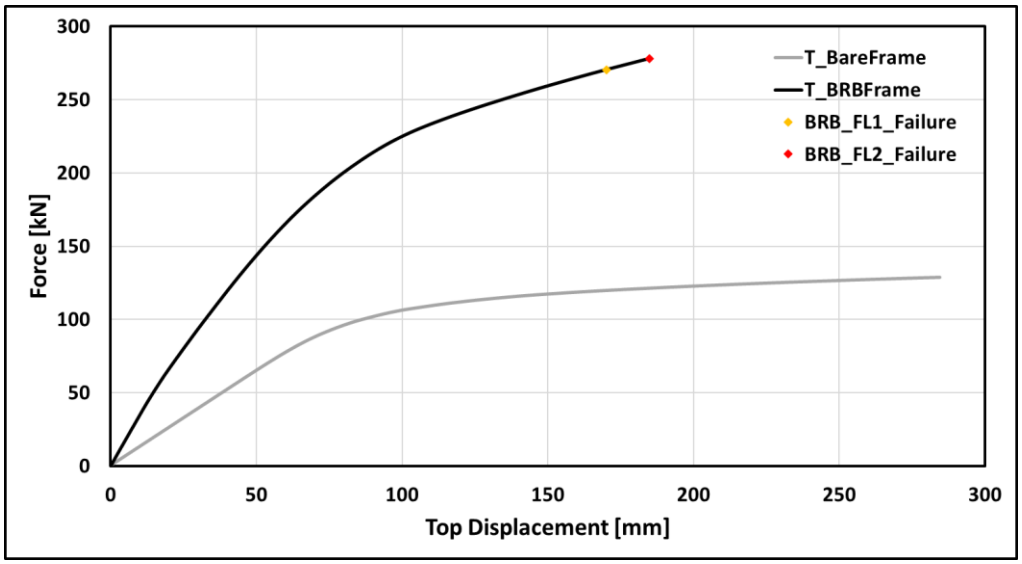

Figure 5-5 *Pushover curve: Bare Frame and BRB Frame (test conditions)*

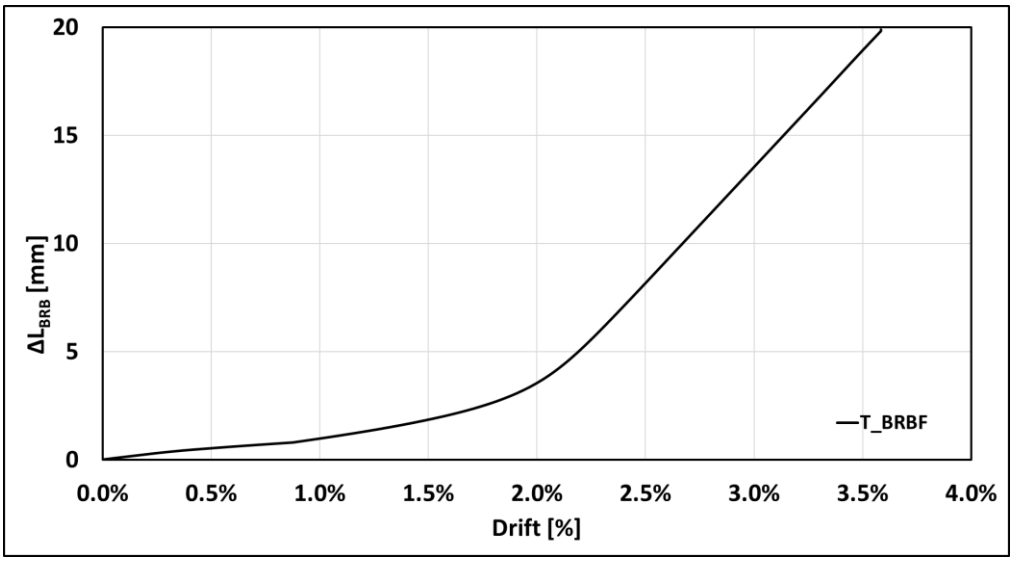

Figure 5-6 *First floor BRB elongation against top displacement*

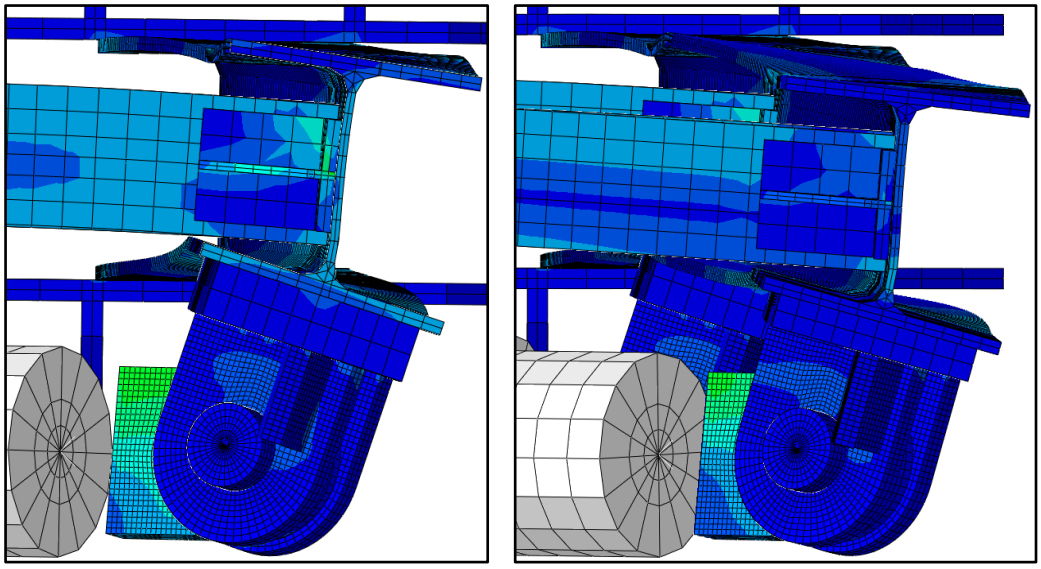

(a) (b)

Figure 5-7 *Column cross-sectional deformation for an interstory drift of 3.5%: (a) first floor, (b) second floor;*

The basic BRB frame kinematic behaviour shown in Figure 5-8 illustrates that, under the assumption of small changes of angles, BRB axial deformation can be calculated in accordance with Eq. (5-1):

$$\Delta_{bx} = \Delta_x \cdot cos(\alpha) \tag{5-1}$$

where Δ_x is the design storey drift, and α is the BRB angle of inclination with respect to the horizontal[16]. Given this, the BRB failure should occur for a story drift of 1%. Therefore, it is clear that due to different factors, the integration of external BRBs in the tested conditions does not allow achieving the same performance as when BRBs are placed in-plane within the frame.

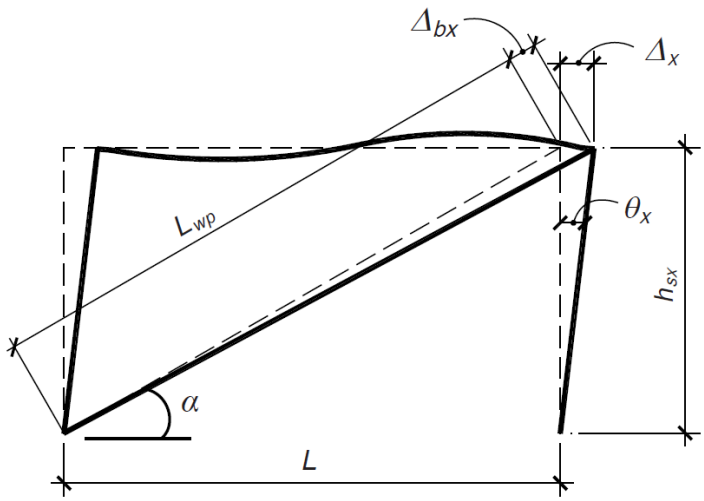

Figure 5-8 *Basic BRB frame kinematic behaviour*[16]

5.3 Identification of the Limiting Parameters

Given the outcomes of the previous section, the aim of this paragraph is to identify the design parameters which affect the effectiveness of the retrofit intervention. To this aim, the following two models were created and analysed:

- An equivalent model with BRBs positioned in-plane with respect to the frame;
- An equivalent model with BRBs positioned externally with respect to the frame aided with torsional and distortional constraints for the columns and the joints.

The first model was considered as a reference since it represents the typical retrofit solution when implementing BRBs in an existed structure. Hence, the results of that model could provide a good reference to identify the design parameters that affect the performance of the intervention.

5.3.1 In-Plane BRBs

Figure 5-9 shows the Bare Frame model retrofitted with internal BRBs. The Bare frame model corresponds exactly to the one described in 5.2. The whole diagonal braces (*i.e.*, the *hollow elastic element* and the *rigid element*) were modelled as illustrated in 4.2.3, while the BRB device was modelled in accordance with 5.1.2. It is worth mentioning that, in this model, the length of the hollow elastic element was slightly reduced to allow the inclusion of the gusset plates. The gusset plates considered in this model are shown in Figure 5-10. The shape of the gusset plates was designed to minimize their area at the effective stress transfer zone [70] hence limiting the increase in the rotational strength and stiffness of the joints. The gusset plates were designed in accordance with the specification given in EN 1993-1-8 [71]

for bolted connection. Moreover, in accordance with AISC 341-16 [29] specifications, the thickness of the gusset plates was defined to ensure that the buckling capacity of the gusset plate was greater than the BRBs maximum compressive force [72]. The outcomes of this model are shown in 5.3.3.

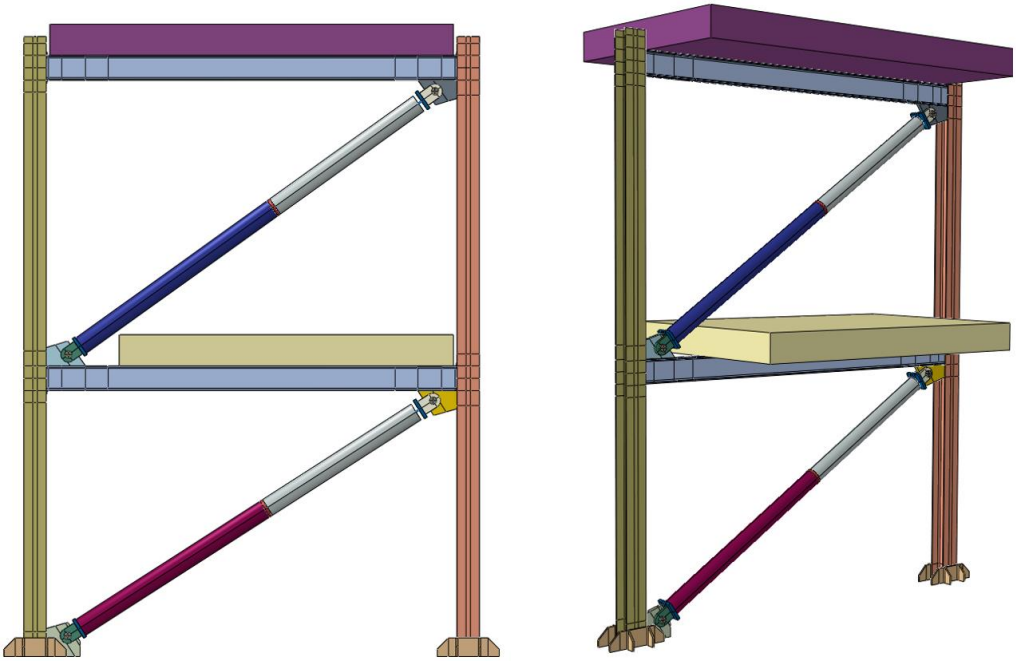

Figure 5-9 *3D InPlane BRBs Frame Abaqus Model*

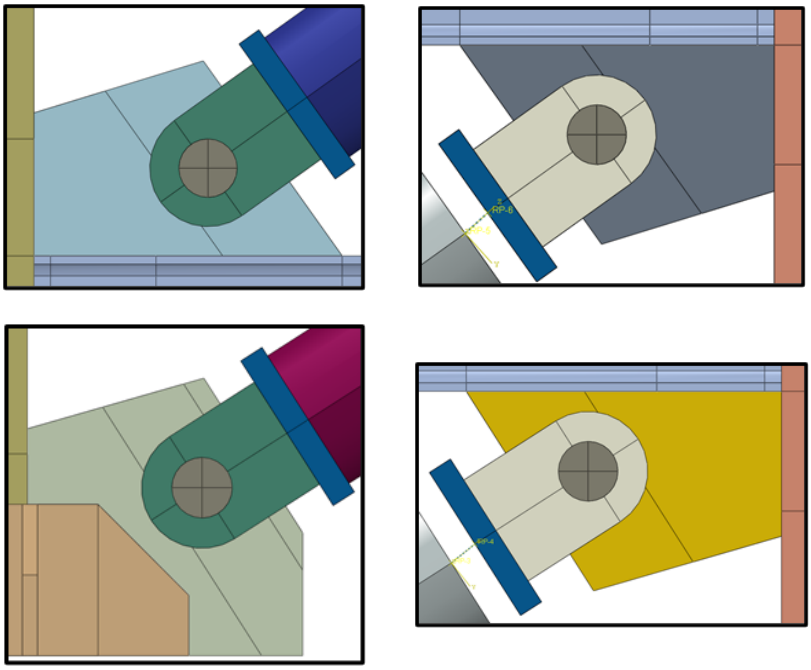

Figure 5-10 *Gusset plates details*

5.3.2 External BRBs with torsional and distorsional constraints

Given the outcomes of the experimental campaign and considering what illustrated in Figure 5-7, it is possible to assume that the parameters influencing the behaviour of the retrofitted frame are mainly two: the torsional stiffness and the distortional deformability of the column. To prove this assumption, additional constraints were introduced in the BRB Frame model to prevent distortional deformations of the column's cross-section and global torsional rotation of the column.

Figure 5-11a shows the Bare Frame model retrofitted with external BRBs. The BRB Frame corresponds exactly to the one described in 5.2. To avoid the distortional deformation of the column, a rigid body constraint was created to tie the displacements of the column's cross-section to the displacements of the Reference Point located at its geometric centre. This constraint was applied in one cross-section for each connection zone between BRBs and frame Figure 5-11b. In addition, to prevent global torsional deformation of the column, rotation around the vertical axis and out-of-plane displacements of each RP were constrained. The outcomes of this model are shown in 5.3.3.

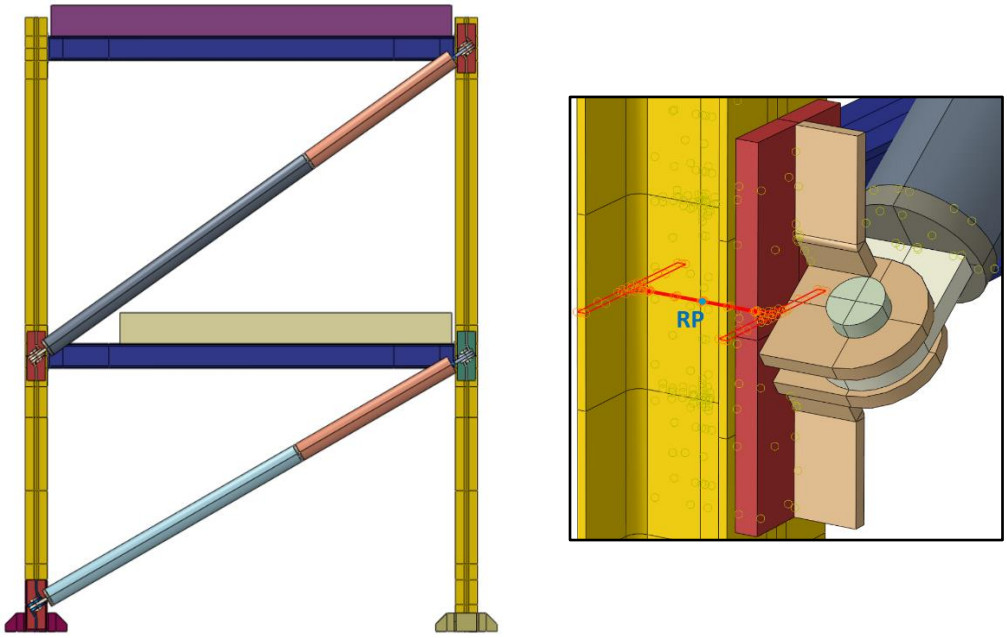

(a) (b)

Figure 5-11 *3D external BRBs Frame with torsional and distorsional constraints: (a) Abaqus Model; (b) Rigid Body Constraint*

5.3.3 Outcomes

The outcomes of the models described in 5.3.1 and 5.3.2 are here presented and compared. It is worth mentioning that the pushover curve related to the bare frame

model (T_BareF) and the BRB frame model in the tested conditions (T_BRBF) are here presented to draw more general conclusions.

As mentioned in 5.2, the placement of BRBs results in an increase in frame stiffness and strength. However, when comparing the results obtained from the frame with external BRBs under the tested conditions (T_BRBF) with those obtained from the frame with internal BRBs (T_BRBF_InPl), it can be seen that the retrofit technique, under the conditions present during the test, does not guarantee the same performances resulting from the placement of internal BRBs. In fact, it can be seen that the stiffness of the frame with internal BRBs is significantly higher; moreover, the BRBs failure due to reaching maximum elongation occurs at lower displacements (Figure 5-12). The latter aspect, together with the graph shown in Figure 5-13, proves that the dissipative capacity of the frame with internal BRBs is definitely greater than the dissipative capacity of the frame with external BRBs under the tested conditions. In fact, it is evident that for the same storey drift, the BRB's elongation is much greater when placed inside the frame.

On the other hand, the comparison between the model with internal BRBs (T_BRBF_InPl) and the model with external BRBs together with torsional (TC) and distortional (DC) constraints (T_BRBF_TC_DC) shows that the latter two aspects have a significant influence on the effectiveness of the intervention. In fact, when the distortional and torsional deformation of the column is prevented, the retrofit intervention involving external BRBs and the one with internal BRBs show very similar results.

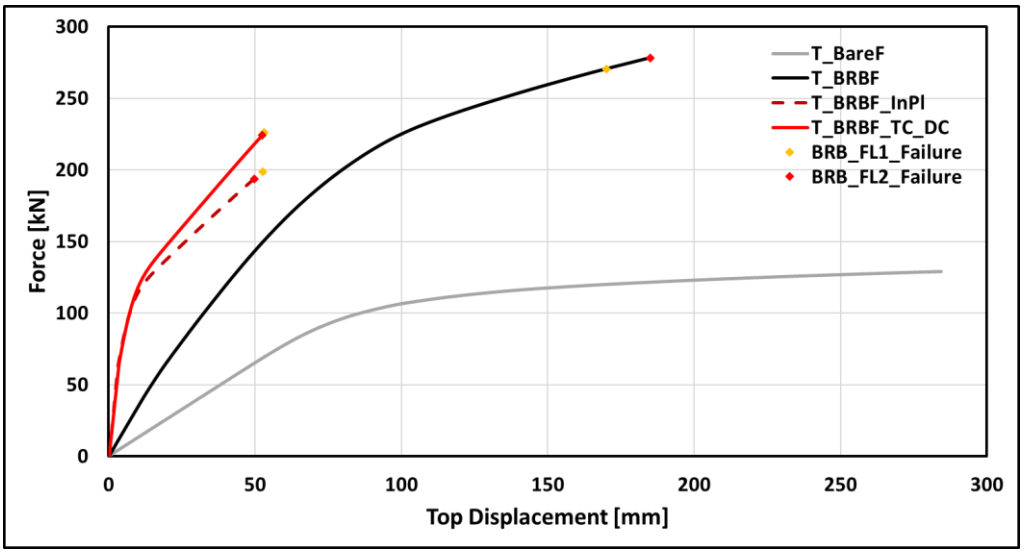

Figure 5-12 *Pushover curve*

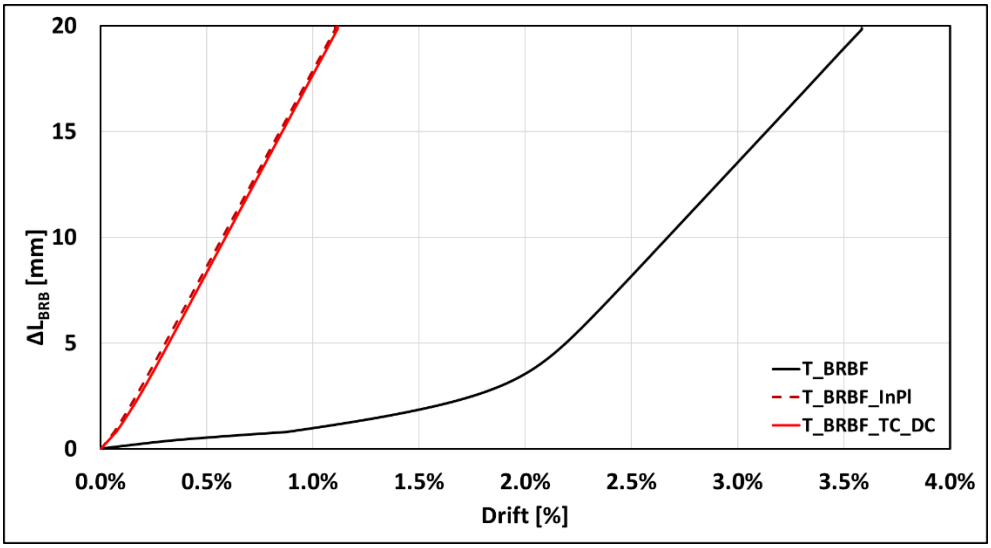

Figure 5-13 *First floor BRB elongation against top displacement*

5.4 Influence of the Limiting Parameters

Once identified the design parameters (*i.e.*, torsional stiffness and distortional deformations) that affect the effectiveness of the intervention, the influence of each parameter on the retrofitted frame's response is investigated in this chapter. To this end, the following two models were created and analysed:

- External BRBs with torsional constraints (TC);
- External BRBs with distortional constraints (DC).

5.4.1 External BRBs with torsional constraints

In this model, the aim is to prevent torsional rotation of the column while leaving the distortion unrestricted. The BRB Frame (Figure 5-14a) was modelled in accordance with 5.2. The torsional constraint was modelled by constraining the out-of-plane displacements of the inner flange of the column. These constraints were applied in limited areas for each connection node between the BRBs and the frame (Figure 5-14b).

The pushover analysis on this model proves that the performance improvements of the retrofitted frame are very limited when only global torsional rotation of the column is prevented. In fact, as shown in Figure 5-15, the stiffness and strength of the frame remain almost unchanged. In addition, the behaviour of the BRB against the storey drift remains almost unaltered (Figure 5-16).

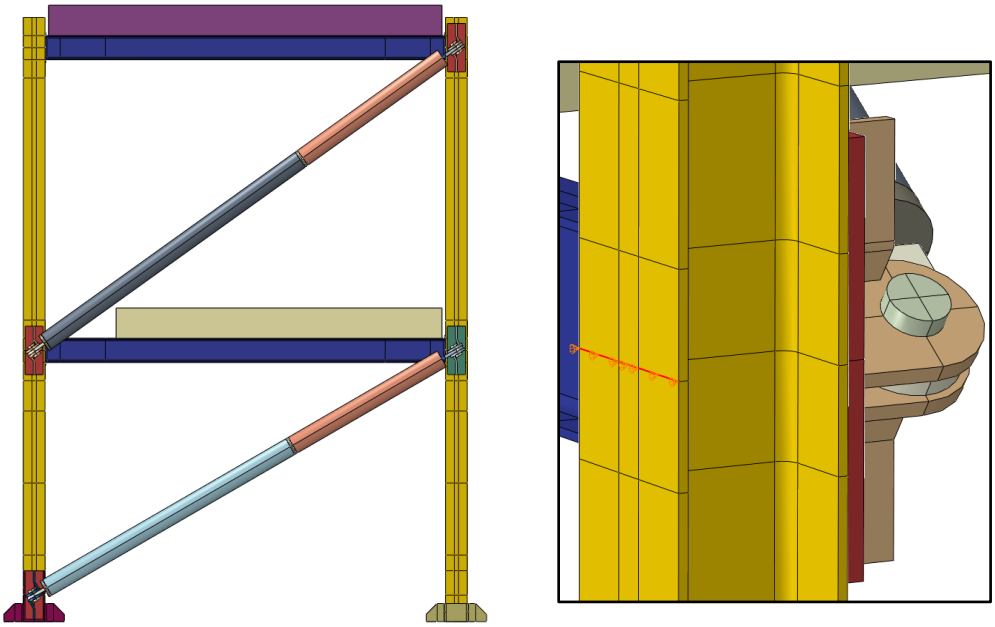

(a) (b)

Figure 5-14 *BRB frame 3D Abaqus model with torsional constraints: (a) Whole Model; (b) Detail of the torsional constraint*

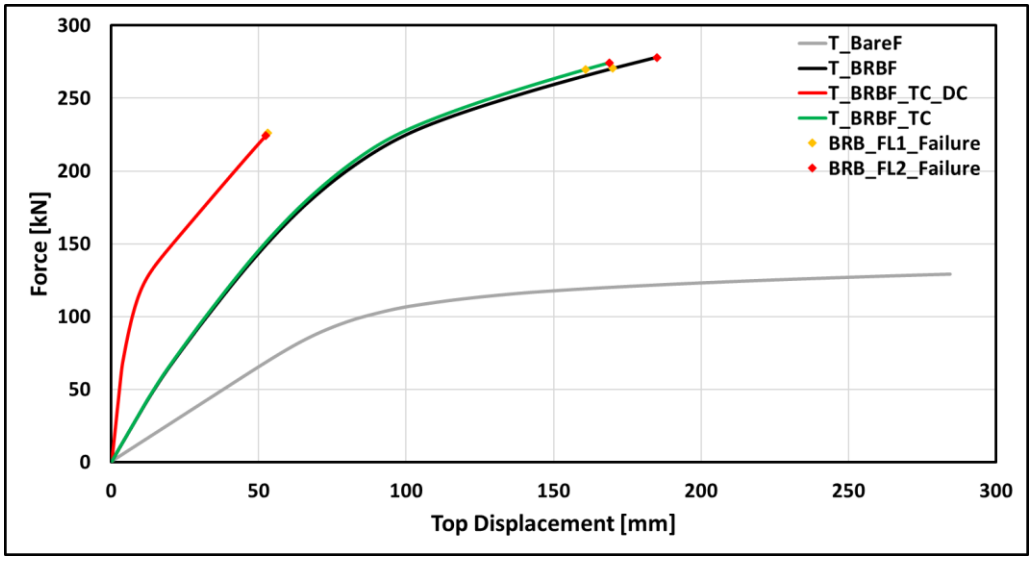

Figure 5-15 *Pushover curve*

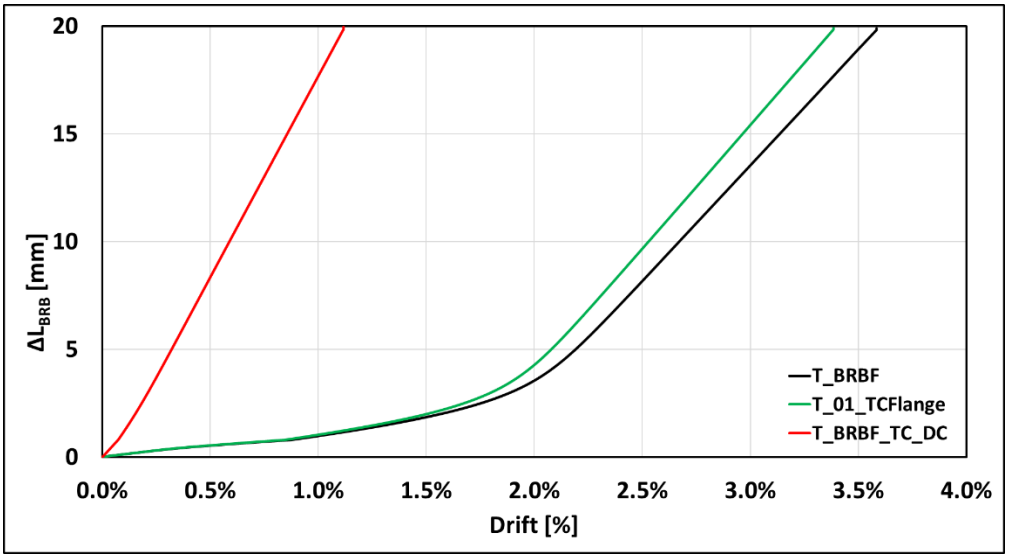

Figure 5-16 *First floor BRB elongation against top displacement*

5.4.2 External BRBs with distortional constraints

In this model, the aim is to prevent the column distortional deformation while leaving the torsional rotation unrestricted. The BRB frame (Figure 5-17a) was modelled in accordance with 5.2. To avoid the distortional deformation of the column, a rigid body constraint was created to tie the displacements of the column's cross-section to the displacements of the Reference Point located at its geometric centre. This constraint was applied in one cross-section for each connection zone between the BRBs and the frame Figure 5-17b.

The pushover analysis on this model proves that the application of a distortional constraint at the column nodes results in a significant increase in frame stiffness (Figure 5-18). Nevertheless, this intervention does not lead to a significant increase in the dissipative capacity of the frame. In fact, although the BRB behaviour differs from that obtained for the model without additional constraints, the additional torsional constraints do not allow the yielding of the devices for small drift (Figure 5-19).

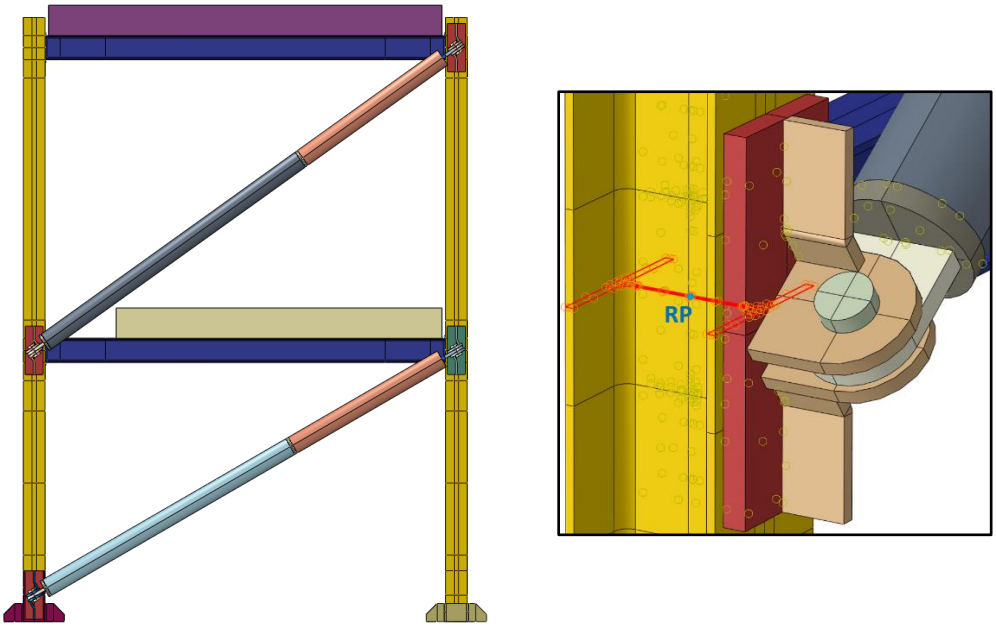

(a) (b)

Figure 5-17 *BRB frame 3D Abaqus model with distortional constraints: (a) Whole Model; (b) Detail of the distortional constraint*

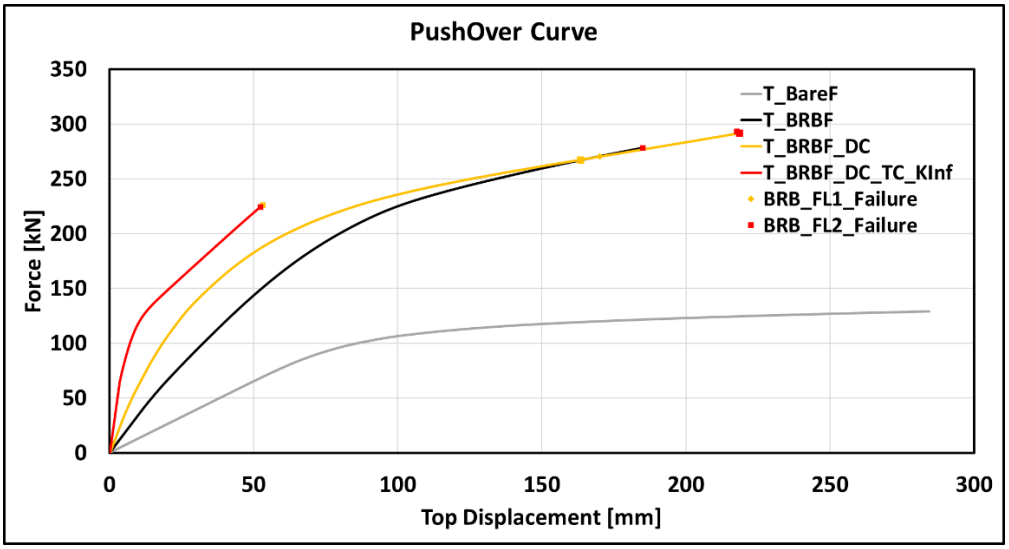

Figure 5-18 *Pushover curve*

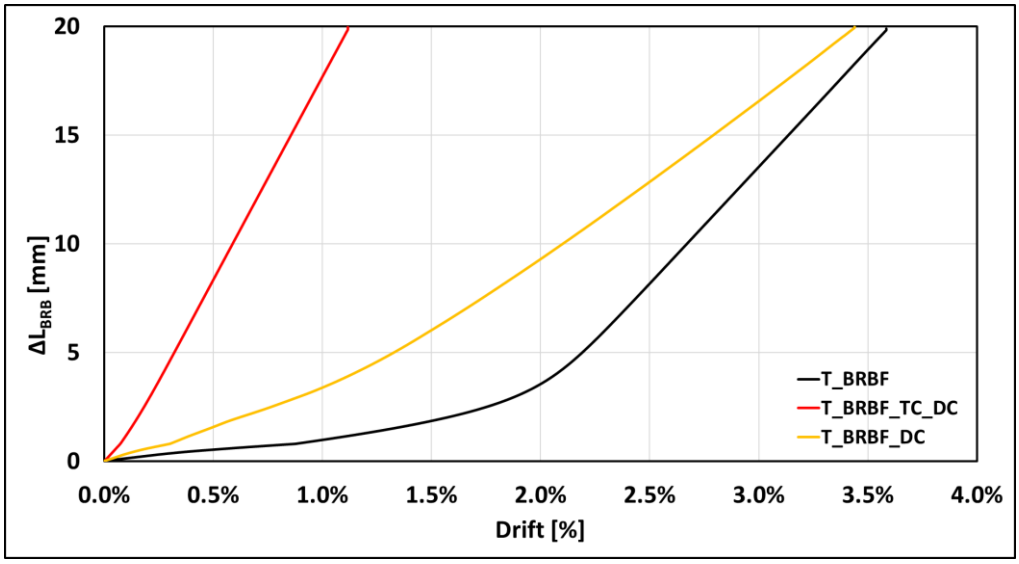

Figure 5-19 *First floor BRB elongation against top displacement*

5.5 Parametric Analysis

5.5.1 Considered Models

In the previous section, the influence of torsional and distortional stiffness on the performance of the retrofitted frame was studied separately. It was observed that by preventing torsional rotation of the column, the response of the frame remained almost unchanged. On the other hand, preventing a distortional deformation of the column only resulted in a slight increase in the initial stiffness of the frame.

In this section, the aim is to investigate the influence of torsional column stiffness when distortional deformation is prevented. To this aim, the following model was considered. The BRB Frame (Figure 5-20a) was modelled in accordance with 5.2. To avoid the distortional deformation of the column, a rigid body constraint was considered as described in 5.4.2. The different torsional stiffness of the column was modelled by placing a rotational spring connecting the ground with each RP (Figure 5-20b). It is worth mentioning that the introduction of a rotational spring can be useful to account for the rotational stiffness of a column with a greater profile as well as for the additional constraints which arise in a 3D frame (*i.e.*, connections with transverse beams, floor slabs and infills).

The stiffness values assigned to the springs were defined by evaluating the pure torsional stiffness (*i.e.*, related to the *pure torsional moment*, also identified as *St Venant's torsion*) of the reference sections and amplifying them by means of coefficients (α). Table 5-6 shows the stiffness values assigned to the torsional springs placed at each floor.

The pushover curves of all the models with different torsional stiffness are shown in Figure 5-21. As can be seen from the graph, the torsional stiffness of the column becomes relevant when column distortion is prevented. In fact, it can be seen that at higher torsional stiffnesses, the performance of the frames increasingly approaches the limit case of a retrofitted frame with internal BRBs. This outcome is also shown in Figure 5-22.

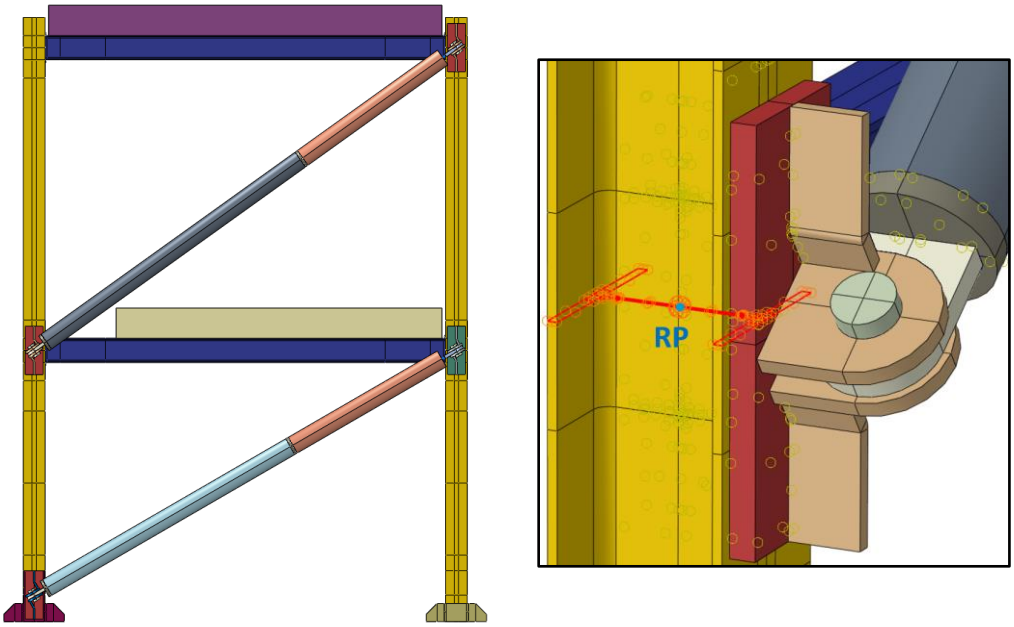

(a) (b)

Figure 5-20 *BRB Frame 3D Abaqus model with distortional constraints: (a) Whole Model; (b) Detail of the distortional constraint and torsional spring.*

Table 5-6 *Torsional Spring stiffness*

Coeff.	Torsional Stiffness [Nmm]		
	Base	Floor 1	Floor 2
$\alpha = 0.5$	2.7E+07	2.7E+06	1.3E+06
$\alpha = 1$	5.5E+07	5.3E+06	2.5E+06
$\alpha = 2.5$	1.4E+08	1.3E+07	6.3E+06
$\alpha = 5$	2.7E+08	2.7E+07	1.3E+07
$\alpha = 10$	5.5E+08	5.3E+07	2.5E+07
$\alpha = 50$	2.7E+09	2.7E+08	1.3E+08
$\alpha = 100$	5.5E+09	5.3E+08	2.5E+08
$\alpha = 500$	2.7E+10	2.7E+09	1.3E+09

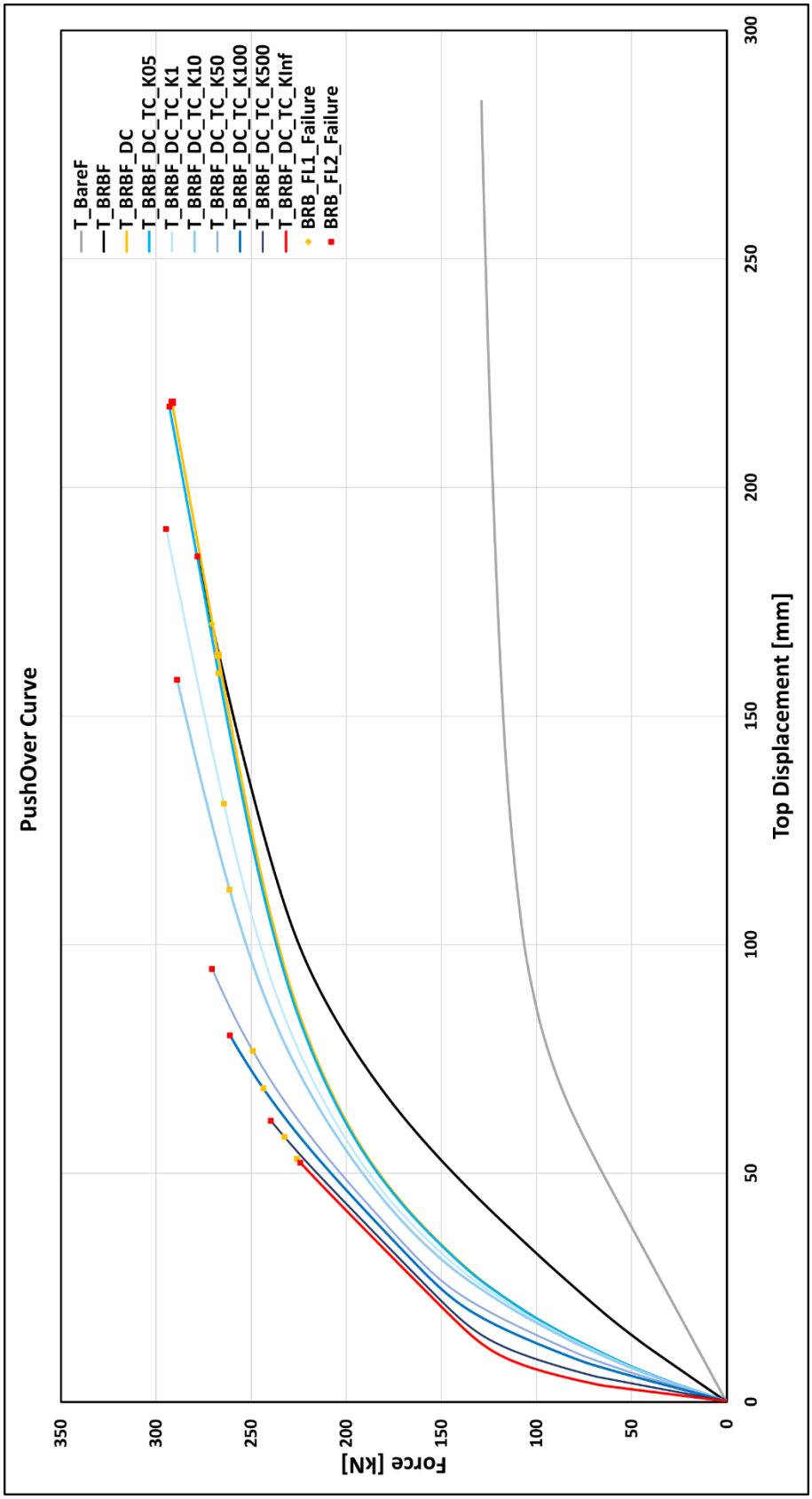

***Figure 5-21** Pushover curves*

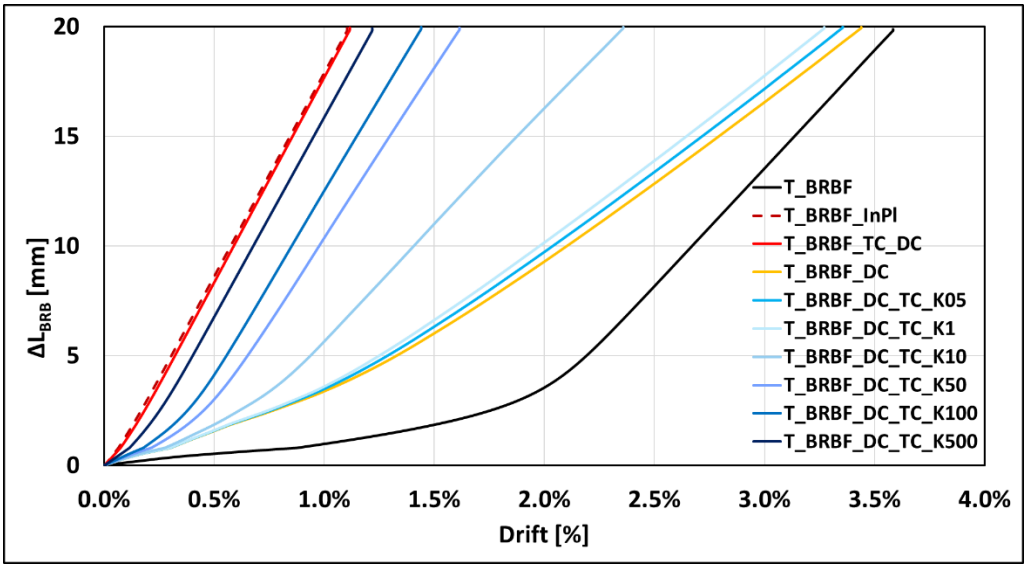

Figure 5-22 *First floor BRB elongation against top displacement*

5.5.2 Outcomes

The results shown so far can be useful to outline design recommendations. Although extensive details on the methodology used for BRBs design can be found elsewhere in literature [17,19,73–77], a brief outline of the design process and the parameters involved is here presented to introduce the key aspects.

The primary objectives that dictate the BRBs design process comprise of (a) defining BRBs dimensions such that they produce a controlled increase of the base shear capacity of the system, that is, the base shear of the dissipative system ($V_{d,1}$) when added to the base shear of the bare frame ($V_{f,1}$); (b) distributing the stiffness of BRBs among the stories such that the first mode shape of the bare frame remains unchanged following the retrofit implementation. This aims at avoiding drastic changes to the moments distribution within the MRF; (c) distributing the BRBs strengths among the stories to ensure simultaneous yielding of BRB devices. This condition is usually sought in the design in order to maximize the dissipation capacity of the system; (d) calibrating the stiffness and ductility of the BRBs such that the device failure occurs at a design displacement (d_u) defined as per the ductility capacity of the bare frame. It is noteworthy that The BRB design procedure is based on the displacement distribution of the first vibration mode and uses nonlinear static analysis and a single degree-of-freedom (SDoF) simplification for the definition of some design parameters that are related to the retrofit objectives, such as the design displacement (d_u); the target ductility of the dissipative braces (μ_d), and the base shear capacity of the dissipative system ($V_{d,1}$). The design method provides the strength $F_{d,i}$, and stiffness $K_{d,i}$ of the BRBs at each story. Following

this, the components' properties, such as length, area, and materials of BRB devices and elastic braces, can be easily derived according to a series arrangement[17].

Considering the above, it seems clear that the definition of the design displacement (d_u) trough pushover analysis represents a fundamental step when designing a BRB retrofit intervention. Therefore, the results obtained from this thesis work turn out to be crucial for properly designing retrofit interventions by means of external BRBs. In fact, the results show that the torsional stiffness of the column significantly influences the displacement value associated with the BRB crisis. In light of this, the increase in displacement observed in the performed analyses was linked to some key design parameters, such as the BRB yield force (F_y), the BRB eccentricity (e) and the column torsional stiffness (K_t). To this aim, in the graph (Figure 5-23) is presented a dimensionless parameter (β) defined by Eq.(4-7) was plotted against the ratio between the storey drift displacement (IDR) associated with the BRB crisis of each model with external BRBs to the IDR at which the BRBs fail in the model with internal BRBs. Therefore, this graph could represent a simple tool to evaluate the increase in displacement associated with the crisis of the dissipative element in retrofits solutions with external BRBs.

$$\beta_i = \frac{F_y \cdot e}{K_t} = \frac{F_y \cdot e}{K_0 + \alpha \cdot \left(\frac{G \cdot I_t}{L_i}\right)} \cong \frac{F_y \cdot e}{(1+\alpha) \cdot \frac{G \cdot I_t}{L_i}} \qquad (5\text{-}2)$$

It is worth mentioning that the torsional stiffness considered here is the sum of the effective torsional stiffness of the node (K_0) and the additional stiffness introduced through the rotational spring (K_α).

The figure shows that the results obtained can be approximated through a lognormal function.

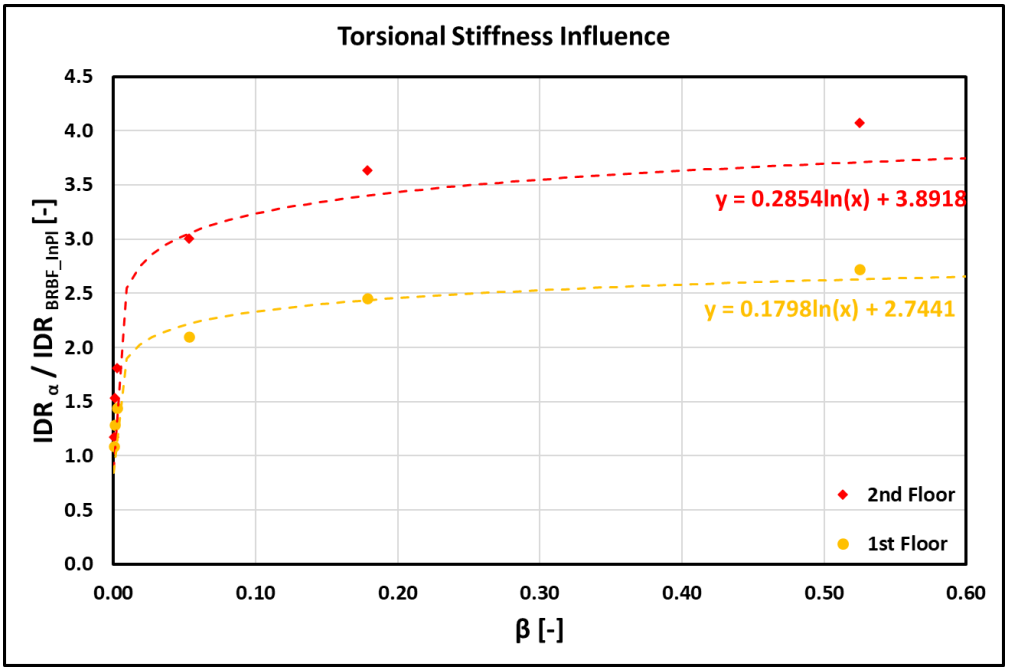

Figure 5-23 *Torsional Stiffness Influence on Top Displacement*

In addition, the graph shows that three different approaches can be followed to limit column deformability effects: (1) modifying the BRB yield force, (2) modifying the BRB eccentricity, (3) acting on column torsional stiffness. In the first scenario, it is possible to select BRBs with yield strengths to enable their activation while leaving the torsional stiffness of the existing columns unaltered. In the second case, the effects related to the placement of external BRBs could be limited by reducing the eccentricity of the connection. However, it is noteworthy that this approach has restrictions as it is constrained by geometric limitations. Finally, it would be possible to consider a combined intervention aimed at connecting the BRBs while increasing the torsional stiffness of the column. Nevertheless, it is worth emphasising that the initial analysed model (5.2) does not take into account the additional torsional constraints provided by the orthogonal beams, slab and non-structural elements in a real 3D structure. Therefore, increasing the torsional stiffness of the column could be not necessary where the torsional constraint at the nodes appears to be already satisfactory.

5.6 Possible Solutions

5.6.1 Preventing column distortion

Paragraphs 5.4 and 5.5 have shown that the column torsional stiffness significantly affects the behaviour of the retrofitted frame by means of external BRBs. However, it has also been shown that a high torsional stiffness hardly modifies the behaviour of the frame if the column's distortional deformations are not prevented. Therefore, assuming that the nodal torsional stiffness in a 3D frame turns out to be sufficient, the aim of this section consists in identifying the best intervention type to avoid the distortional deformability of the column.

To this end, three different types of intervention were considered. Firstly, two stiffening plates were placed in the middle of the joint (Figure 5-24). Then, four stiffening plates were placed within the node area: two plates at each end of the panel node (Figure 5-25). Finally, six stiffening plates were considered: two plates at each end of the panel nodal and two plates in the centre of the node (Figure 5-26).

The pushover curves reported in Figure 5-17 demonstrate that the placement of two stiffening plates (T_R_2Pl) prevents distortional deformation of the column in the nodal area. As a result, the frame presents a stiffness increase equal to the one observed in the frame discussed in section 5.4.2. Based on further analysis, it is evident that the introduction of 6 stiffening plates is completely equivalent to the inclusion of four stiffening plates, resulting in a slight increase in stiffness and strength. Therefore, based on these analyses, it appears that the inclusion of four plates seems to be the best compromise between the performance and invasiveness of the intervention.

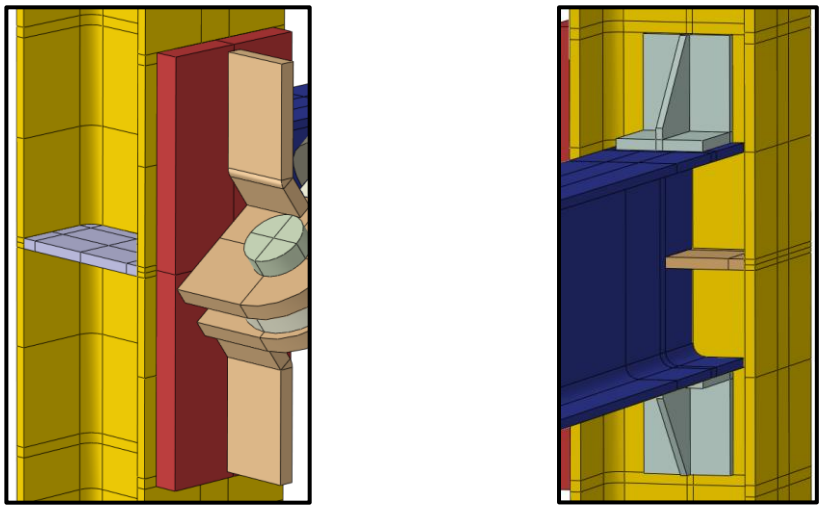

(a) (b)

Figure 5-24 *Retrofit solution: one additional plate: (a) external view, (b) internal view;*

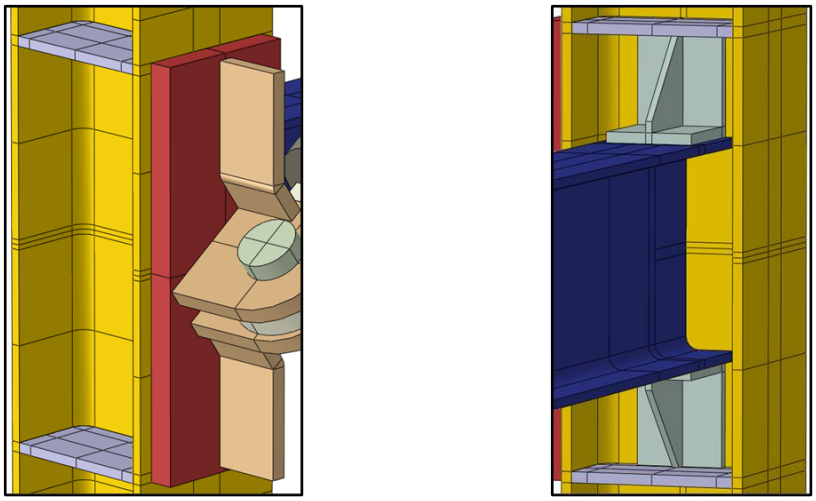

(a) (b)

Figure 5-25 *Retrofit solution: two additional plate: (a) external view, (b) internal view;*

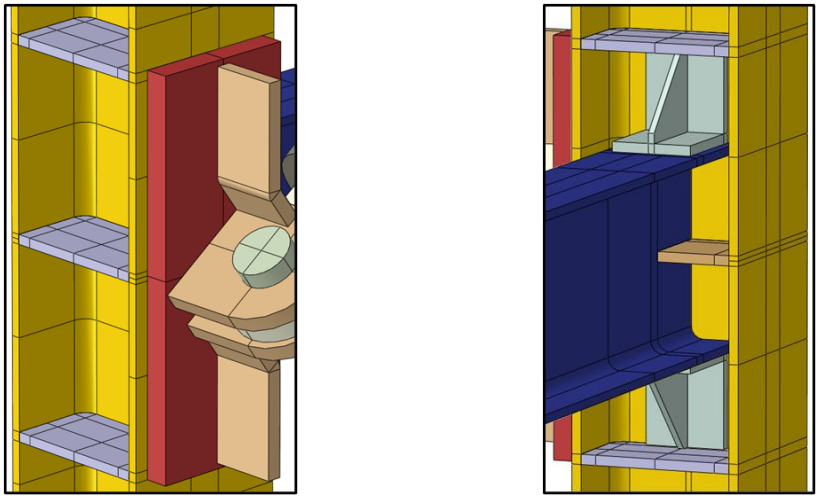

(a) (b)

Figure 5-26 *Retrofit solution: three additional plate: (a) external view, (b) internal view;*

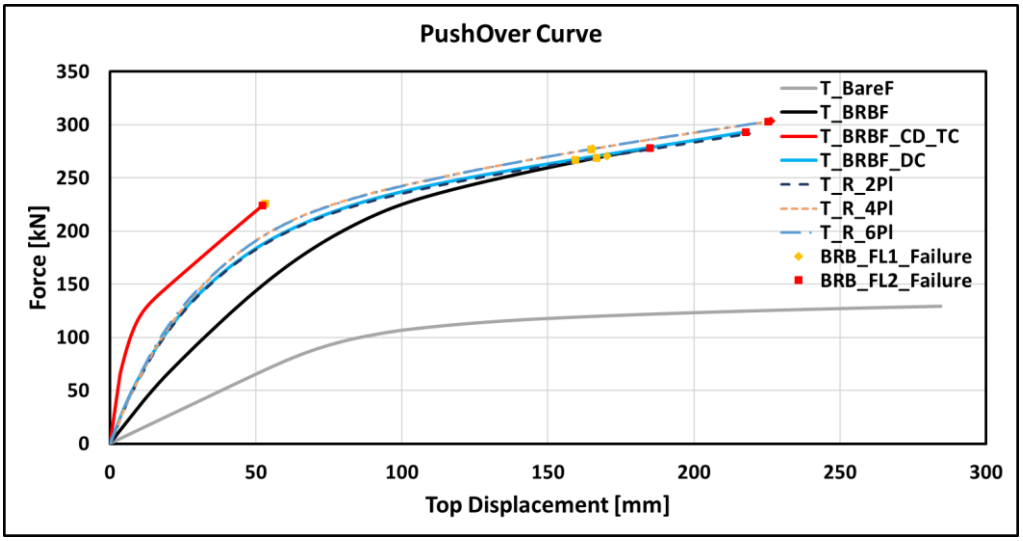

Figure 5-27 *Pushover curves*

5.6.2 Influence of a 3D configuration

All the above considerations have been conducted on a single frame. As already seen in the previous section (5.5), the torsional stiffness of the column panel zone significantly affects the structural behaviour. In this section, an attempt is made to assess the structural behaviour of the frame retrofitted with external BRBs by explicitly accounting for the additional torsional constraint provided by the orthogonal beams, the slab and the additional frames.

The considered FE model (Figure 5-28) was built according with the modelling strategies adopted in the previous Section (4). The FE model reflect the 3:4 scaled prototype building introduced in Section 3. However, to reduce computational time, only half of the model was built with appropriate boundary conditions to account for the symmetry of the structure. In addition, column distortional deformability was prevented introducing the solutions described in Section 5.6.1 (Figure 5-29). It is worth mentioning that to reduce the slab influence, only the effective thickness of the slab was considered (*i.e.*, 7.7mm).

The result shown in Figure 5-30 and Figure 5-31 demonstrate that when assessing the structural behaviour of the retrofitted frame with external BRBs, the additional torsional constraint provided by the 3D structure cannot be neglected. It is worth mentioning that the above results show that the actual three-dimensional configuration is equivalent to the single frame model equipped with a rotational spring (5.5.1) whose stiffness is defined by equation (5-2) considering the "α" parameter equal to "500". In fact, the BRB failure occurs at an IDR of nearly 30% of the one observed in the single-frame model with no additional stiffening plates (T_BRBF model). Moreover, the reduced IDRs at the failure of BRBs were less than 20% larger than those of the model with internal BRBs

(T_BRBF_DC_TC_KInf), indicating that the retrofit scheme using external BRBs with the stiffening plates can lead to approximately the same structural performance as the conventional retrofit approach using internal BRBs. In particular

Figure 5-28 *3D Abaqus model*

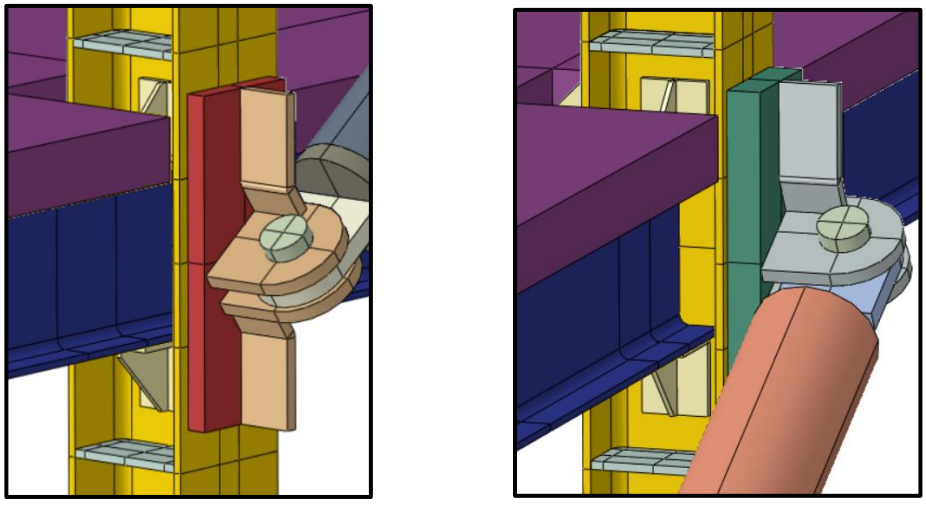

(a) (b)

Figure 5-29 *Details of the additional stiffening plates;*

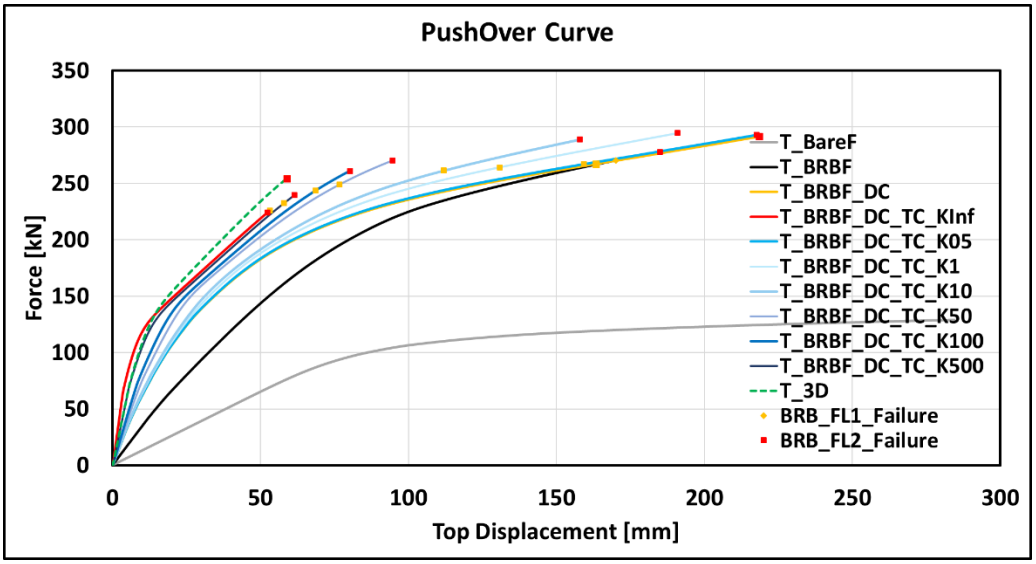

Figure 5-30 *Pushover curves*

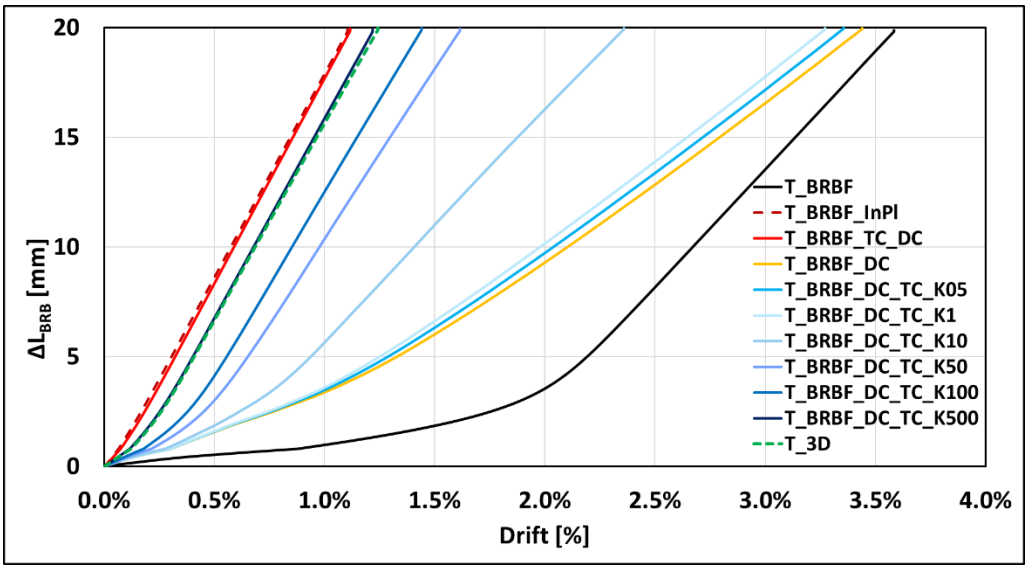

Figure 5-31 *First floor BRB elongation against storey drift*

6 Conclusions

The need to reduce the invasiveness of the seismic retrofitting intervention by means of BRBs contributed to inspire the HITFRAMES[1] research project on which this thesis is founded. The main outcomes of the experimental campaign proved that further considerations were needed to increase the effectiveness of the intervention. De facto, the inclusion of diagonal braces, as carried out in the laboratory, allowed to increase the stiffness of the frame but not its dissipative capacity.

The above considerations inspired this dissertation. Indeed, the main objective of the study was to identify the design parameters that limited the effectiveness of the intervention and then investigate solutions that would allow design recommendations to be outlined. To this aim, the following methodological approach has been adopted. First, a non-linear FEM detailed (Abaqus) model was developed and validated against the experimental results. Thereafter, the validated model was subjected to pushover analysis aimed at identifying the key design parameters that influenced the effectiveness of the intervention and evaluating their influence on the frame behaviour. Finally, based on what was observed in the previous step, design recommendations were outlined.

The present study demonstrated that neglecting the torsional and distortional deformability of the column during the design process leads to a drastic performance reduction of the retrofitted frame. In particular, pushover analyses have shown that without torsional and distortional constraints, BRB yielding occurs at larger inter-storey drifts, thus making BRB inclusion ineffective. Therefore, to achieve similar performance between retrofit intervention through external BRBs and internal BRBs, it is required that in the former, distortional deformability of the column in the nodal zone is prevented and that an adequate torsional constraint is provided for the column. Hence, the retrofitting solution by means of external BRBs turns out to be effective in cases in which the other structural elements (*e.g.*, orthogonal beams, slab, infills) are able to guarantee an adequate torsional restraint for the column, and at least four stiffening plates can be placed in the nodal zone. However, when torsional restraint appears to be inadequate, it is still possible to vary the strength or eccentricity of the BRB to reduce the column deformability effects.

6.1 Future works

Although the present thesis work allowed the identification of preliminary design recommendations, further studies are needed to improve the proposed seismic retrofit strategy. In particular, the following tasks are proposed as future research topics:

- Improvement of the methodology for the modelling of BRB devices, which is currently limited to a symmetric cyclic behaviour. A more refined procedure should instead be able to capture the BRB strength increase in compression;
- Further consideration on the 3D model of the structure to explicitly consider the torsional constraints offered by orthogonal beams;
- Assess the feasibility and effectiveness of the intervention for structures with other column profiles (*e,g,*. rectangular hollow sections);
- Design improvements to increase the nodal torsional stiffness when it proves to be inadequate;
- Extend the studies to a larger number of frames to explicitly account for the variation of several key design parameters (*e.g.*, BRB yield strength, BRB ultimate strength, BRB eccentricity, node torsional stiffness) and identify a more accurate relationship linking these parameters to the performance of the retrofitted frame.

Bibliography

1. Di Sarno L, Freddi F, D'Aniello M, Kwon O-S, Wu J-R, Gutiérrez-Urzúa F, et al. Assessment of existing steel frames: Numerical study, pseudo-dynamic testing and influence of masonry infills. J Constr Steel Res. 2021;185:106873. doi:10.1016/j.jcsr.2021.106873

2. Eurocode 8: Design Of Structures For Earthquake Resistance - Part 1: General Rules, Seismic Actions And Rules For Buildings. :13.

3. Eurocode 8: Design Of Structures For Earthquake Resistance - Part 3: Assessment And Retrofitting Of Buildings. :11.

4. Iunio I. Dinamica delle Strutture ed Ingegneria Sismica - Principi ed Applicazioni [Internet]. Hoepli; 2021. 528 p. Available from: https://www.hoepli.it/libro/dinamica-delle-costruzioni-e-ingegneria-sismica/9788820397203.html

5. Bozorgnia Y, Bertero VV. Earthquake Engineering: From Engineering Seismology to Performance-Based Engineering. CRC Press; 2004. 958 p.

6. Field Manual: Postearthquake Safety Evaluation of Building (2nd Edition) [Internet]. Applied Technology Council; [cited 2022 Jul 14]. Available from: https://store.atcouncil.org/index.php?dispatch=products.view&product_id=32

7. NEHRP Gidelines for the Seismic Rehabilitation of Buildings. Vol. FEMA 273. Applied Technology Council. [Washington, D.C.: Federal Emergency Management Agency]; 1997.

8. Performance-based Seismic Engineering of Buildings [Internet]. Vol. I. Structural Engineers Assn. of California (SEAOC), Vision 2000 Committee.; 1995 [cited 2022 Jul 14]. Available from: https://www.seaoc.org/store/viewproduct.aspx?id=11238558

9. Fajfar P. A Nonlinear Analysis Method for Performance-Based Seismic Design. Earthq Spectra. 2000;16(3):573–92. doi:10.1193/1.1586128

10. Deierlein GG, Reinhorn AM, Willford MR. Nonlinear Structural Analysis For Seismic Design - A Guide for Practicing Engineers [Internet]. National Institute of Standards and Technology; 2010. Available from: https://nehrp.gov/pdf/nistgcr10-917-5.pdf

11. Gutiérrez-Urzúa F, Freddi F, Di Sarno L. Comparative analysis of code-based approaches for seismic assessment of existing steel moment resisting frames. J Constr Steel Res. 2021;181:106589. doi:10.1016/j.jcsr.2021.106589

12. Vidic T, Fajfar P, Fischinger M. Consistent inelastic design spectra: Strength and displacement. Earthq Eng Struct Dyn. 1994;23(5):507–21. doi:10.1002/eqe.4290230504

13. D'Aniello M, Mazzolani F. STEEL DISSIPATIVE BRACING SYSTEMS FOR SEISMIC RETROFITTING OF EXISTING STRUCTURES: THEORY AND TESTING. :316.

14. Chen CC, Lu LW. Development and experimental investigation of a ductile CBF system. Proceedings of the 4th National Conference on Earthquake Engineering. Vol.2. :575–84.

15. Clark W, Kasai K, Aiken ID, Kimura I. Evaluation of design methodologies for structures incorporating steel unbonded braces for energy dissipation. Proceedings of the 12th World Conference on Earthquake Engineering. 2000;

16. Kersting RA, Fahnestock LA, Lopez WA. Seismic design of steel buckling-restrained braced frames: a guide for practicing engineers [Internet]. Gaithersburg, MD: National Institute of Standards and Technology; 2016 Sep [cited 2022 Jun 25] p. NIST GCR 15-917-34. Report No.: NIST GCR 15-917-34. doi:10.6028/NIST.GCR.15-917-34

17. Freddi F, Ghosh J, Kotoky N, Raghunandan M. Device uncertainty propagation in low-ductility RC frames retrofitted with BRBs for seismic risk mitigation. Earthq Eng Struct Dyn. 2021;50(9):2488–509. doi:10.1002/eqe.3456

18. Freddi F, Tubaldi E, Zona A, Dall'Asta A. Seismic performance of dual systems coupling moment-resisting and buckling-restrained braced frames. Earthq Eng Struct Dyn. 2021;50(2):329–53. doi:10.1002/eqe.3332

19. Freddi F, Tubaldi E, Ragni L, Dall'Asta A. Probabilistic performance assessment of low-ductility reinforced concrete frames retrofitted with dissipative braces: SEISMIC PERFORMANCE OF LOW-DUCTILITY RC FRAMES WITH DISSIPATIVE BRACES. Earthq Eng Struct Dyn. 2013;42(7):993–1011. doi:10.1002/eqe.2255

20. Ballio G, Mazzolani F, Bernuzzi C, Landolfo R. Strutture di Acciaio. Teoria e Progetto [Internet]. 2ª. Hoepli; 2020. 704 p. Available from: https://www.hoepli.it/libro/strutture-di-acciaio/9788820391805.html

21. Zona A, Dall'Asta A. Elastoplastic model for steel buckling-restrained braces. J Constr Steel Res. 2012;68(1):118–25. doi:10.1016/j.jcsr.2011.07.017

22. Freddi F, Galasso C, Cremen G, Dall'Asta A, Di Sarno L, Giaralis A, et al. Innovations in earthquake risk reduction for resilience: Recent advances and challenges. Int J Disaster Risk Reduct. 2021;60:102267. doi:10.1016/j.ijdrr.2021.102267

23. Uang C-M, Nakashima M, Tsai K-C. Research and Application of Buckling-Restrained Braced Frames. Steel Structures. 2004;301–13.

24. Morfuni F, Freddi F, Galasso C. Resilience-Based Design of Dual Moment-Resisting Frames with Buckling-Restrained Braces. :133.

25. Tremblay R, Dehghani M, Fahnestock L, Herrera R, Canales M, Clifton C, et al. Comparison of seismic design provisions for buckling restrained braced frames in Canada, United States, Chile, and New Zealand. Structures. 2016;8:183–96. doi:10.1016/j.istruc.2016.06.004

26. Shuhaibar C, Lopez WA, Sabelli R. Buckling-restrained braced frames. Seminar on Response Modification Technologies for Performance-Based Seismic Design. 2002;

27. Zona A, Ragni L, Dall'Asta A. Sensitivity-based study of the influence of brace over-strength distributions on the seismic response of steel frames with BRBs. Eng Struct. 2012;37:179–92. doi:10.1016/j.engstruct.2011.12.026

28. Vigh LG, Zsarnóczay Á, Balogh T. Eurocode conforming design of BRBF – Part I: Proposal for codification. J Constr Steel Res. 2017;135:265–76. doi:10.1016/j.jcsr.2017.04.010

29. ANSI/AISC 341-16: Seismic Provisions for Structural Steel Buildings. 2016;480.

30. American Society of Civil Engineers, editor. Minimum design loads for buildings and other structures. Reston, Va: American Society of Civil Engineers : Structural Engineering Institute; 2010. 608 p. (ASCE standard).

31. Aiken ID, Mahin SA, Uriz P. Large-scale testing of buckling-restrained braced frames. In: Japan Passive Control Symposium. 2002.

32. Tsai KC, Hsiao BC, Lai JW, Chen CH, Lin ML, Weng YT. Pseudo dynamic experimental response of a full scale CFT/BRB composite frame. In: Proc, Joint NCREE/JRC Workshop on Int Collaboration on Earthquake Disaster Mitigation Research. 2003.

33. Tsai KC, Loh CH, Hwang YC, Weng CS. Seismic retrofit of building structures with dampers in Taiwan. In: Symposium of Seismic Retrofit of Buildings and Bridges with Base Isolation and Dampers. Kyoto University Japan; 2003.

34. Lin ML. Bi-directional sub-structural pseudo-dynamic tests of a full-scale 2-story BRBF, Part 2: Compressive behavior of gusset plates. In: Proceedings of the 8th US National Conference on Earthquake Engineering, 2006 4. 2006.

35. Tsai KC, Weng YT, Wang KJ, Tsai CY, Lai JW, Lin JL. Bi-directional sub-structural pseudo-dynamic testing of a full scale 2-Story BRBF, Part 1:

Seismic design, analytical and experimental performance assessments. In: 8th US National Conference on Earthquake Engineering. 2006.

36. Roeder CW. Seismic performance of special concentrically braced frames with buckling restrained braces. In: 8th National Conference on Earthquake Engineering (8th NCEE), 2006 4. 2006.

37. Fahnestock LA, Ricles JM, Sause R. Experimental Evaluation of a Large-Scale Buckling-Restrained Braced Frame. J Struct Eng. 2007;133(9):1205–14. doi:10.1061/(ASCE)0733-9445(2007)133:9(1205)

38. Di Sarno L, Manfredi G. Seismic retrofitting with buckling restrained braces: Application to an existing non-ductile RC framed building. Soil Dyn Earthq Eng. 2010;30(11):1279–97. doi:10.1016/j.soildyn.2010.06.001

39. Lorenzo GD, Colacurcio E, Filippo AD, Formisano A, Massimilla A, Landolfo R. STATE-OF-THE-ART ON STEEL EXOSKELETONS FOR SEISMIC RETROFIT OF EXISTING RC BUILDINGS. :19.

40. Gioiella L, Tubaldi E, Gara F, Dezi L, Dall'Asta A. Modal properties and seismic behaviour of buildings equipped with external dissipative pinned rocking braced frames. Eng Struct. 2018;172:807–19. doi:10.1016/j.engstruct.2018.06.043

41. Di Sarno L, Paolacci F, Sextos AG. Seismic performance assessment of existing steel buildings: a case study. In: Key Engineering Materials. Trans Tech Publ; 2018. p. 1067–76.

42. Di Sarno L, Wu J-R. Seismic assessment of existing steel frames with masonry infills. J Constr Steel Res. 2020;169:106040.

43. Freddi F, Dimopoulos CA, Karavasilis TL. Experimental Evaluation of a Rocking Damage-Free Steel Column Base with Friction Devices. J Struct Eng. 2020;146(10):04020217. doi:10.1061/(ASCE)ST.1943-541X.0002779

44. da Silva LS, Simões R, Gervásio H. Design of Steel Structures: Eurocode 3: Design of steel structures, Part 1-1 – General rules and rules for buildings [Internet]. 1st ed. Wiley; 2012 [cited 2022 Jun 27]. doi:10.1002/9783433601099

45. Iso EN. 6892-1. Metallic materials-Tensile testing-Part 1: Method of test at room temperature. Int Organ Stand. 2009;

46. Jennings PC, Scholl RE, Earthquake Engineering Research Institute Committee on Experimental Research. Experimental research needs for improving earthquake-resistant design of buildings: [overview and recommendations] / EERI Committee on Experimental Research ; prepared on behalf of the committee by P. Jennings and R. Scholl. Berkeley, Calif.: Earthquake Engineering Research Institute; 1984. ii+43. (Report (Earthquake Engineering Research Institute) ; no. 84-02).

47. Mahin SA, Shing PB, Thewalt CR, Hanson RD. Pseudodynamic Test Method—Current Status and Future Directions. J Struct Eng. 1989;115(8):2113–28. doi:10.1061/(ASCE)0733-9445(1989)115:8(2113)

48. Nakashima M, Kato H, Takaoka E. Development of real-time pseudo dynamic testing. Earthq Eng Struct Dyn. 1992;21(1):79–92.

49. Nakashima M. Development, potential, and limitations of real–time online (pseudo–dynamic) testing. Chapman SJ, editor. Philos Trans R Soc Lond Ser Math Phys Eng Sci. 2001;359(1786):1851–67. doi:10.1098/rsta.2001.0876

50. Sadeghian V, Kwon O-S. Discussion of "Fast and Slow Cyclic Tests for Reinforced Concrete Columns with an Improved Axial Force Control" by Yunbyeong Chae, Jinhaeng Lee, Minseok Park, and Chul-Young Kim. J Struct Eng. 2020;146(7):07020001.

51. Mojiri S, Kwon O-S, Christopoulos C. Development of a ten-element hybrid simulation platform and an adjustable yielding brace for performance evaluation of multi-story braced frames subjected to earthquakes. Earthq Eng Struct Dyn. 2019;48(7):749–71.

52. Takanashi K, Udagawa K, Seki M, Okada T, Tanaka H. Nonlinear earthquake response analysis of structures by a computer-actuator on-line system. Bull Earthq Resist Struct Res Cent. 1975;8:1–17.

53. Pegon P, Pinto AV. Pseudo-dynamic testing with substructuring at the ELSA Laboratory. Earthq Eng Struct Dyn. 2000;29(7):905–25. doi:10.1002/1096-9845(200007)29:7<905::AID-EQE941>3.0.CO;2-P

54. Shing PB, Mahin SA. Pseudodynamic method for seismic performance testing: theory and implementation. Rep No UCBEERC-84. 1984;1.

55. Luzi L, Puglia R, Russo E, ORFEUS W 5. Engineering strong motion database, version 1.0. Ist Naz Geofis E Vulcanol Obs Res Facil Eur Seismol Doi. 2016;10.

56. Smith M. Abaqus/CAE User's Guide, Version 6.14. Dassault Systèmes Simulia Corp; 2009.

57. Lubliner J. Plasticity Theory. Pearson Education;

58. Choung JM, Cho SR. Study on true stress correction from tensile tests. J Mech Sci Technol. 2008;22(6):1039–51. doi:10.1007/s12206-008-0302-3

59. Bridgman PW. Studies in Large Plastic Flow and Fracture: With Special Emphasis on the Effects of Hydrostatic Pressure [Internet]. Studies in Large Plastic Flow and Fracture. Harvard University Press; 2013 [cited 2022 Jul 13]. doi:10.4159/harvard.9780674731349

60. Aronofsky J. Evaluation of Stress Distribution in the Symmetrical Neck of Flat Tensile Bars. J Appl Mech. 2021;18(1):75–84. doi:10.1115/1.4010223

61. Zhang Z, Hauge M, Ødegård J, Thaulow C. Determining material true stress–strain curve from tensile specimens with rectangular cross-section. 1999; doi:10.1016/S0020-7683(98)00153-X

62. Ling Y, Incorporated A. Uniaxial True Stress-Strain after Necking. undefined [Internet]. 2004 [cited 2022 Jul 13]; Available from: https://www.semanticscholar.org/paper/Uniaxial-True-Stress-Strain-after-Necking-Ling-Incorporated/16694f61de9799413445d61f53065e29ad74f6fc

63. Scheider I, Brocks W, Cornec A. Procedure for the Determination of True Stress-Strain Curves From Tensile Tests With Rectangular Cross-Section Specimens. J Eng Mater Technol. 2004;126(1):70–6. doi:10.1115/1.1633573

64. Bernuzzi C, Cordova B. Structural Steel Design to Eurocode 3 and AISC Specifications [Internet]. Wiley; 2016. 536 p. Available from: https://www.wiley.com/en-us/Structural+Steel+Design+to+Eurocode+3+and+AISC+Specifications-p-9781118631287

65. Blaž Č, Darko B. Seismic resistance of welded beam-to-column connections in hybrid moment and braced frames. University of Ljubljana; 2015.

66. Lemaitre J, Chaboche J-L. Mechanics of Solid Materials [Internet]. Cambridge University Press; 1990. 584 p. Available from: https://doi.org/10.1017/CBO9781139167970

67. Zub C, Dubina D, Sato A, Văcăreanu RS, Chiorean C-G. Seismic protection of building framed structures with Buckling Restrained Braces (Protecția antiseismică a structurilor în cadre cu contravântuiri cu flambaj împiedecat). Politehnica University Timisoara; 2018 [cited 2022 Jun 28]. Available from: http://rgdoi.net/10.13140/RG.2.2.13375.12969

68. Zub CI, Stratan A, Dogariu A, Dubina D. Development of a Finite Element Model for a Buckling Restrained Brace. Proc ROMANIAN Acad Ser A. Volume 19, Number 4/2018, pp. 581–588:8.

69. Zub CI, Stratan A, Dubina D. Modelling the cyclic response of structural steel for FEM analyses. Herisanu N, Razzaghi M, Vasiu R, editors. ITM Web Conf. 2019;29:02011. doi:10.1051/itmconf/20192902011

70. Whitmore RE. Experimental Investigation of Stresses in Gusset Plates [Internet]. Engineering Experiment Station, University of Tennessee, Knoxville; 1952. (Bulletin (University of Tennessee (Knoxville campus). Engineering Experiment Station))). Available from: https://books.google.it/books?id=ER9ZJAAACAAJ

71. BS EN B. Eurocode 3: Design of steel structures-Part 1-8: Design of joints. BS EN. 1993;1(2005):8.

72. Thornton WA. Bracing connections for heavy construction. Eng J. 1984;21(3):139–48.

73. Dall'Asta A, Ragni L, Tubaldi E, Freddi F. Design methods for existing r.c. frames equipped with elasto-plastic or viscoelastic dissipative braces. :9.

74. Ragni L, Zona A, Dall'Asta A. Analytical expressions for preliminary design of dissipative bracing systems in steel frames. J Constr Steel Res. 2011;67(1):102–13. doi:10.1016/j.jcsr.2010.07.006

75. Maley TJ, Sullivan TJ, Corte GD. Development of a Displacement-Based Design Method for Steel Dual Systems With Buckling-Restrained Braces and Moment-Resisting Frames. J Earthq Eng. 2010;14(sup1):106–40. doi:10.1080/13632461003651687

76. Sabelli R, Mahin S, Chang C. Seismic demands on steel braced frame buildings with buckling-restrained braces. Eng Struct. 2003;25(5):655–66. doi:10.1016/S0141-0296(02)00175-X

77. Castaldo P, Tubaldi E, Selvi F, Gioiella L. Seismic performance of an existing RC structure retrofitted with buckling restrained braces. J Build Eng. 2021;33:101688. doi:10.1016/j.jobe.2020.101688

Appendix A

The present appendix presents a comparison between the experimental results and Abaqus results concerning the bare frame subjected to the seismic sequence scaled by 0.75 and 1. Finally, a comparison of the main results obtained for the different scaling factors is reported.

A.1. Scaled Ground Motion (SF = 0.75)

The procedure described in Section 4.1.2.1 was repeated considering the ground motion scaled by a scale factor of "0.75". Therefore, the following graphs are completely analogous to the ones previously presented.

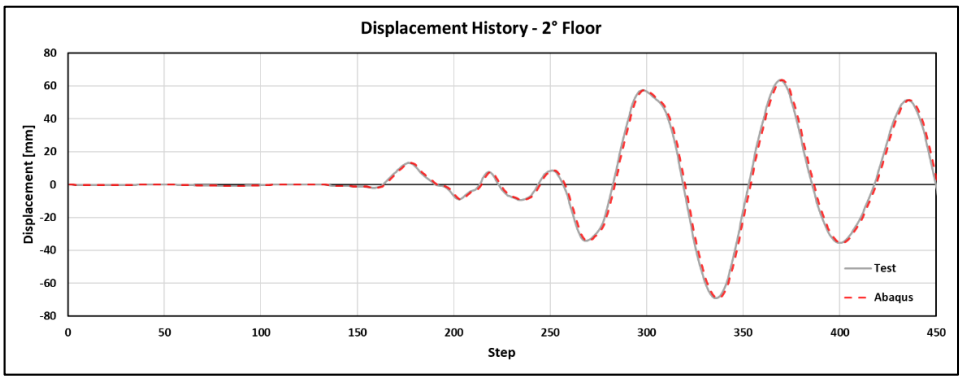

(a)

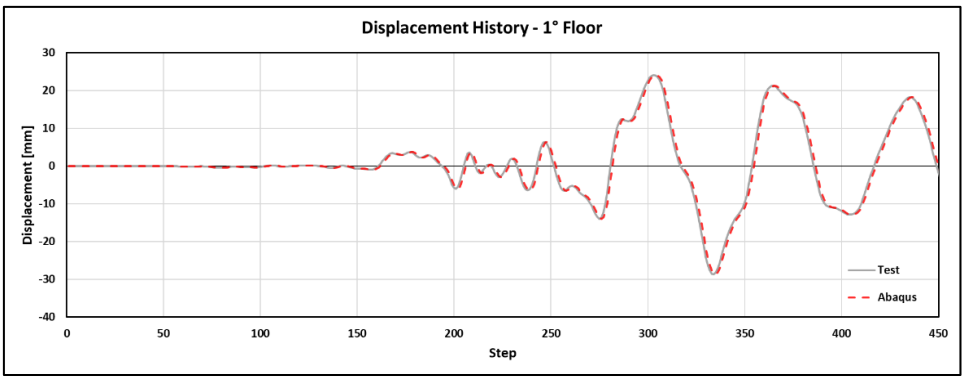

(b)

Figure A1-1 *Displacement History: (a) Second Floor; (b) First Floor*

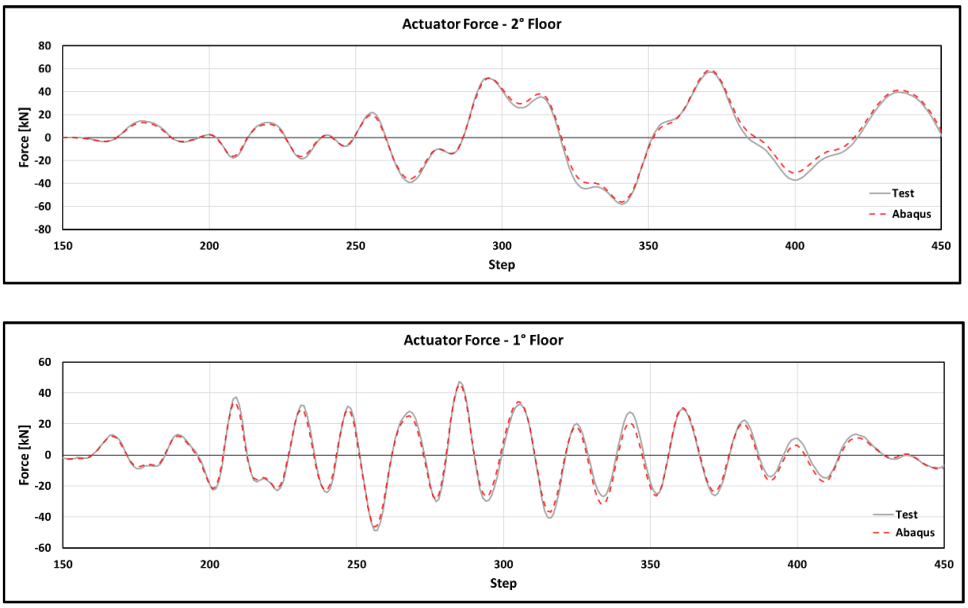

(a)

(b)

Figure A1-2 *Actuator Force: (a) Second Floor; (b) First Floor*

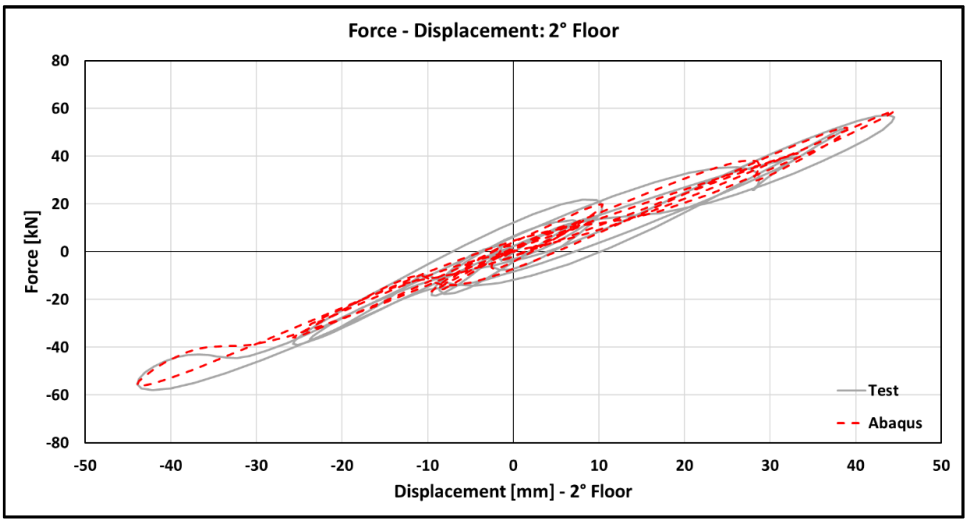

(a)

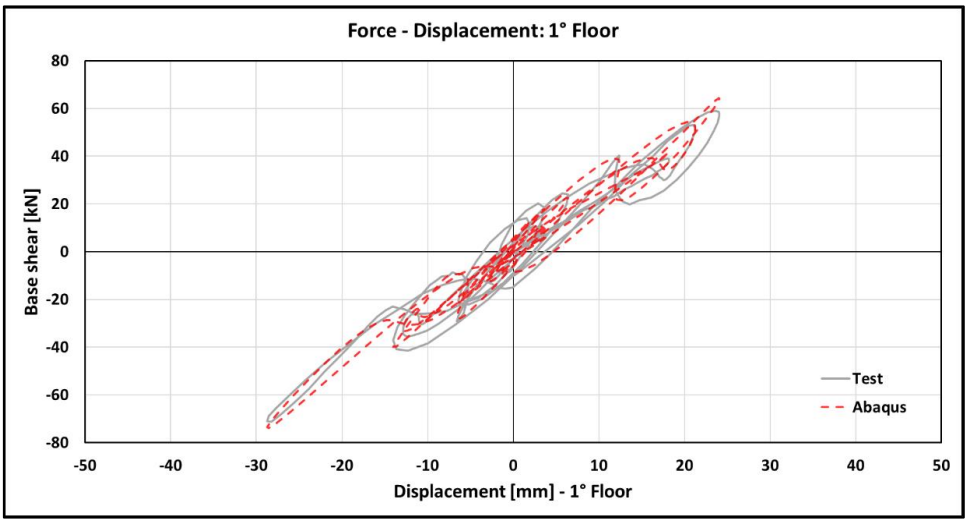

(b)

Figure A1-3 *Floor Stiffeness: (a) Second Floor; (b) First Floor*

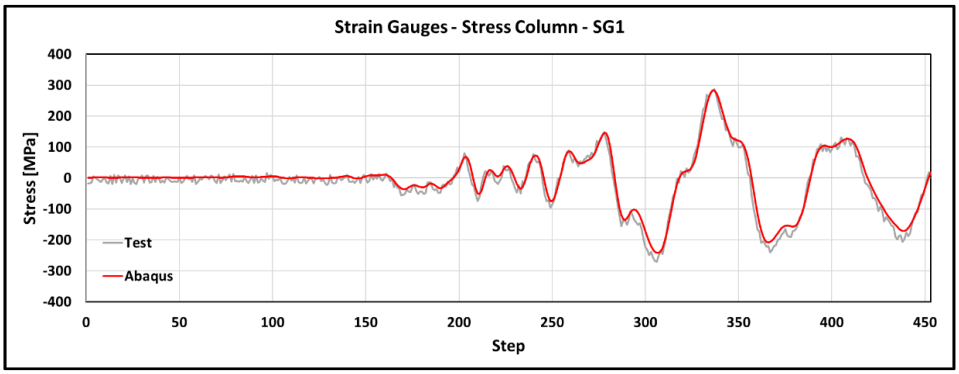

(a)

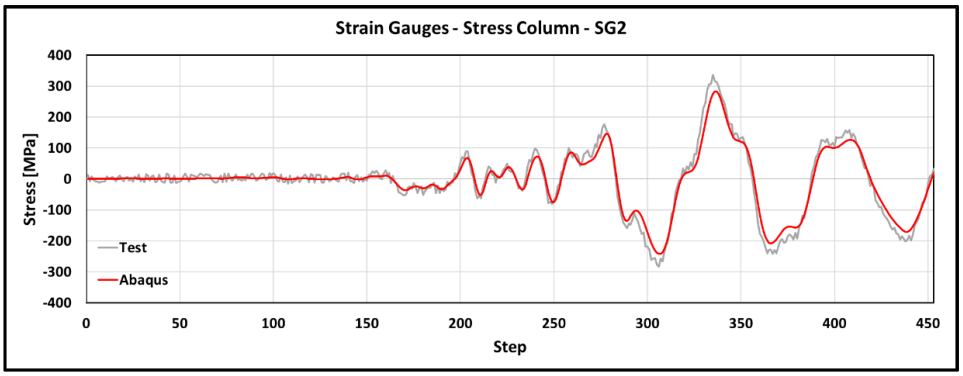

(b)

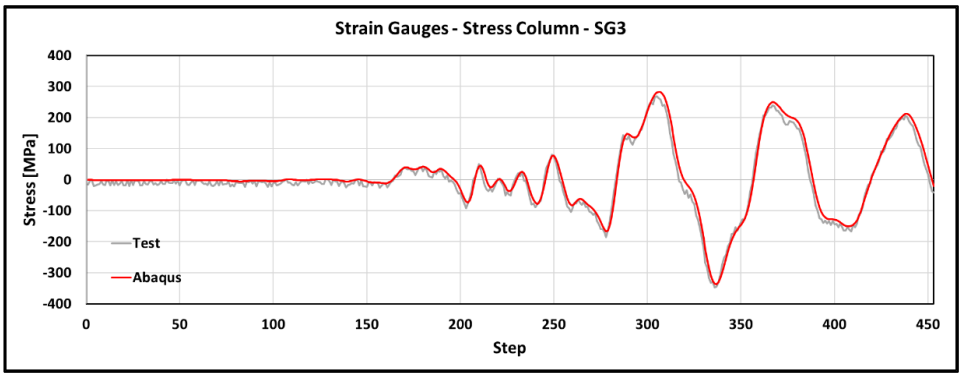

(c)

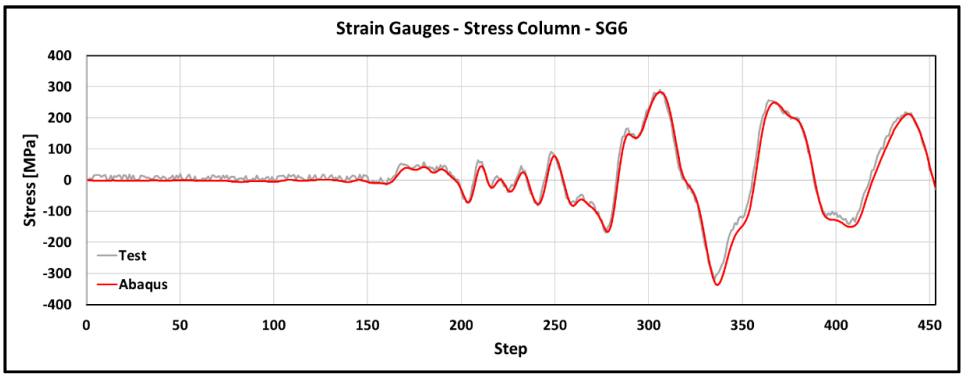

(d)

Figure A1-4 *Column Flange Strain Gauges - Detail 1: (a) SG1, (b) SG2, (c) SG3, (d) SG6*

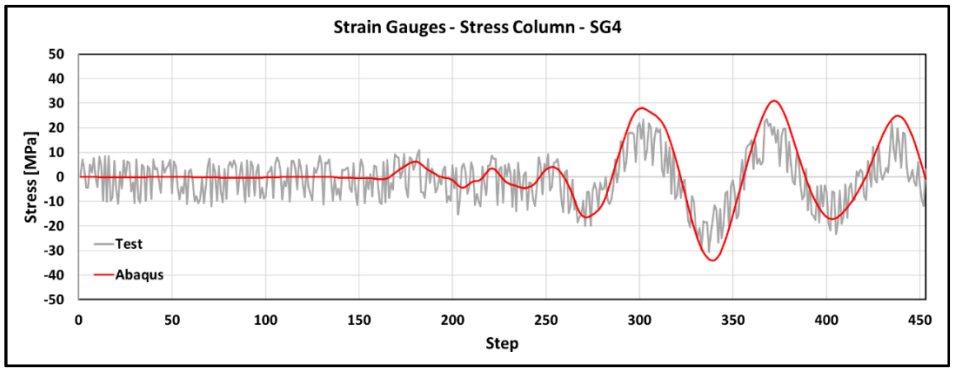

(a)

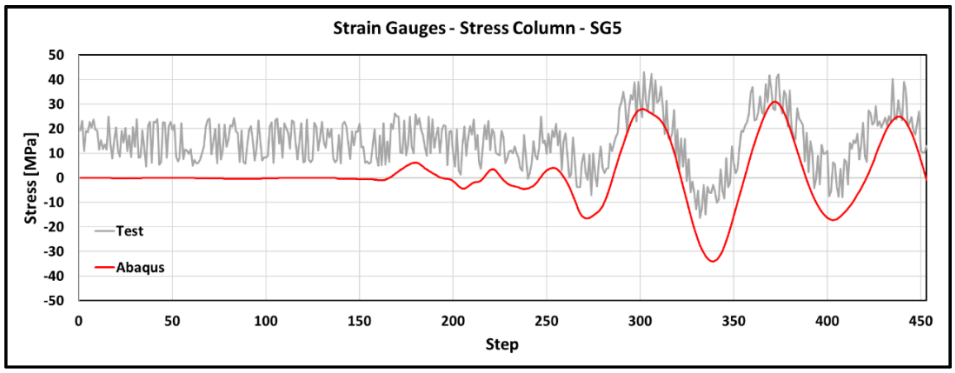

(b)

Figure A1-5 *Column Web Strain Gauges - Detail 1: (a) SG4, (b) SG5*

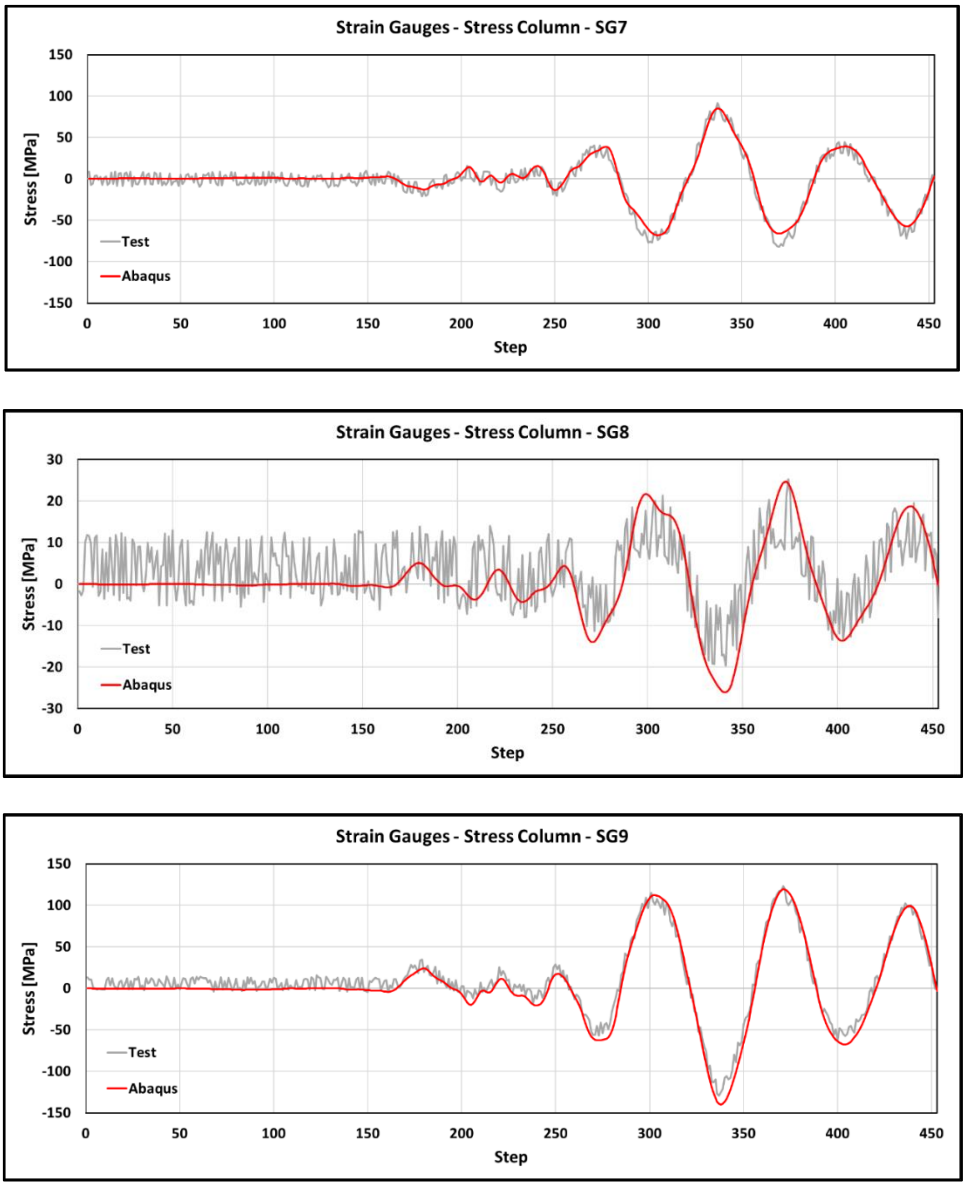

Figure A1-6 *Column Flange Strain Gauges - Detail 2: (a) SG7, (b) SG8, (c) SG9*

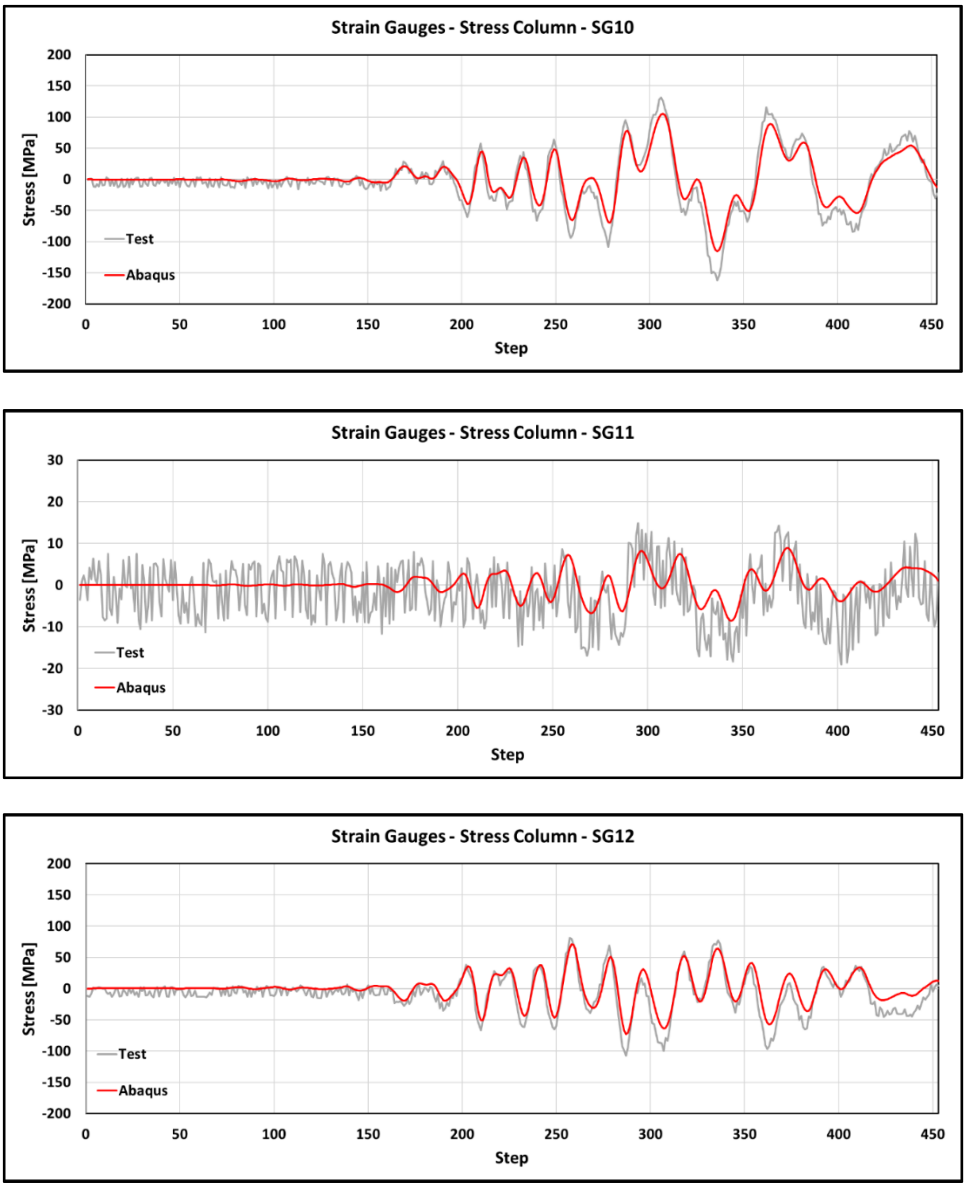

(a)

(b)

(c)

Figure A1-7 *Column Flange Strain Gauges - Detail 3: (a) SG10, (b) SG11, (c) SG12*

A.2. Scaled Ground Motion (SF = 1)

The procedure described in Section 4.1.2.1 was repeated considering the ground motion scaled by a scale factor of "1". Therefore, the following graphs are completely analogous to the ones previously presented.

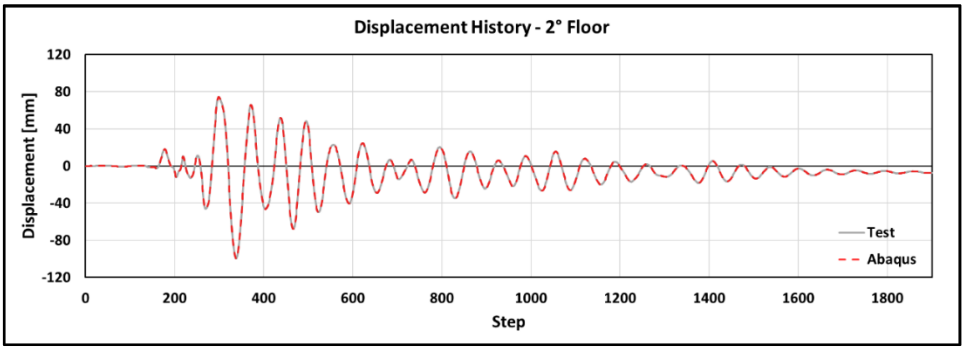

(a)

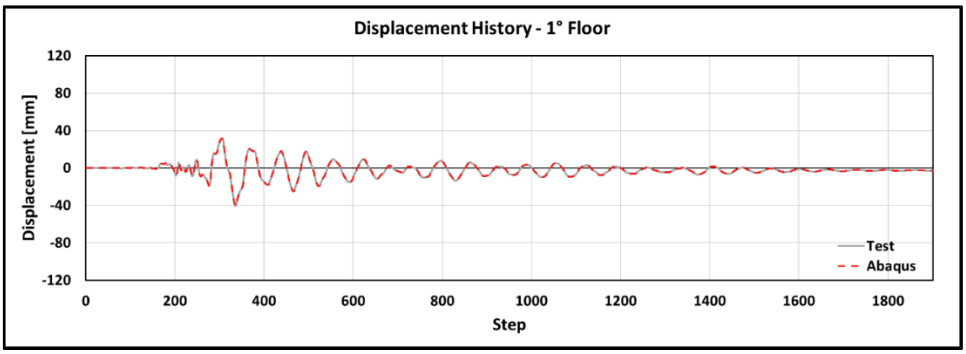

(b)

Figure A2-1 *Displacement History: (a) Second Floor; (b) First Floor*

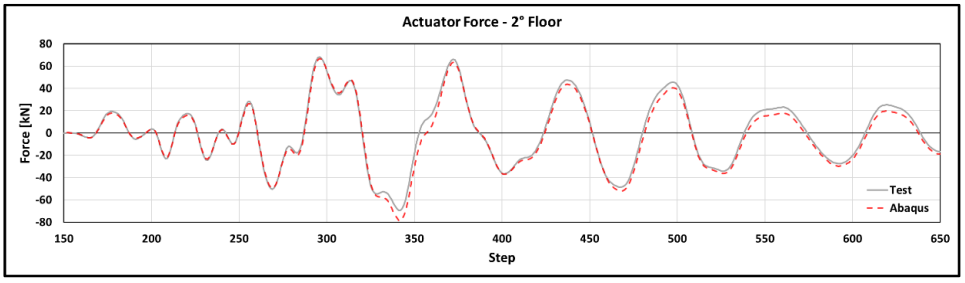

(a)

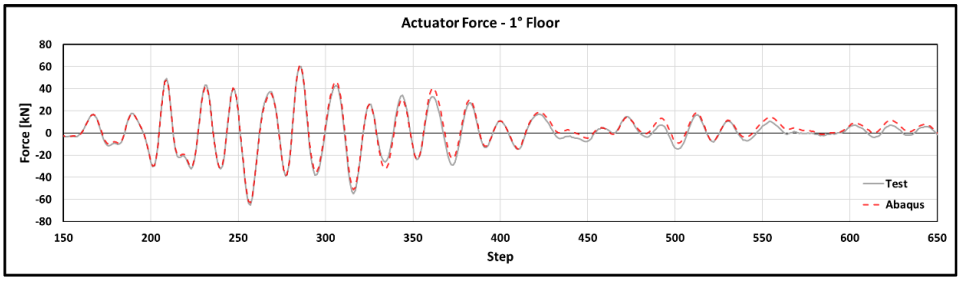

(b)

Figure A2-2 *Actuator Force: (a) Second Floor; (b) First Floor*

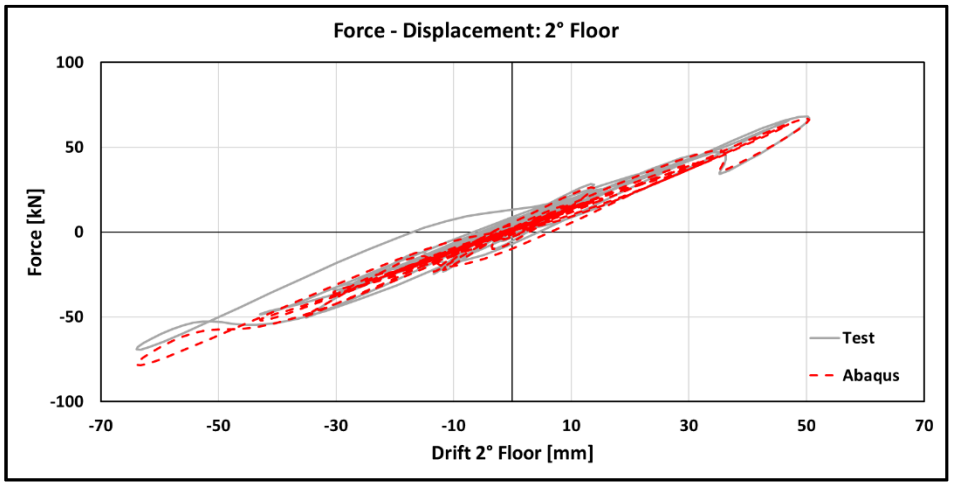

(a)

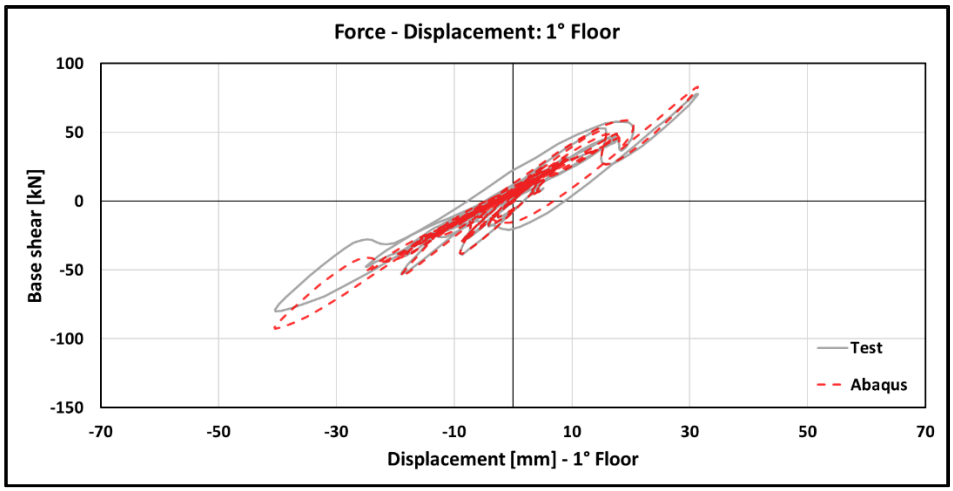

(b)

Figure A2-3 *Floor Stiffness: (a) Second Floor; (b) First Floor.*

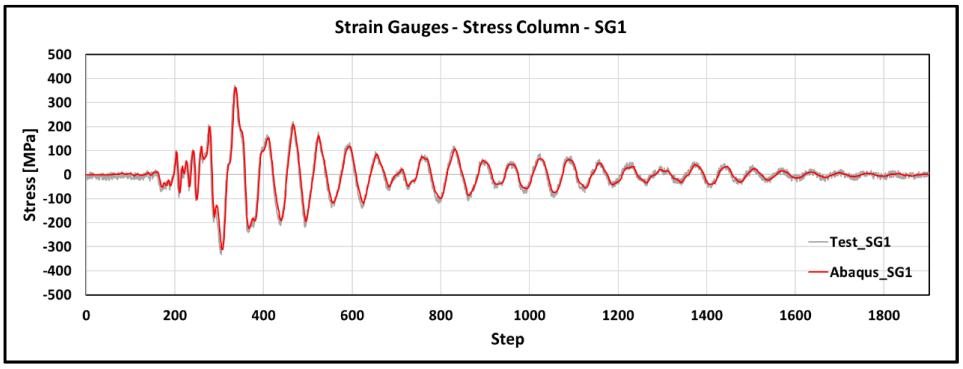

(a)

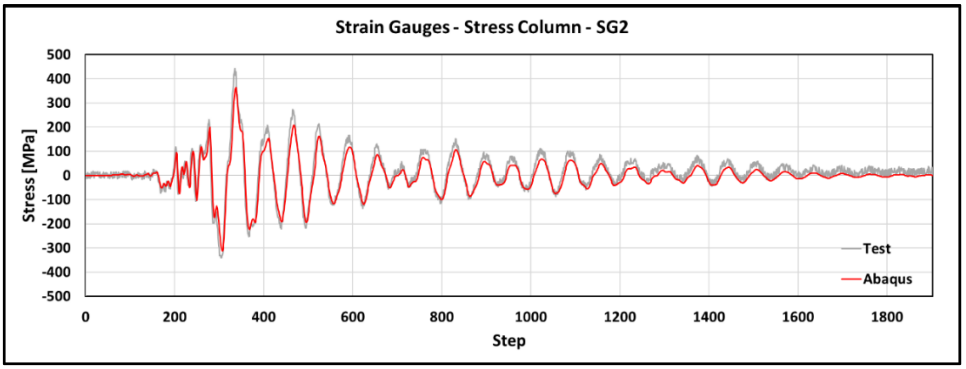

(b)

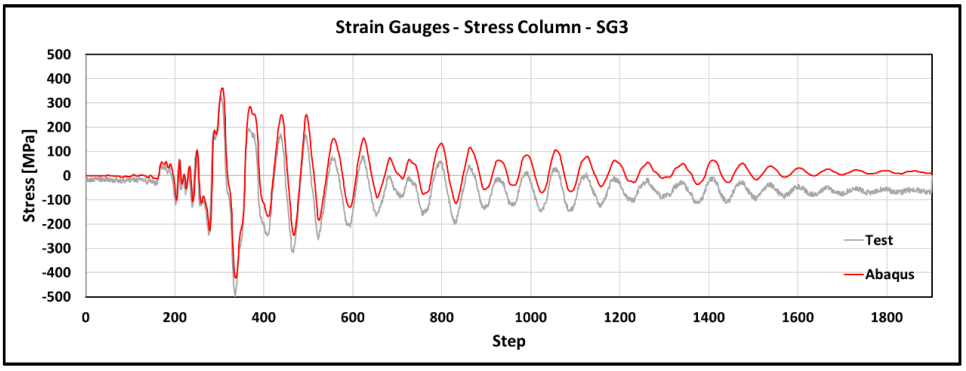

(c)

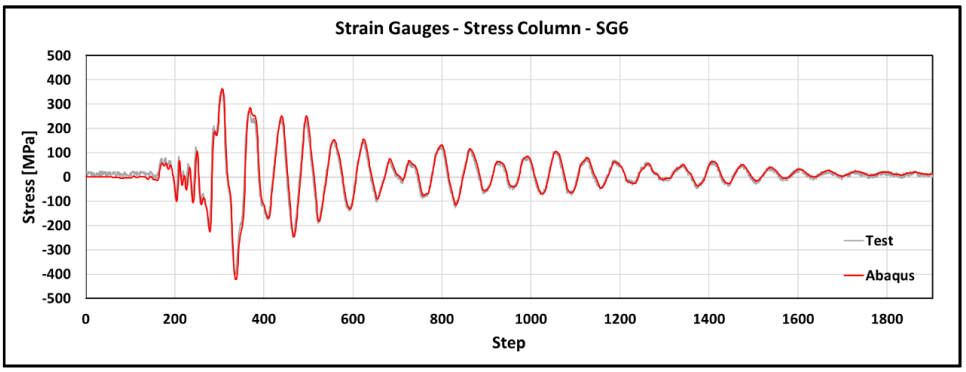

(d)

Figure A2-4 *Column Flange Strain Gauges - Detail 1: (a) SG1, (b) SG2, (c) SG3, (d) SG6*

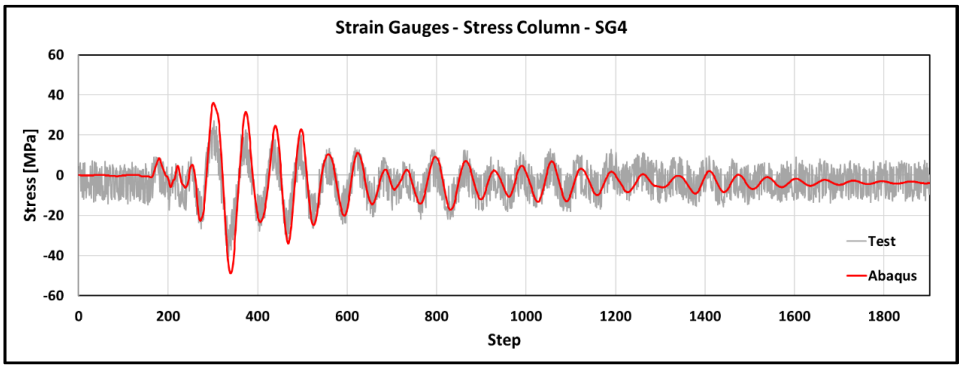

(a)

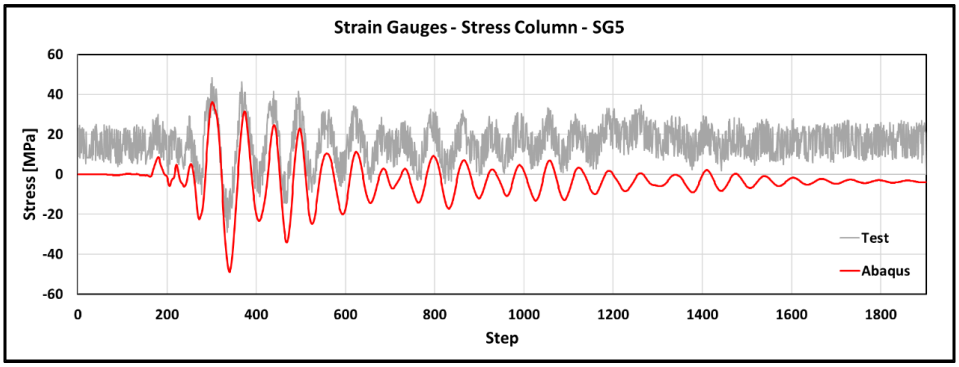

(b)

Figure A2-5 *Column Web Strain Gauges - Detail 1: (a) SG4, (b) SG5*

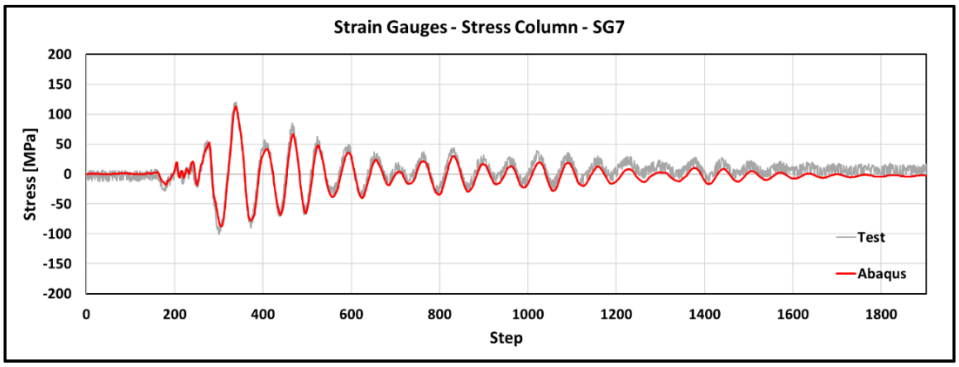

(a)

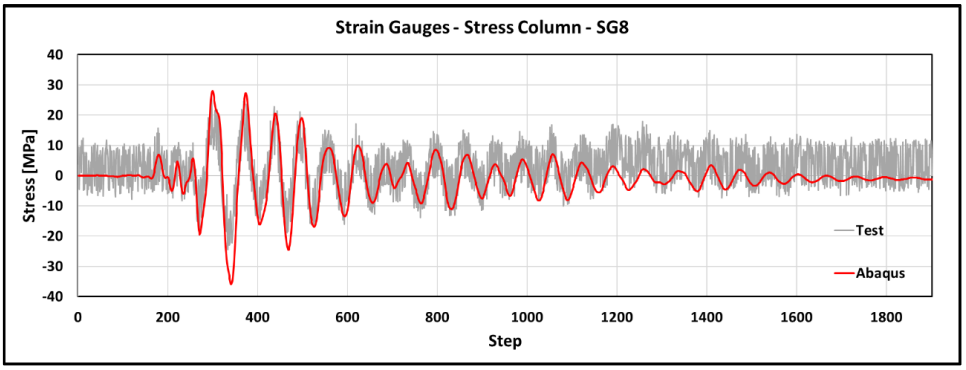

(b)

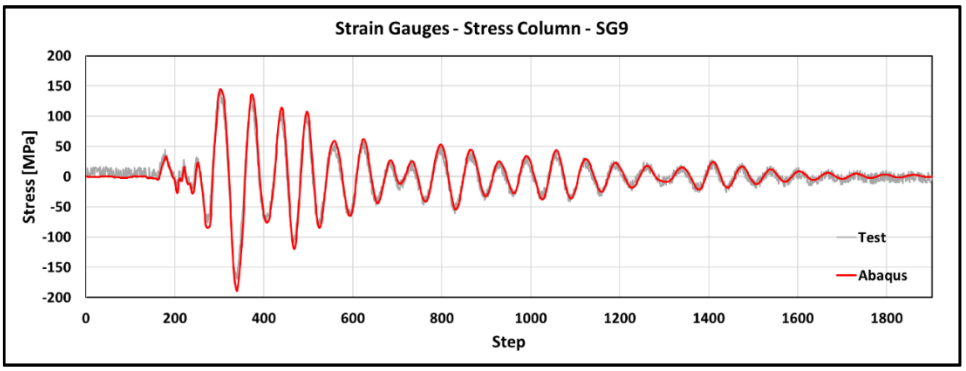

(c)

Figure A2-6 *Column Flange Strain Gauges - Detail 2: (a) SG7, (b) SG8, (c) SG9*

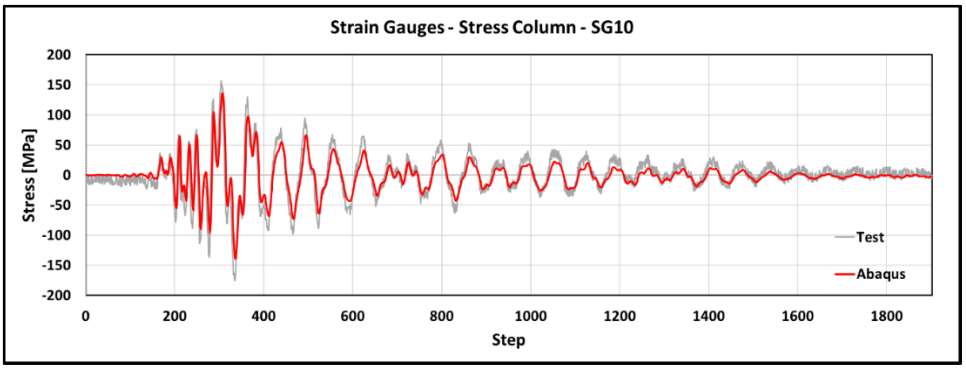

(a)

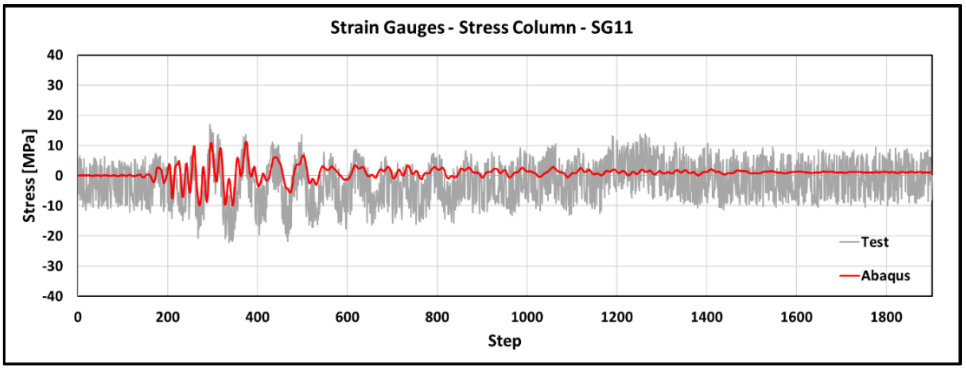

(b)

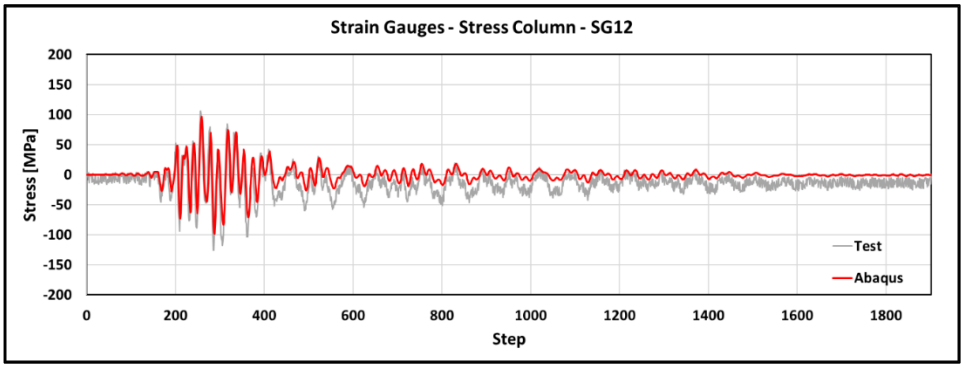

(c)

Figure A2-7 *Column Flange Strain Gauges - Detail 3: (a) SG10, (b) SG11, (c) SG12*

A.3. Comparison between scale factors

Figure A3-1 and Figure A3-2 summarise the results shown in the previous section and in 4.1.2. As already mentioned, these data prove that the Abaqus model can be considered as valid, *i.e.*, equivalent to the real model.

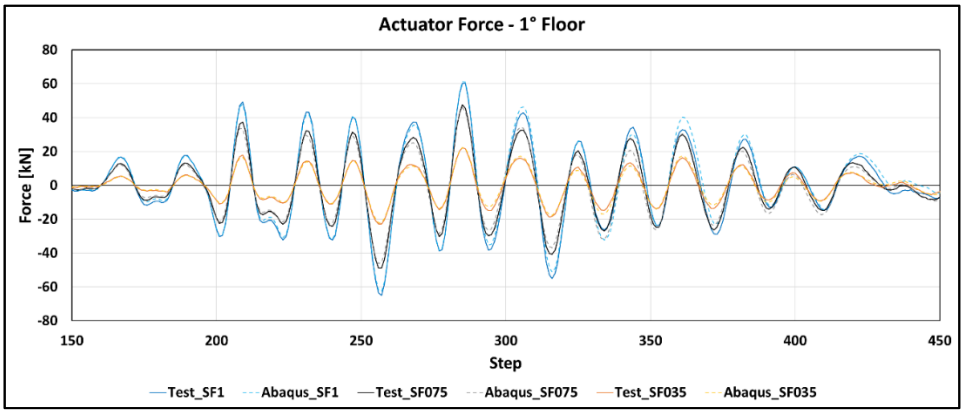

(a)

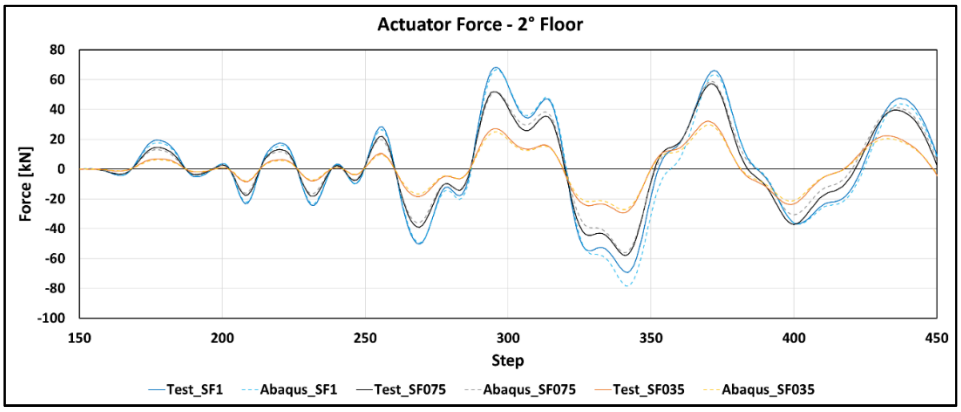

(b)

Figure A3-1 *Actuator Force: (a) First floor; (b) Second floor*

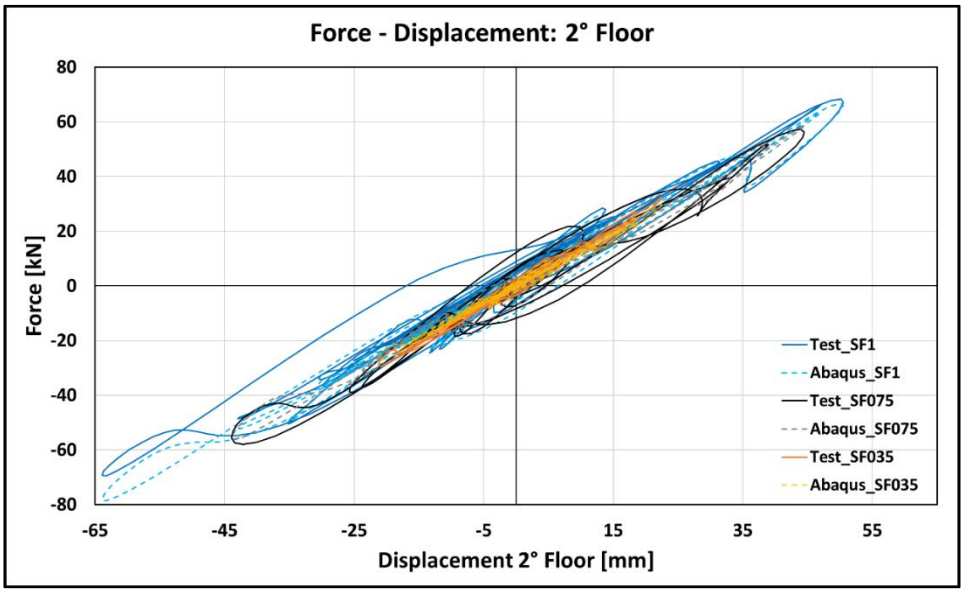

(a)

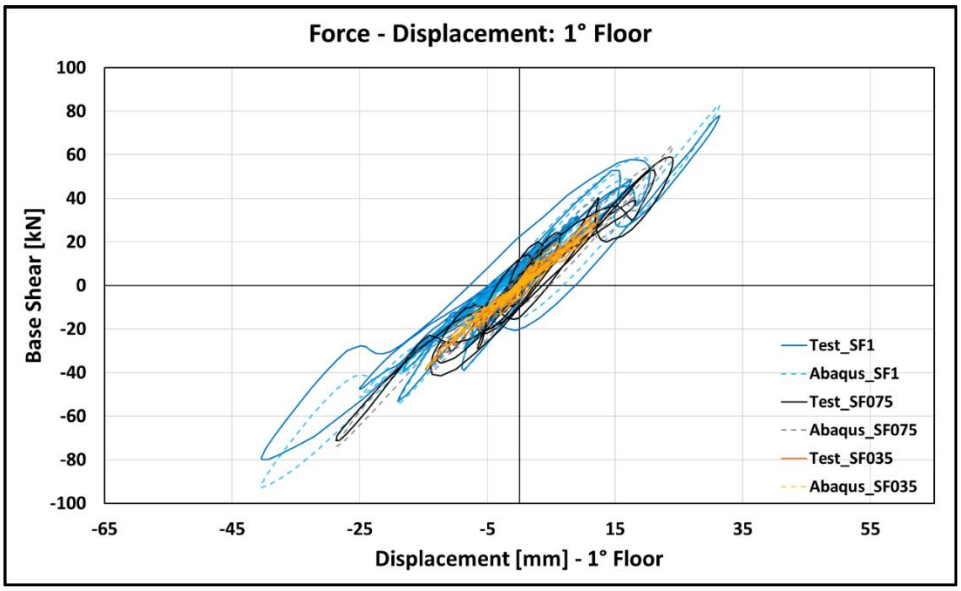

(b)

Figure A3-2 *Floor stiffness: (a) Second floor; (b) First floor*

Appendix B

The present appendix presents a comparison between the experimental results and Abaqus results concerning the BRB frame subjected to the seismic sequence scaled by 1.5.

B.1. Scaled Ground Motion (SF = 1.5)

The procedure described in Section 4.2.4.2 was repeated considering the ground motion scaled by a scale factor of "1.5". Therefore, the following graphs are completely analogous to the ones previously presented.

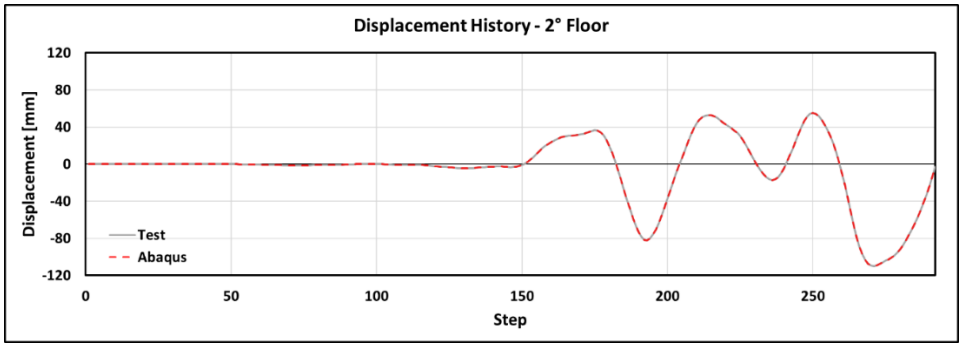

(a)

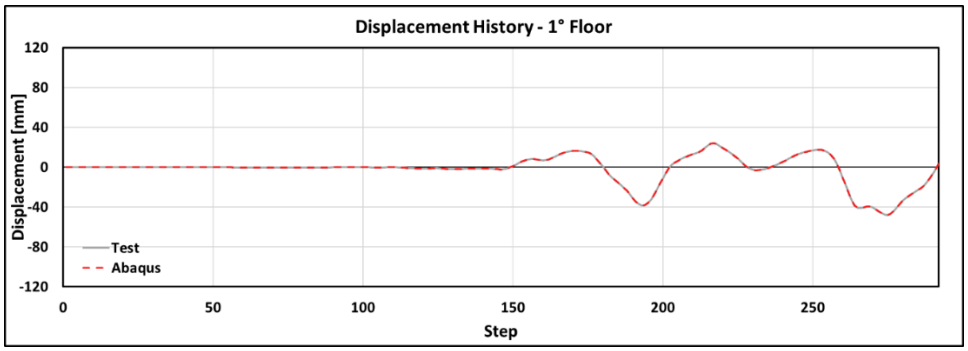

(b)

Figure B1-1 *Displacement History: (a) Second Floor; (b) First Floor*

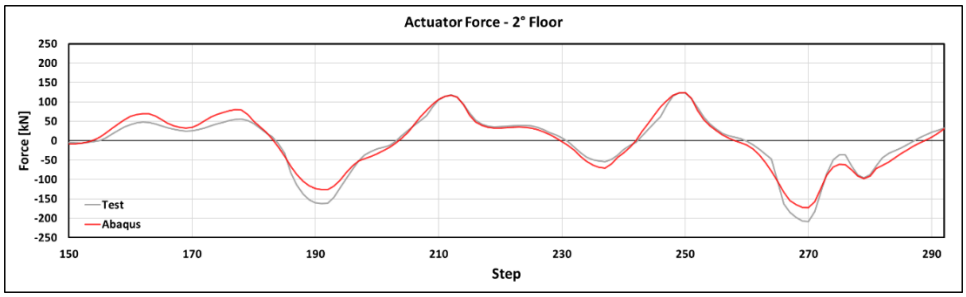

(a)

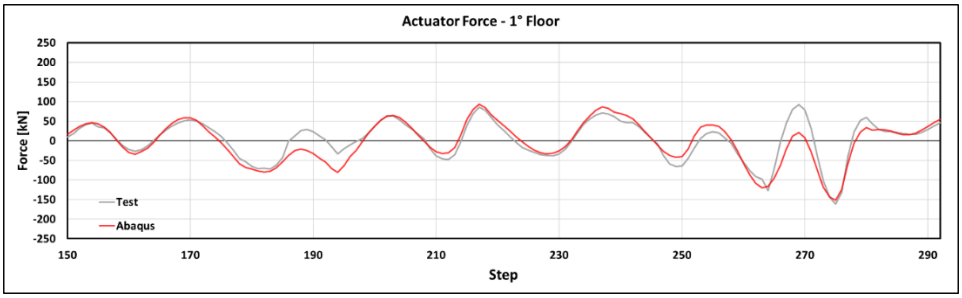

(b)

Figure B1-2 *Actuator Force: (a) Second Floor; (b) First Floor*

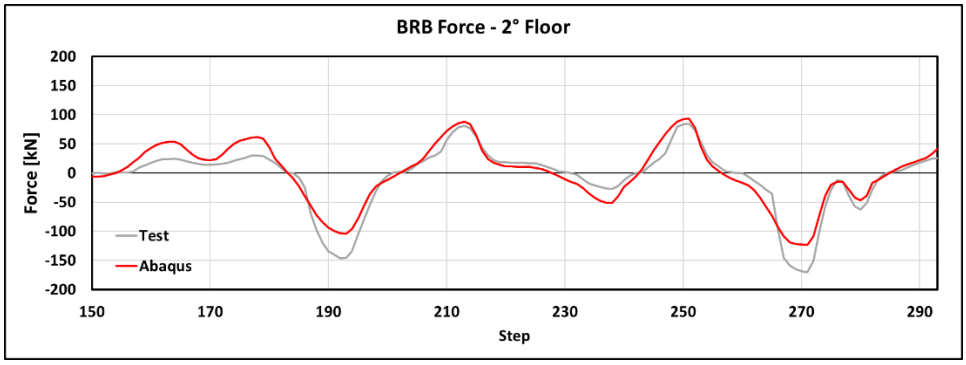

(a)

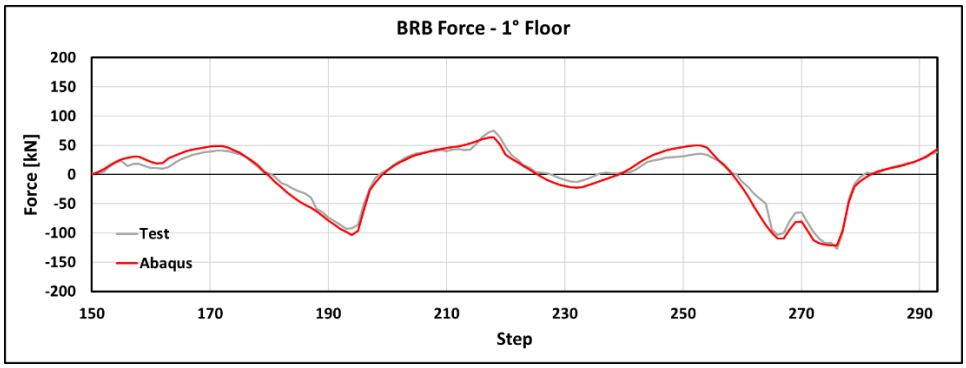

(b)

Figure B1-3 *BRB Force: (a) Second Floor; (b) First Floor*

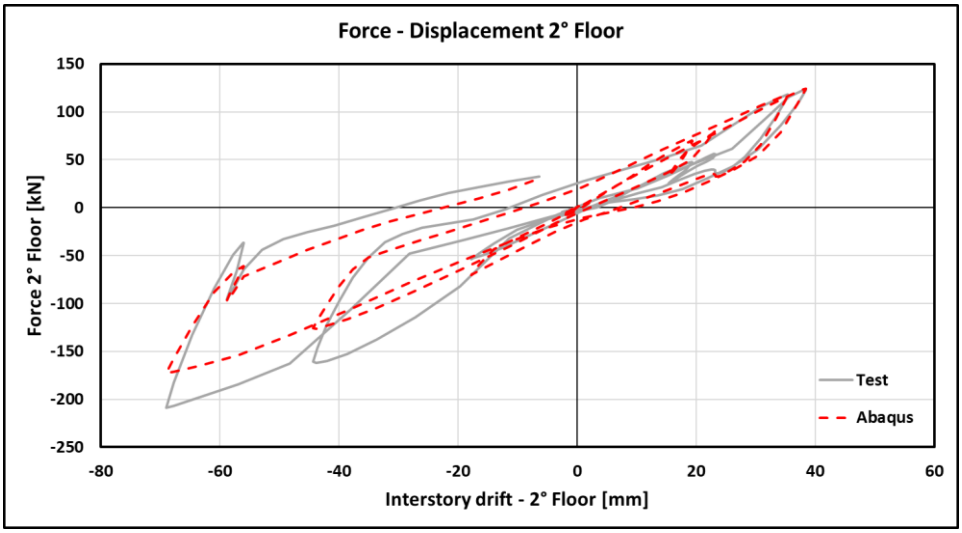

(a)

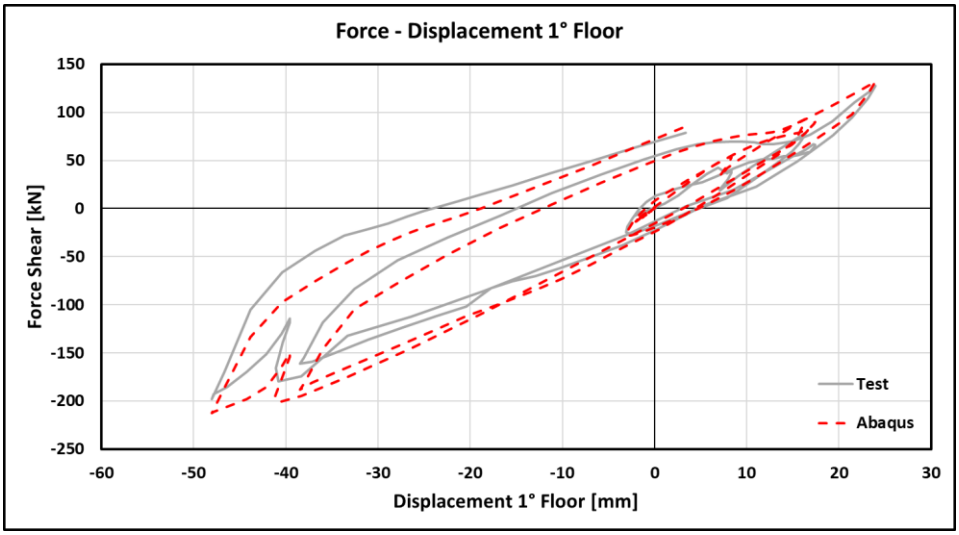

(b)

Figure B1-4 *Floor Stiffness: (a) Second Floor; (b) First Floor*

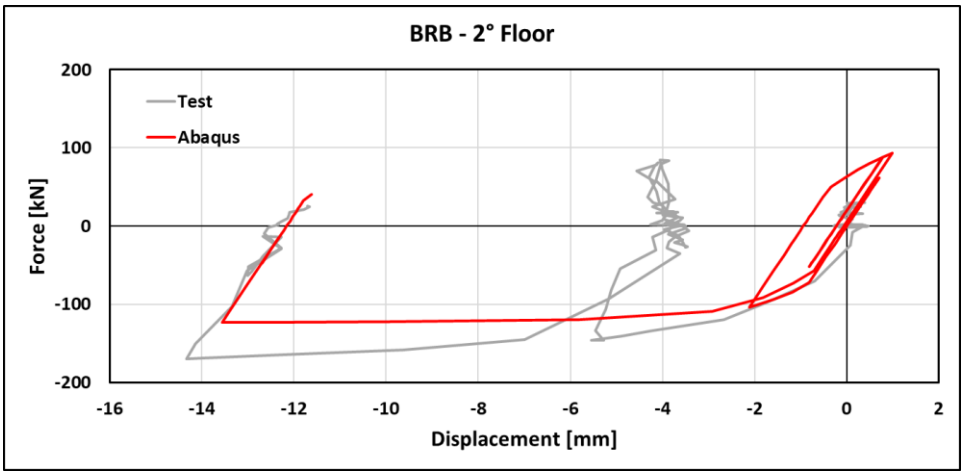

(a)

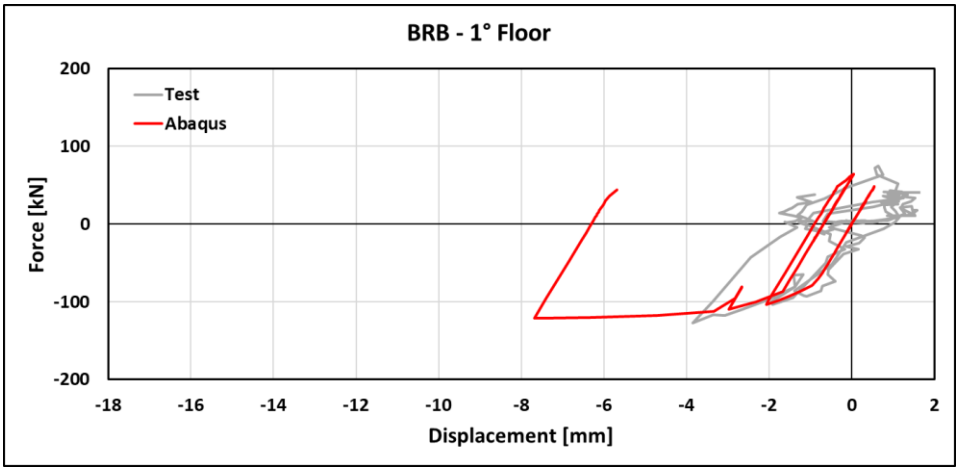

(b)

Figure B1-5 *BRB behaviour: (a) Second Floor; (b) First Floor*

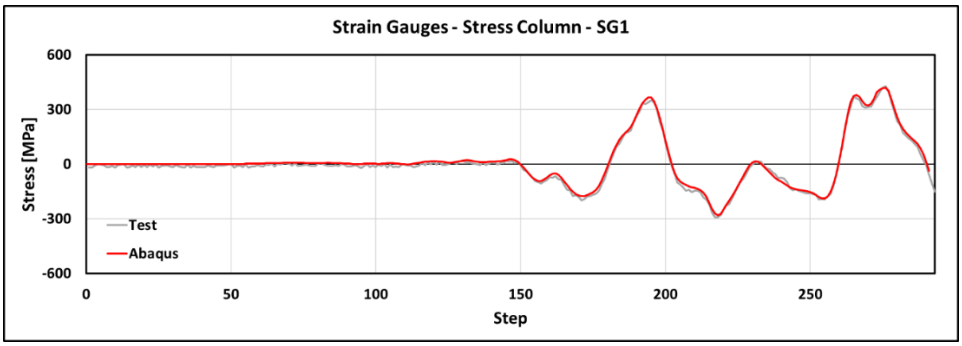

(a)

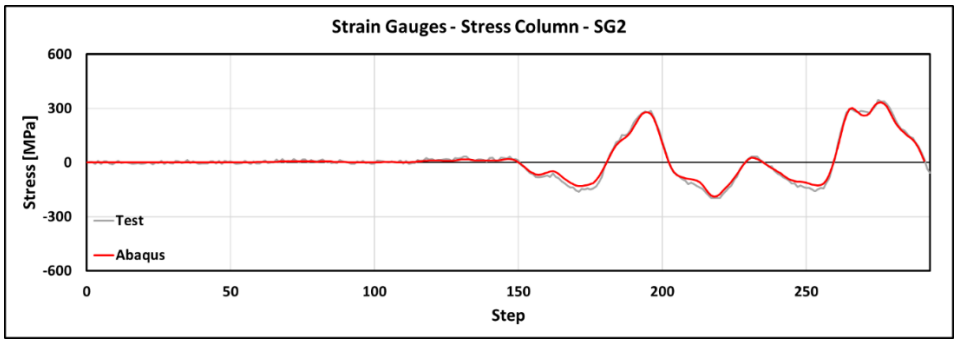

(b)

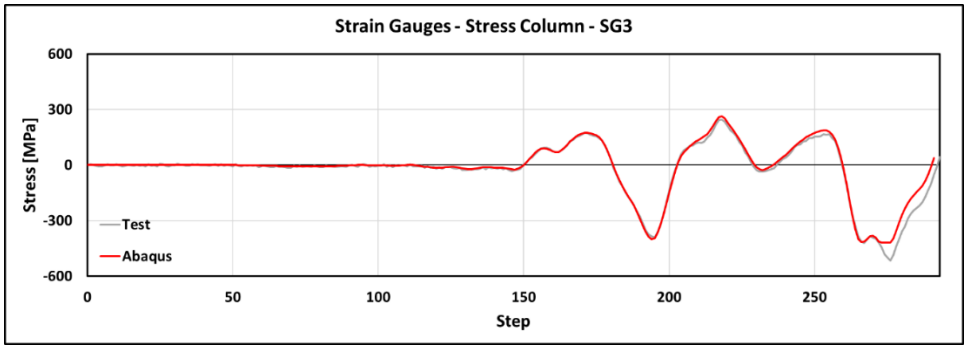

(c)

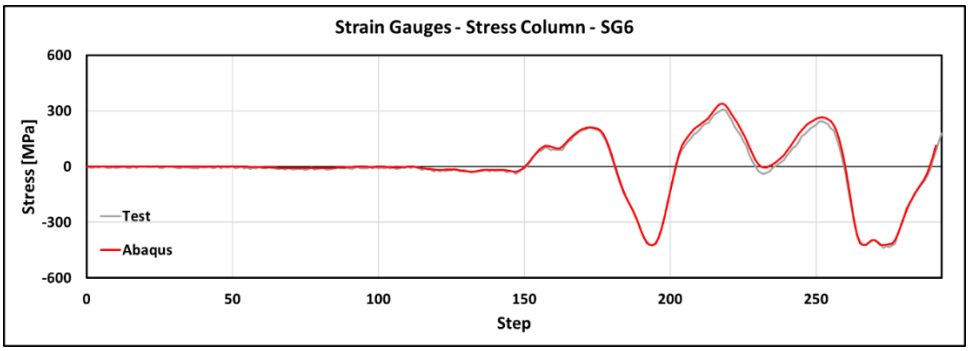

(d)

Figure B1-6 *Column Flange Strain Gauges - Detail 1: (a) SG1, (b) SG2, (c) SG3, (d) SG6*

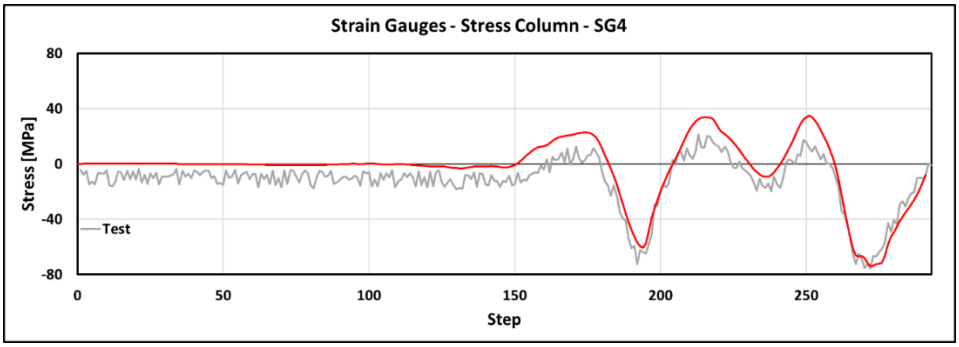

(a)

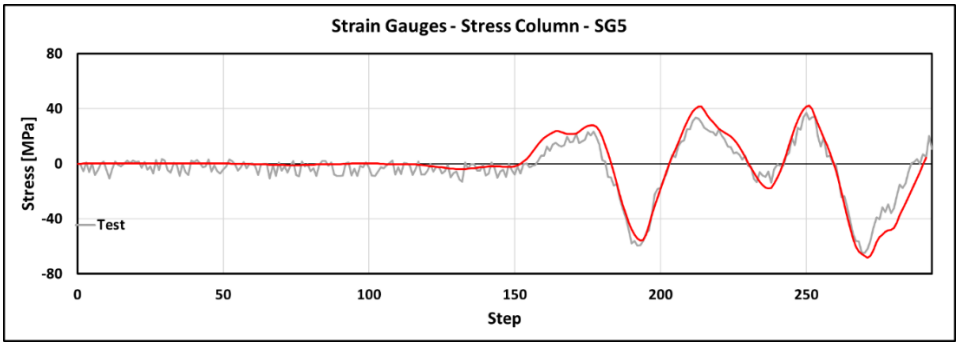

(b)

Figure B1-7 *Column Web Strain Gauges - Detail 1: (a) SG4, (b) SG5*

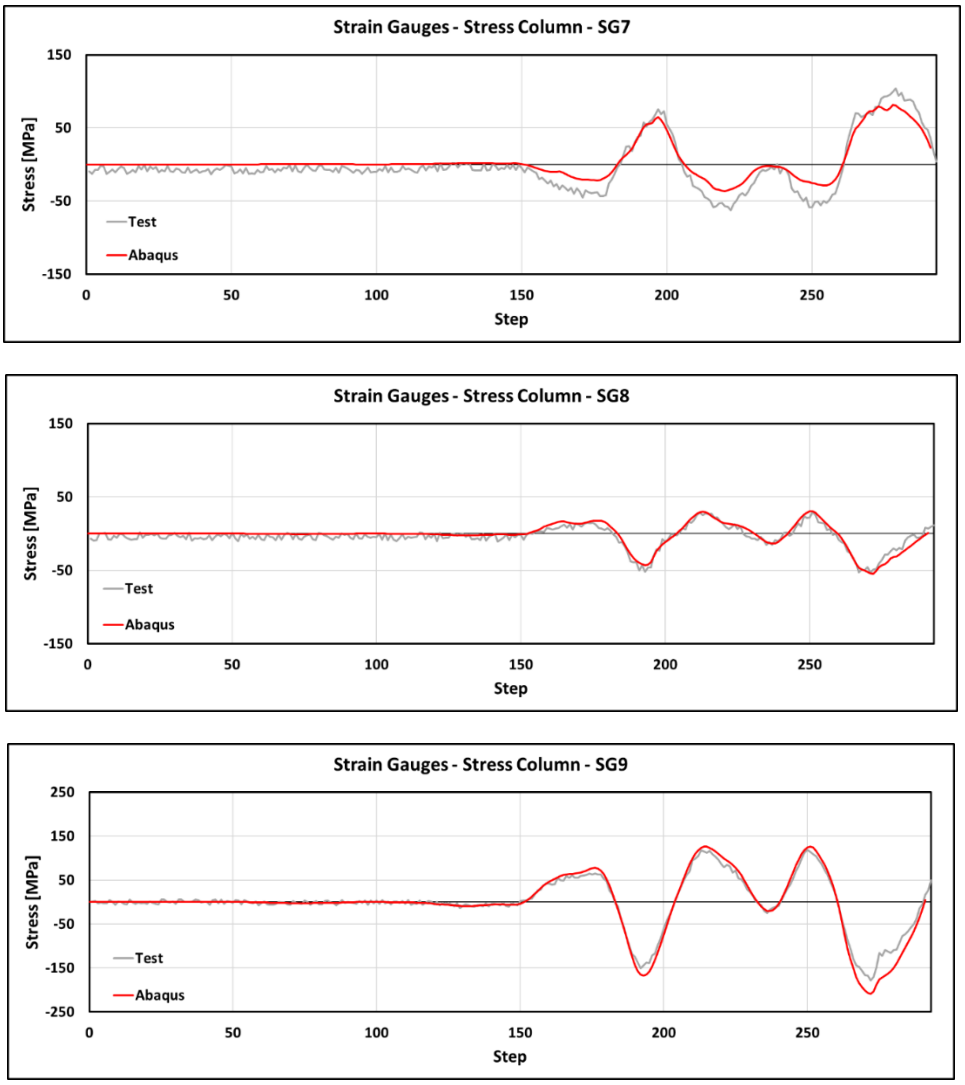

Figure B1-8 *Column Flange Strain Gauges - Detail 2: (a) SG7, (b) SG8, (c) SG9*

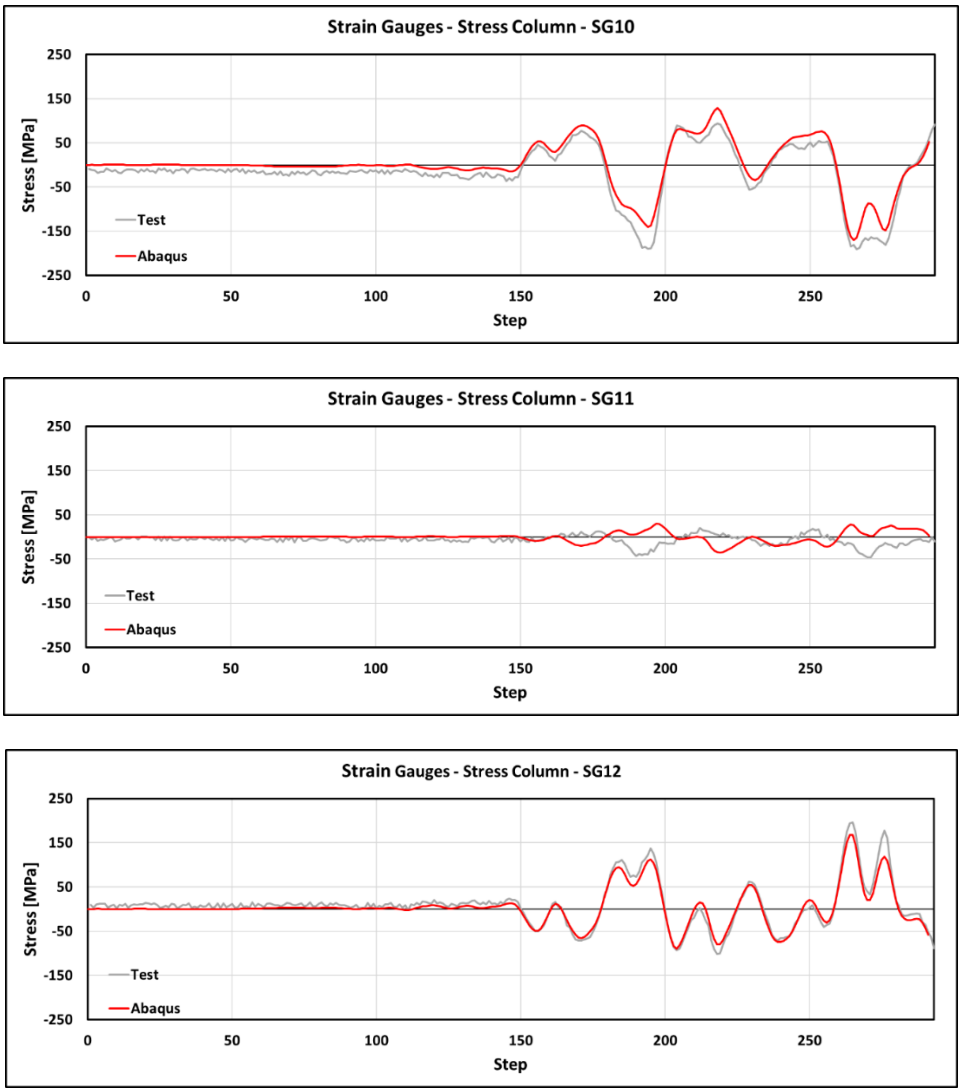

Figure B1-9 *Column Flange Strain Gauges - Detail 3: (a) SG10, (b) SG11, (c) SG12*

Acknowledgments

This thesis is the result of a collaboration between Dipartimento di Strutture per l'Ingegneria e l'Architettura (DIST, UniNA, Napoli) and Department of Civil, Environmental and Geomatic Engineering (CEGE, UCL, London) within the framework of the Erasmus+ project. Therefore, I sincerely want to express my gratitude to all the people and institutions involved in this project.

My sincerest appreciation goes to Professor Raffaele Landolfo, who introduced me to steel structures and allowed me to deepen my knowledge in an international environment. I am really grateful for the opportunity given to me.

A special mention goes to Dr Fabio Freddi who mentored me throughout the dissertation work. While abroad, he showed me his great ability to balance extreme professionalism with humanity. He made me realise that no successful research work can be achieved without a strong and cohesive team. Indeed, I would like to thank the whole UCL research group for welcoming me so warmly and for making me feel part of the family. I really appreciated the time we spent together.

All my family deserves my highest gratitude. To my parents for raising, educating and loving me; you are and always will be my greatest inspiration source. To my sister, my other half; despite disagreeing most of the time, I couldn't imagine a life without you. To Fernanda and Mariano, thank you for the support and love you constantly give me, you are my second parents. To all my grandparents. Origins are something you cannot choose, and I can only be proud of mine. Thank you all for everything you have done and will keep doing for me.

A special word of thanks goes to all my friends for sharing and turning every moment of these years into a very special one. Thank you for always being there. Among all, to Sergio and Simone, for putting up with me all these years; you will always represent a fundamental touchstone. To Mino, the most human and empathetic person I know; thank you for all the attention you dedicate to your friends. To Paolo and Roberto, for making every moment of the Bachelor's degree unforgettable. To Antimo and Raffaele, thank you for letting me grow with you throughout my Master's degree; I couldn't have wished for better mates. To Massimino, more than a classmate, for his constant support over the years. To Guido and Francesco, friends I know I can count on since day one.

To Elisabetta. What I believe to be the most important thing in life is to be able to find a partner who shares the same values, interests and ambitions as yours. I now believe I have found her and I hope to share many more "outdoor trips" by your side.